INVESTIGATION OF THIN SEMICONDUCTOR COATINGS AND THEIR ANTIMICROBIAL PROPERTIES

A THESIS SUBMITTED TO
THE GRADUATE SCHOOL OF NATURAL AND APPLIED SCIENCES
OF
MIDDLE EAST TECHNICAL UNIVERSITY

BY

ARCAN ERKAN

IN PARTIAL FULFILLMENT OF THE REQUIREMENTS
FOR
THE DEGREE OF MASTER OF SCIENCE
IN
CHEMICAL ENGINEERING

JULY 2005

Approval of the Graduate School of Natural and Applied Sciences

Prof. Dr. Canan Özgen
Director

I certify that this thesis satisfies all the requirements as a thesis for the degree of Master of Science.

Prof. Dr. Nurcan Baç
Head of Department

This is to certify that we have read this thesis and that in our opinion it is fully adequate, in scope and quality, as a thesis and for the degree of Master of Science.

Prof. Dr. Ufuk Bakır
Co-Supervisor

Assoc. Prof. Dr. Gürkan Karakaş
Supervisor

Examining Committee Members

Prof. Dr. Timur Doğu	(METU, CHE)	
Assoc. Prof. Dr. Gürkan Karakaş	(METU, CHE)	
Prof. Dr. Ufuk Bakır	(METU, CHE)	
Prof. Dr. Hayrettin Yücel	(METU, CHE)	
Prof. Dr. Hüseyin A. Öktem	(METU, BIO)	

I hereby declare that all information in this document has been obtained and presented in accordance with academic rules and ethical conduct. I also declare that, as required by these rules and conduct, I have fully cited and referenced all material and results that are not original to this work.

Name, Last name: Arcan Erkan

Signature :

ABSTRACT

INVESTIGATION OF THIN SEMICONDUCTOR COATINGS AND THEIR ANTIMICROBIAL PROPERTIES

Erkan, Arcan

M.S., Department of Chemical Engineering

Supervisor: Assoc. Prof. Dr. Gürkan Karakaş

Co-Supervisor: Prof. Dr. Ufuk Bakır

July 2005, 121 pages

Regular disinfection of surfaces is required in order to reduce the number of microorganisms, unable to transmit infections and maintaining the surfaces sterilized. For this purpose, antimicrobial thin film coatings on the various surfaces such as glass and ceramic surfaces, capable of killing harmful microorganisms are being investigated.

Generally a semiconducting material which can be activated by UV light tends to exhibit a strong antimicrobial activity. With holes (h^+) and hydroxyl radicals (OH*) generated in the valence band, electrons and the superoxide ions (O_2^-) generated in the conduction band, illuminated semiconductor photocatalysts can inactivate microorganisms by participating in a series of oxidation reactions leading to carbon dioxide.

The aim of this current study was developing semiconductor coatings, increasing the photocatalytic activity of these coatings by metal doping, particularly palladium doping, and investigating the antimicrobial properties of these coatings.

In this study, glass surfaces were coated with titanium dioxide (TiO_2), tin dioxide (SnO_2) and palladium doped TiO_2 and SnO_2 sol-gels. After achieving thin, dense and strong coatings, antimicrobial properties of the coatings were investigated by applying the indicator microorganisms directly onto the coated glasses. Different cell wall structure of microorganisms can strongly affect the photocatalytic efficiency of the coatings. Hence *Escherichia coli* as a Gr (-) bacteria, *Staphylococcus aereus* as Gr (+) bacteria, *Saccharomyces cerevisiae* as a yeast and *Aspergilus niger* spores were used in the experiments.

Photocatalytic efficiency of TiO_2 was better than SnO_2 coatings. Palladium doping increased the antimicrobial activity of both coatings. The reduction efficiencies were found to decrease in the following order of *E. coli* [Gr (-)] > *S. aereus* [Gr (+)] > *S.cerevisiae* (yeast) > *A. niger* spores. The complexity and the density of the cell walls increased in the same order. As a result of this study, with the coating that shows the best photocatalytic activity, 98% of *Escherichia coli*, 87% of *Staphylococcus aereus*, 43% *Saccharomyces cerevisiae* were killed after 2 hours illumination.

Keywords: Semiconductor coatings, photocatalysis, antimicrobial surface, TiO_2, SnO_2, palladium doping

ÖZ

YARI İLETKEN İNCE KAPLAMALARIN GELİŞTİRİLMESİ VE BU KAPLAMALARIN ANTİMİKROBİYAL ÖZELLİKLERİ

Erkan, Arcan
Yüksek Lisans, Kimya Mühendisliği Bölümü
Tez Yöneticisi: Doç. Dr. Gürkan Karakaş
Ortak Tez Yöneticisi: Prof. Dr. Ufuk Bakır

Temmuz 2005, 121 sayfa

Yüzeylerin düzenli dezenfekte edilmesi, yaşayan mikroorganizmaların sayısının azaltılması, enfeksiyonların yayılmasının engellenmesi ve yüzeylerin mikrop barındırmaması için gereklidir. Bu amaçla zararlı mikroorganizmaları öldürebilen ve cam ve seramik yüzeylere kaplanabilecek antimikrobiyal ince film kaplamalar geliştirilmektedir.

Genel olarak, yarı iletken bir malzeme UV ışığı ile aktif olduğunda güçlü bir antimikrobiyal özellik göstermektedir. UV ışığı altında aktif hale gelmiş bir yarı iletken, valans bandında oluşan boşluk (h^+) ve hidroksil radikalleri (OH*), iletim bandında oluşan elektron ve oksijen radikalleri (O_2^-) ile yüzeye temas halindeki mikroorganizmaları, oksidasyon tepkimeleri ile öldürmektedir.

Bu çalışmanın amacı, yukarıda bahsedilen gelişmelerin sağlanması yolunda yarı iletken filmler geliştirmek, cam yüzeyleri bu yarı iletken ince filmlerle kaplamak suretiyle bu yüzeylere çok fonksiyonluluk kazandırmak ve bu filmlerin antibakteriyel özelliklerini araştırmaktır. Bu filmlerin fotokatalitik etkisinin yarı iletken kaplama malzemesine metal iyonu ekleyerek arttırıldığı

bilinmektedir. Malzemelerin yapılarına paladyum eklenerek, filmlerin fotokatalitik aktivitesi üzerindeki etkileri araştırılmıştır.

Bu çalışmada, cam yüzeyler titanyum dioksit (TiO_2), kalay oksit (SnO_2) ve paladyum eklenmiş TiO_2 and SnO_2 sol-jel solüsyonları ile kaplanmıştır. İnce ve dayanıklı kaplamalar elde ettikten sonra kaplamaların antimikrobiyal özellikleri araştırılmıştır. Kaplamaların antimikrobiyal özelliklerinin araştırılmasında *Escherichia coli,* Gr (-) bakteri, *Staphylococcus aereus,* Gr (+) bakteri, *Saccharomyces cerevisiae,* maya, ve *Aspergilus niger* sporları, küf sporu, olarak kullanılmıştır. Bu mikroorganizmaların sıvı kültürleri direk olarak kaplanmış cam yüzeylere uygulanmış ve zamana bağlı olarak canlı kalan mikroorganizma sayısı incelenmiştir. Yarı iletkenlerin farklı mikroorganizmalar üzerindeki fotokatalitik aktiviteleri hücre duvar yapılarına göre farklılık göstermektedir. Bu nedenle bu çalışmada farklı mikroorganizmalar kullanılmıştır.

TiO_2 yüzey kaplaması SnO_2 yüzey kaplamasına göre daha daha iyi fotokatalitik etki göstermektedir. Paladyum eklemek, her iki kaplamanın da antimikrobiyal aktiviesini arttırmıştır. Fotokatalitik aktivitenin farklı mikroorganizmalar üzerindeki etkisi, *E. coli* [Gr (-)] > *S. aereus* [Gr (+)] > *S.cerevisiae* (maya) > *A. niger* sporları sırasına göre azalmaktadır. Hücre duvarlarının kompleks ve yoğun yapıları da aynı yönde artmaktadır. Bu çalışmanın sonunda, en iyi fotokatalitik aktivite gösteren kaplama ile, PdO- TiO_2, 2 saat iluminasyon sonucunda yüzeye temas halindeki mikroorganizmaların sayısında; *Escherichia coli, %98, Staphylococcus aereus*, %87*, Saccharomyces cerevisiae*, %43, azalma görülmüştür. En iyi fotokatalitik aktivite paladyum dopinglenmiş TiO_2 kaplamalar ile elde edilmiştir.

Anahtar Sözcükler: yarı iletken kaplamalar, fotokataliz, antimikrobiyal yüzeyler, TiO_2, SnO_2, paladyum katkılama

Dedicated to my family…

ACKNOWLEDGEMENTS

This thesis could not have been written without the long-time and encouraging support of my supervisor, Assoc. Prof. Gürkan Karakaş and my co-supervisor Prof. Dr. Ufuk Bakır. I present my sincere gratitude to my thesis supervisors for their valuable advice and guidance throughout this study. It was a pleasing honor for me to work with them.

I was delighted to conduct my experiments in the Environmental Catalysis Laboratory with my colleagues during this study. I would like to thank my dear friends Burcu Mirkelamoğlu, Başak Kurbanoğlu, Alp Yürüm and Müge Arifoğlu for their contributions and cordiality.

I also wish to give my special thanks to all my friends in our research group in Industrial Biotechnology Laboratory. I am especially grateful to Ayşegül Ersayın, Didem Sutay, Aytaç Kocabaş, Beril Korkmaz, Deniz Öztürk, Emel Göksu, Özlem Ak for their valuable help, cooperation and friendship.

Additional thanks go to the staff and the technicians of Chemical Engineering Department.

I am, also, very grateful to my homemates Işın Sancar and Pelin Toprak; my dear friends Taşkın Irmak, Salih Obut, Özge Güvenir and Eser Dinçer for their helps and support.

My special thanks go to Yalaz Yalçın for being right beside me whenever I needed and his endless cordiality.

Finally, I would like to express my deepest thanks to my family and my love Güray Güven for unceasing patience, supporting, encouraging and loving me all through my life. It would not have been possible without their endless understanding and love to complete this study.

TABLE OF CONTENTS

PLAGIARISM iii

ABSTRACT iv

ÖZ vi

DEDICATION viii

ACKNOWLEDGEMENTS ix

TABLE OF CONTENTS x

LIST OF TABLES xv

LIST OF FIGURES xvi

NOMENCLATURE xxi

CHAPTER

1. INTRODUCTION 1

2. LITERATURE SURVEY 5

2.1 Environmental Applications of Semiconductor Photocatalysis 5

2.2 Semiconductors 6

2.3 Determination of Optical Absorption Edge Energy of the Films Depending on the spectra 9

2.4 Semiconductor Photocatalysis 11

2.5 Precursors 12

2.5.1 Alkoxides 12

2.5.2 Mixed Ligand Precursors 13

2.6 Solution Processes and Chemical Routes 13

2.7 Production Techniques For Thin Films 14

2.7.1 Sol-gel Processes 15

2.8 Film Formation 18

2.9 Contact Angle 19

2.10 Hydrophilicity 21

2.11 Hydrophobicity 22

2.12 Coating Process for Deposition of Sol-gel Films 23

2.12.1 Dip Coating 24

2.12.2 Spin Coating 25

2.13 Thermal Treatment 29

2.13.1 Drying 29

2.13.2 Annealing 30

2.14 Photocatalytic Process Mechanism 31

2.15 Increasing the Photocatalytic Activity 32

2.15.1 Microscopic Conduction in Solids 34

2.16 Photocatalytic Activity on Microbial Cells 34

2.17 Main Cell Types and Their Cell Wall Structures 36

2.17.1 Procaryotic Cells 37

2.17.1.1. Gram Negative Bacteria 39

2.17.1.2. Gram Positive Bacteria 40

2.17.2 Eucaryotic Cells 42
2.17.2.1 Fungi 43
2.17.2.2 Yeasts and Molds 44
3. EXPERIMENTAL PROCEDURE 46
3.1 Preparation of Monolayers 46
3.1.1 Pretreatment of the Glasses 46
3.1.2 Preparation of Coating Solutions 46
3.1.2.1 Sol-Gel Preparation of Titanium Dioxide 46
3.1.2.2 Sol-Gel Preparation of Tin Dioxide 48
3.1.2.3 Palladium Doping to TiO_2 and SnO_2 Solutions 49
3.1.3 Coating of the Films 49
3.1.4 Heat Treatment of the Films 49
3.2 Analysis of the Films 50
3.3 Anti-Bacterial Test 50
3.3.1 Microorganisms and Growth 50
3.3.2 Illumination 51
3.3.3 Irradiation and Testing the Anti-Bacterial Effect 52
4. RESULTS AND DISCUSSION 53
4.1 Determination of Optical Absorption Edge Energy of the Films Depending on the Spectra 53
4.2 Film Morphology 56
4.2.1 SEM analysis for TiO_2 and PdO-TiO_2 deposited Glass Substrates 56
4.2.2 SEM analysis for SnO_2 and PdO-SnO_2 deposited Glass Substrates 58
4.3 Reusability of the Films 60

4.4 Antimicrobial Properties of the Films 60

4.5 Photocatalytic Effect on Microbial Cells 64

4.5.1 Antimicrobial Effect Against *Escherichia coli* 64

4.5.1.1 TiO_2 Films 64

4.5.1.2 Palladium Doped TiO_2 Films 65

4.5.1.3 SnO_2 Films 68

4.5.1.4 Palladium Doped SnO_2 Films 69

4.5.2. Antimicrobial Effect Against *Staphylococus aereus* 72

4.5.2.1 Isolation and Identification Test Results of *S. aereus* 72

4.5.2.2 TiO_2 Films 72

4.5.2.3. Palladium Doped TiO_2 Films 74

4.5.2.4. SnO_2 Films 76

4.5.2.5. Palladium Doped SnO_2 Films 77

4.5.3 Antimicrobial Effect Against *Saccharomyces cerevisiae* 80

4.5.3.1 TiO_2 Films 80

4.5.3.2 Palladium Doped TiO_2 Films 82

4.5.3.3. SnO_2 Films 84

4.5.3.4. Palladium Doped SnO_2 Films 85

4.5.4 Antimicrobial Effect Against *Aspergilus niger* 89

5. CONCLUSION 97

6. RECOMMENDATION 98

7. REFERENCES 99

8. WEB REFERENCES 105

9. APPENDICES 107

A. MEDIUM AND AGAR BASES 107

B. SAMPLE CALCULATIONS 110

C. DATA OF GRAPHICS 115

LIST OF TABLES

2.1 Some advantages of the sol-gel method.....17

2.2 Some disadvantages of the sol-gel method.....17

4.1 The comparison of the number of survived cells in dark experiments with the number of cells in the original liquid culture.....63

4.2 The increasing effect of Palladium doping TiO_2 and SnO_2 coatings.....96

9.1 Data of Figure 4.1, UV-Vis spectra of TiO_2 and PdO-TiO_2 deposited glass substrates.....115

9.2 Data of Figure 4.2, UV-Vis spectra of SnO_2 and PdO-SnO_2 deposited glass substrates.....116

9.3 Data of Figure 4.16, Survival ratio of *E. coli* under illumination on TiO_2 and PdO-TiO_2 coated glass substrates 118

9.4 Data of Figure 4.21, Survival ratio of *E. coli* under illumination on SnO_2 and PdO-SnO_2 coated glass substrates 119

9.5 Data of Figure 4.27, Survival ratio of *S. aereus* under illumination on TiO_2 and PdO-TiO_2 coated glass substrates.....119

9.6 Data of Figure 4.30, Survival ratio of *S. aereus* under illumination on SnO_2 and PdO-SnO_2 coated glass substrates.....120

9.7 Data of Figure 4.37, Survival ratio of *S. cerevisiae* under illumination on TiO_2 and PdO-TiO_2 coated glass substrates 121

LIST OF FIGURES

2.1 Band Gap Energies of metals, insulators and semiconductors..... 7
2.2 n-type/p-type semiconductors 8
2.3 The relation between optical absorbance edge energy and the onset of intense optical absorption. 10
2.4 Sol-gel Process 16
2.5 Contact angle and hydrophilicity relation 20
2.6 Hydrophilic property of coated tile. 22
2.7 The dip-coating technique 25
2.8 Stage one in spin-coating technique 26
2.9 Stage two in spin-coating technique 27
2.10 Stage three in spin-coating technique 28
2.11 Stage four in spin-coating technique 29
2.12 Photocatalytic process on the surface of the semiconductor 32
2.13 Depletion layer of a semiconductor 33
2.14 Conduction through particles 34
2.15 Main types of microbial cells 37
2.16 Typical procaryotic cell structure 38
2.17 Classification of procaryotes.....39
2.18 Typical gram-negative cell wall structure 40
2.19 Typical gram-positive cell wall structure 41
2.20 Comparison of cell wall complexity of gram-positive and gram-negative bacteria 42
2.21 Cell wall structure of a filamentous fungi 43
2.22 Cell wall structure of a yeast cell 44
3.1 Flow diagram for the sol-gel processing of TiO_2 thin films 47
3.2 Flow diagram for the sol-gel processing of SnO_2 thin films.....48
3.3 Comparison of spectral distribution of solar simulator with the natural light 51
4.1 UV-Vis spectra of TiO_2 and PdO-TiO_2 deposited glass substrates.....54
4.2 UV-Vis spectra of SnO_2 and PdO-SnO_2 deposited glass substrates 55
4.3 SEM micrograph of TiO_2 film surface, x10,000 magnification.....56

4.4 SEM micrograph of surface defects over the TiO_2 film surface, x10,000 magnification 57
4.5 SEM micrograph of PdO-TiO_2 film surface, x10,000 magnification 58
4.6 SEM micrograph of surface defects over the PdO-TiO_2 film surface, x10,000 magnification 58
4.7 SEM micrograph of SnO_2 film surface, x1,000 magnification 59
4.8 SEM micrograph of PdO-SnO_2 film surface, x1,000 magnification 60
4.9 Number of *E. coli* cells in the 200µl microbial suspension that applied on the surfaces, [352±5 CFU/200µl were counted] 61
4.10 Number of *E. coli* cells in the microbial suspension of 200µl applied on the uncoated surface and illuminated i.e., the UVA effect alone [350±7 CFU/200µl were counted].. 62
4.11 Number of *E. coli* cells in the microbial suspension of 200µl applied on the TiO_2 coated surface and kept in the dark [350±5 CFU/200µl were counted]. 62
4.12 Number of *E. coli* cells survived on uncoated (control) glass surface, [350±7 CFUs/200µl were counted]. 64
4.13 Number of *E. coli* cells survived on TiO_2 coated glass surface [50±4 CFUs/200µl were counted] 65
4.14 Number of *E. coli* cells survived on uncoated (control) glass surface, [356±5 CFUs/200µl were counted] 66
4.15 Number of *E. coli* cells survived on PdO-TiO_2 coated glass surface [8±1 CFUs/200µl were counted] 67
4.16 Survival ratio of *E. coli* under illumination on TiO_2 and PdO-TiO_2 coated glasses (initial number of E. coli: 352±5 CFUs/200µl).....67
4.17 Number of *E. coli* cells survived on uncoated (control) glass surface, [352±5 CFUs/200µl were counted].....68
4.18 Number of *E. coli* cells survived on SnO_2 coated glass surface [153±4 CFUs/200µl were counted].....69
4.19 Number of *E. coli* cells survived on uncoated (control) glass surface, [351±2 CFUs/200µl were counted].....70
4.20 Number of *E. coli* cells survived on PdO-SnO_2 coated glass surface [109±1 CFUs/200µl were counted].....70
4.21 Survival ratio of *E. coli* under illumination on SnO_2 and PdO-SnO_2 coated glasses (initial number of *E. coli*: 352±5 CFUs/200µl).....71

4.22 Number of residual cells of *E. coli* under illumination on TiO_2, PdO-TiO_2, SnO_2 and PdO-SnO_2 coated glasses (initial number of *E. coli*: 352±5 CFUs/200µl) 71
4.23 Identification results of *S. aereus* on Baird-Parker agar 72
4.24 Number of *S. aereus* cells survived on uncoated (control) glass surface, [337±5 CFUs/200µl were counted].....73
4.25 Number of *S. aereus* cells survived on TiO2 coated glass surface [44±6 CFUs/200µl were counted].....73
4.26 Number of *S. aereus* cells survived on uncoated (control) glass surface, [335±7 CFUs/200µl were counted].....75
4.27 Number of *S. aereus* cells survived on PdO-TiO_2 coated glass surface [7±2 CFUs/200µl were counted] 75
4.28 Survival ratio of *S. aereus* under illumination on TiO_2 and PdO-TiO_2 coated glasses (initial number of *S. aereus*: 330±5 CFUs/200µl).....76
4.29 Number of *S. aereus* cells survived on uncoated (control) glass surface, [327±7 CFUs/200µl were counted] 77
4.30 Number of *S. aereus* cells survived on SnO_2 coated glass surface [69±3 CFUs/200µl were counted] 77
4.31 Number of *S. aereus* cells survived on uncoated (control) glass surface, [332±7 CFUs/200µl were counted].....78
4.32 Number of *S. aereus* cells survived on PdO-SnO_2 coated glass surface, [33±3 CFUs/200µl were counted] 78
4.33 The survival ratio of *S. aereus* under illumination on SnO_2 and PdO-SnO_2 coated glasses (Initial number of *S. aereus*: 330±5 CFUs/200µl).....79
4.34 Number of residual cells of *S. aereus* under illumination on TiO_2, PdO-TiO_2, SnO_2 and PdO-SnO_2 coated glasses (initial number of *S. aereus*: 352±5 CFUs/200µl) 80
4.35 Number of *S. cerevisiae* cells survived on uncoated (control) glass surface, [432±12 CFUs/200µl were counted].....81
4.36 Number of *S. cerevisiae* cells survived on TiO_2 coated glass surface [233±8 CFUs/200µl were counted].....81
4.37 Number of *S. cerevisiae* cells survived on uncoated (control) glass surface, [430±8 CFUs/200µl were counted] 83

4.38 Number of *S. cerevisiae* cells survived on PdO-TiO_2 coated glass surface [150±6 CFUs/200µl were counted] 83
4.39 Survival ratio of *S. cerevisiae* under illumination on TiO_2 and PdO-TiO_2 coated glass substrates (initial number of *S. cerevisiae*: 434±8 CFUs/200µl) 84
4.40 Number of S*. cerevisiae* cells survived on uncoated (control) glass surface, [436±8 CFUs/200µl were counted] 85
4.41 Number of *S. cerevisiae* cells survived on SnO_2 coated glass surface [300±9 CFUs/200µl were counted].....85
4.42 Number of *S. cerevisiae* cells survived on uncoated (control) glass surface, [430±8 CFUs/200µl were counted] 86
4.43 Number of *S. cerevisiae* cells survived on PdO-SnO_2 coated glass surface [253±7 CFUs/200µl were counted].....87
4.44 Survival ratio of *S. cerevisiae* under illumination on SnO_2 and PdO-SnO_2 coated glass substrates (initial number of *S. cerevisiae*: 434±8 CFUs/200µl) 88
4.45 Number of residual cells of *S. cerevisiae* under illumination on TiO_2, PdO-TiO_2, SnO_2 and PdO-SnO_2 coated glasses (initial number of E. coli: 434±8 CFUs/200µl).....88
4.46 Growth of *A. niger* spores on the uncoated (control) glass after (A) 2h illumination; (B) 4h illumination (C) 6h illumination (D) 8h illumination. Plates were incubated at 35°C for 29 hours.....90
4.47 Growth of *A. niger* spores on TiO_2 coated glass after (A) 2h illumination; (B) 4h illumination (C) 6h illumination (D) 8h illumination. Plates were incubated at 35°C for 29 hours. 91
4.48 Growth of *A. niger* spores on PdO-TiO_2 coated glass after (A) 2h illumination; (B) 4h illumination (C) 6h illumination (D) 8h illumination. Plates were incubated at 35°C for 29 hours.....92
4.49 Growth of *A. niger* spores on SnO_2 coated glass after (A) 2h illumination; (B) 4h illumination (C) 6h illumination (D) 8h illumination. Plates were incubated at 35°C for 29 hours 93
4.50 Growth of *A. niger* spores on PdO-SnO_2 coated glass after (A) 2h illumination; (B) 4h illumination (C) 6h illumination (D) 8h illumination. Plates were incubated at 35°C for 29 hours.....94

4.51 Comparison of antimicrobial efficiencies of different coatings against different microorganisms after 1 and 2 hours of illumination 96

NOMENCLATURE

Symbols

CoA	coenzyme A
c	speed of light, m/s^2
DNA	deoxyribonucleic acid
e	electron charge
eV	electron-volt
E	Photon energy
E_{bg}/E_g	band gap energy
h	planck's constant
L_c	particle size
n	negative
p	positive
RNA	ribonucleic acid
SnO_2	Tin dioxide
TiO_2	Titanium dioxide
U	substrate withdrawal speed cm/s
UV-Vis	ultraviolet-visible reagion
UVA	ultraviolet A region (near UV)

Greek Letters

λ	wavelength
σ	conductivity
ρ	density of sol
θ	contact angle
μ	mobility of electrons and holes
γ	surface tension
γ_{SV}	solid-vapor surface tension
γ_{SL}	solid-liquid surface tension

η	sol viscosity
η	charge carrier density

Abbreviations

CVD	chemical vapor deposition
MOCVD	metal organic chemical vapor deposition
PECVD	plasma-assisted chemical vapor deposition
SEM	scanning electron microscopy

CHAPTER 1

INTRODUCTION

Because of the ever-growing demand for healthy living, there is a keen interest in materials capable of killing harmful microorganisms. Such materials could be used to coat the surfaces of common objects touched by people in everyday life to render them antiseptic and thus unable to transmit bacterial infections [Tiller et al., 2001].

Particularly in microbiology laboratories and areas of intensive medical use, regular and thorough disinfection of surfaces is required in order to reduce the numbers of bacteria and to prevent bacterial transmission. Conventional methods of manual disinfection with wiping are not effective in the longer term, can not be standardized, and are time-intensive and staff-intensive [Kühn et al., 2003].

From the viewpoint of energy saving and environmental protection, low-temperature, antimicrobial materials synthesis has been highlighted in the past several decades. Because ordinary materials are not antimicrobial, they require modification. A potential alternative may be provided by substrates made of light-guiding materials, coated with specific semiconductors and stimulated by indirect mild ultraviolet A light (320-400nm) [Lin et al., 1998].

The photocatalytic process is emerging as a promising technology for the oxidation/degradation of organic contaminants in environmental control. The process has several advantages when compared to biological and traditional chemical oxidation processes. First the photocatalytic reaction is not specific and, therefore, is capable of destroying a wide spectrum of organic chemicals. Second the process is powerful, often achieving a complete mineralization of organics. Third, the process is immune to organic toxicity. This advantage makes the photocatalytic process particularly attractive for the degradation of recalcitrant and toxic compounds. Four, the process can be applied equally well to liquid and

gaseous streams. Finally, there is a potential to utilize sunlight instead of an artificial light as an UV source, thereby reducing the energy cost for the process. A heterogeneous photocatalytic system consists of semiconductor particles (photocatalyst) which are in close contact with a liquid or gaseous reaction medium. Exposing the catalyst to light excited states are generated which are able to initiate subsequent processes like redox reactions and molecular transformations [Chang et al., 2000].

Due to their electronic structure, which is characterized by a filled valence band and an empty conduction band, semiconductors with their reasonable band gap energies find great attraction through this purpose and these semiconductors (ZnO, CdS, TiO_2, Fe_2O_3) can act as sensitizers for light-induced redox processes. The energy difference between the lowest energy level of the conduction band and the highest energy level of the valence band is the so-called band gap energy E_g. It corresponds to the minimum energy of light required to make the material electrically conductive [Benedix et al., 2000].

Semiconductor photocatalysis is based on the feature that some semiconductors, in particular titanium dioxide (TiO_2), are able to photocatalyse the complete mineralization of many organics and living microorganisms. Semiconductor materials are very effective against microorganisms and organic materials. The semiconductor photocatalysis has been studied for years by many researchers. Although many important fundamental results concerning semiconductor photocatalytic reaction have been clarified by such intensive works, there have been few successful industrial applications in environmental as well as photovoltaic applications. Most of these works utilized powder TiO_2 as a material. In order to avoid the use of powder, which requires stirring during reaction process and has to be separated from the water after photocatalysis, ways have been developing to apply semiconductor coatings on various materials such as glass or ceramic tiles to give the surface of these materials a self-cleaning function utilizing photocatalysis. Not only the self-cleaning functions but also hydrophilic properties were found on photoirradiated TiO_2 surface [Mills et al., 2003].

Some of our choices for photocatalytic semiconductors are TiO_2 (E_g = 3.2 eV), SnO_2 (E_g = 3.5 eV), Fe_2O_3 (E_g = 2.2 eV), CdS (E_g = 2.5 eV), ZnO (E_g = 3.2 eV), ZnS (E_g = 3.6 eV). Among these semiconducting materials, TiO_2 has attracted massive interest since wide spectrum of organic contaminants can be converted to water and CO_2 with its strong oxidation/reduction property, corrosion resistance and non-toxic property and since it is inexpensive, has quite fast reactions and has no side reaction. Photocatalytic water splitting, dye sensitized nanocrystalline solar cells and light induced hydrophilic surfaces are the most striking photocatalytic phenomena reported on TiO_2 surfaces. Hydrophilic property of the surface allows water to spread completely across the surface rather than remain as droplets, thus making the surface anti-fogging and easy to wash [Popielarski, 1998].

One disadvantage of TiO_2 is that the band gap energy is approximately 3.2 eV; therefore UV illumination is necessary to photoactivate this semiconductor. Another disadvantage of TiO_2 is that charge carrier recombination occurs within nanoseconds and in the absence of promoters, hence the photocatalytic activity is low [Trapalis et al., 2003].

A wide range of metal ions, in particular transition metal ions (palladium, platinum, iron, gold, silver, copper, chromium, cobalt), have been used as dopants for semiconductors to decrease the wide band gap energy and hence increase the photocatalytic activity.

The wide band-gap semiconductor TiO_2 has three crystal structures: anatase (at temp < 700^{o}C, tetragonal), rutile (at temp > 700^{o}C, tetragonal) and brookite (orthorhombic). The crystal structures of anatase and rutile phases consist of chains of TiO_6 octahedra. The octahedra structure is more distorted in anatase-TiO_2 than in rutile- TiO_2, resulting in different structures and distinct chemical and physical properties. The most stable crystalline structures are rutile and anatase. Rutile structure is more stable than anatase structure but anatase structure is the most active one [Tang et al., 1995].

The film deposition on the substrate can be formed by dip coating, spin coating, or spray deposition techniques. Dip coating and spin coating techniques are the most widely used coating techniques.

When the semiconductor with light of $\lambda < 400nm$, an electron is promoted from the valence band to the conduction band of the semiconducting oxide to give an electron/hole pair. The valence band potential is positive enough to generate hydroxyl radicals at the surface and the conduction band potential is negative enough to reduce molecular O_2. The hydroxyl radical is a powerful oxidizing agent and attacks organic pollutants present at or near the surface of TiO_2, resulting usually in their complete oxidation to CO_2 [Chang and Wu, 2000].

In this study photocatalytic, semiconductor thin films were prepared by sol-gel processing method. Dip coating technique was used for the coating of the TiO_2, SnO_2 and palladium doped TiO_2 and SnO_2 thin films on the glass substrates. Then, antimicrobial properties of these coatings were determined by using different microbial cells having different cell wall structures. *Escherichia coli, Staphylococcus aereus, Saccharomyces cerevisiae* and *Aspergilus niger* were used as the indicator microorganisms.

CHAPTER 2

LITERATURE SURVEY

2.1. Environmental Applications of Semiconductor Photocatalysis

Semiconductor photocatalysis with the primary focus on titanium dioxide (TiO_2) as a durable photocatalyst has been applied to a variety of problems of environmental interest in addition to water and air purification. It has been shown to be useful for the destruction of microorganisms and viruses, for the inactivation of cancer cells, for odor control, for the photosplitting of water to produce hydrogen gas, for the fixation of nitrogen, and for the clean up of oil spills [Hoffmann et al., 1995].

As mentioned above, one of the most significant environmental applications of semiconductor photocatalysis is photo-induced removal of pollutants from air and water, as well as deodorization, prevention of stains, and sterilization under ambient conditions [Serpone et al., 1988]

The civilian, commercial, and defense sectors of most advanced industrialized nations are faced with a tremendous set of environmental problems related to the remediation of hazardous wastes, contaminated groundwater, and the control of toxic air contaminants.

More recent applications of TiO_2 as a photocatalyst and photoactive material have involved antifouling [Minabe et al., 2000], antibacterial [Kikuchi et al., 1997] and self-cleaning functions [Fukayama et al., 1995]. Much work has been carried out on the photocatalytic decomposition of relatively small organic compounds, either in gas or liquid phase [Schwitzgebel et al., 1995].

Semiconductor photocatalysis is an efficient method for the chemical utilization of solar energy. It is based on the surface trapping of light-generated charges that induce interfacial electron-transfer reactions with a great variety of substrates.

In practice, surface cleaning of building materials like tiles, facades and glass panes causes considerable trouble, high consumption of energy and chemical detergents and, consequently, high costs.

In order to address these significant problems, extensive research is underway to develop advanced analytical, biochemical, and physicochemical methods for the characterization and elimination of hazardous chemical compounds from air, soil, and water, to make surfaces self-cleaning and antimicrobial, to gain materials antifouling property. Advanced physicochemical processes such as semiconductor photocatalysis are intended to be both supplementary and complementary to some of the more conventional approaches to the destruction or transformation of hazardous chemical wastes [Hoffmann et al., 1995].

2.2. Semiconductors

The band theory of solids describes a non-metallic material as having two energy bands: the lower energy valence band, which is completely filled and the upper energy conduction band, which is completely empty at the temperature of absolute zero. The conductivity of a material at any other temperature depends on whether or not there are electrons in the conduction band. The energy gap between filled valence band and empty conduction band is band gap energy [Reddya et al., 2002]. The size of the energy gap has an important effect on the number of electrons that can be excited into conduction band. As shown in Figure 2.1, the valence and conduction bands in a metal coincide and the valence electrons are free to move in the conduction band, which is the reason why metals are good conductors. The energy level of electrons in metals is very high and photons do not increase their energies. In contrast, in insulators the valence and conduction bands are separated by a large gap, called the forbidden energy gap or band gap. For insulators it is very hard to promote an electron from valence band to conduction band. Insulators do not absorb energy; light enters and leaves the insulator [Okudera and Yokogawa, 2001].

In semiconductors the band gap is narrower than that in insulators and thermal excitation of electrons and electron donor or acceptor impurities can

improve the conductivity of a semiconductor. For semiconductors the electrons can be promoted from valence band to conduction band by the energy of photons. At any temperature above absolute zero, there are a number of electrons in the conduction band and the higher the temperature, the more the conductivity. In the case of dopants, the impurity atoms added into the semiconductor crystal either donates extra electrons into the lattice or take away electrons from lattice, thus creating "holes", which are electron deficient spots. Another way to view the addition of impurities in the semiconductor is to say that they introduce new energy states into the structure. In the case of donor impurities, there forms an extra level close to the conduction band, which donates electrons to the conduction band, increasing the charge carrier density and thus the conductivity. In the case of acceptor impurities the levels created by the holes are close to the valence band and they provide a means for flow for the valence band electrons. Semiconductors absorb mostly the UV spectrum and the excited electrons jump the band gap energy and fill the conduction band [Fujishima et al., 2000].

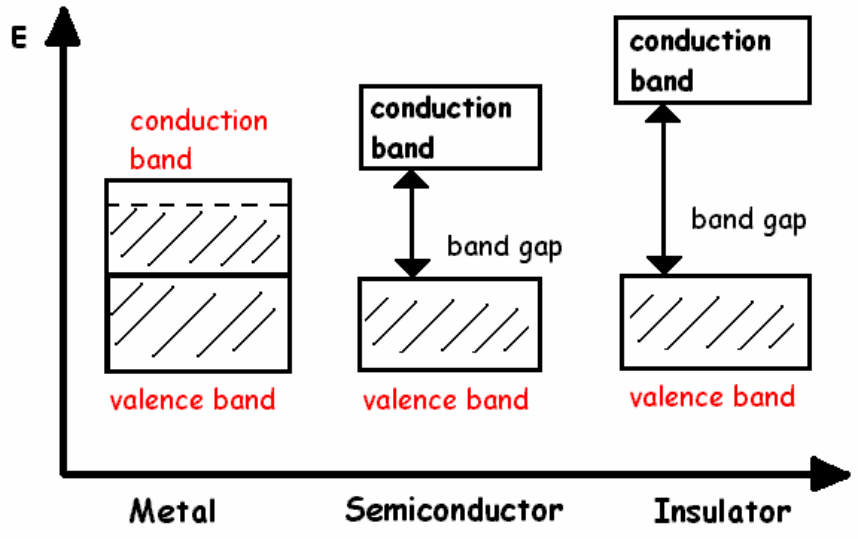

Figure 2.1 Band Gap Energies of metals, insulators and semiconductors

Semiconductors are classified into two groups according to the major source of electrical conduction in their structure. In n-type semiconductors, the major carriers are electrons whereas in p-type semiconductors, the major carriers are holes. SnO_2 and TiO_2 are n-type semiconductors.

In a pure semiconductor there are not enough free electrons and holes to be of much use. Their number can be greatly increased however by adding an impurity, called a donor. If the donor gives up some extra free electrons we get an n-type semiconductor (n for (-)). If the donor soaks up some of the free electrons we get a p-type semiconductor (p for (+)). In both cases the impurity donates extra current carriers to the semiconductor [Walters et al., 2000].

In n-type semiconductors there are more electrons than holes and they are the main current carriers. In p-type semiconductors there are more holes than electrons and they are the main current carriers. The donor atoms become either (+) ions (n-type) or (-) ions (p-type).

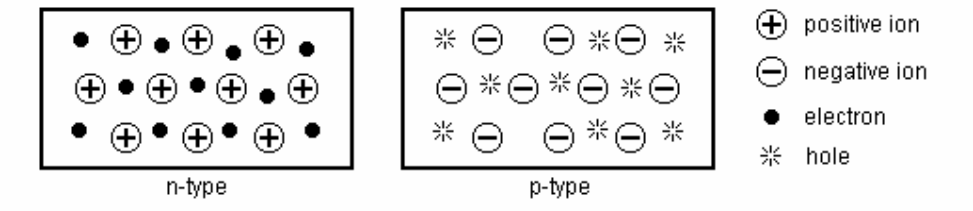

Figure 2.2 n-type/p-type semiconductors [URL 1]

2.3. Determination of Optical Absorption Edge Energy of the Films

Depending on the spectra

It is possible to determine the magnitude of the forbidden band gap energy of semiconductors using their absorbance spectrum in the UV-Visible range. While absorbance in the infrared region corresponds to lower energy levels in a material and is informative about lattice vibrations, the energies in the visible and UV range correspond to the energies of the valence and conduction bands. UV-Vis absorbance and reflectance spectroscopy of semiconductors contain valuable information in the sense of crystallite size, electronic properties of surface, oxidation states of species and metal support interaction. Also the UV-Vis spectroscopy is a powerful characterization technique on the nano-technology because of most of the materials transforms into semiconductors when their crystallite size approaches to the nanometer range.

The fact that, many metals which are conductor at microscale expose semiconductor properties with higher band gap because of excessive amount of surface electrons per molecule and this process is thermodynamically favorable. The behavior of size dependent electronic properties of metal oxide clusters offers tunable and tailored semiconductor properties and promising to yield high technology electronic and optical products [Marzan and Luis, 2003].

The electronic structure of a semiconductor surface should be characterized by considering the cluster size of a material and the terminology must be used carefully. For micro-scale materials, forbidden band gap is described as the minimum energy required to shift one electron from valence band to conduction band, where as the optical absorption edge energy must be considered for nano-sized materials which can be described as the minimum photon energy required to excite an electron from the highest occupied molecular orbital (HOMO) to the lowest unoccupied molecular orbital (LUMO). Depending on the crystallite size of the semiconductor material, either band gap or absorption edge energy must be determined to characterize the property.

The UV-Vis spectroscopy can be utilized to measure band gap or optical absorption edge energy depending on the spectra.

As shown Figure 2.3, the photon energy corresponding to the band gap occurs at the onset of intense optical absorption. This provides an experimental method for the determination of the band gap [Kato et al., 1995].

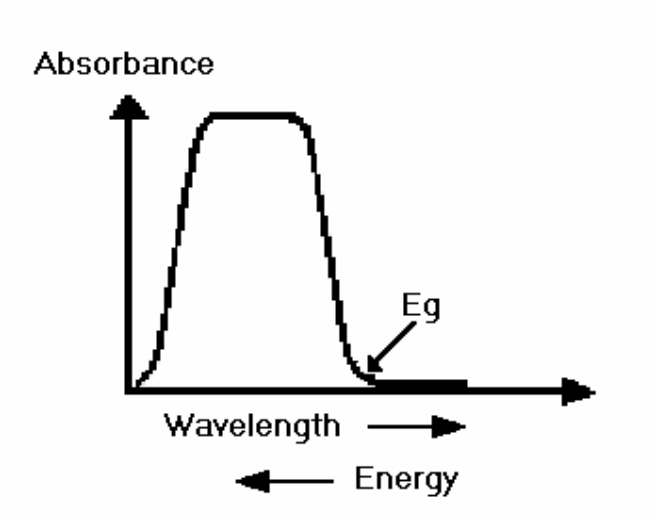

Figure 2.3 The relation between optical absorbance edge energy and the onset of intense optical absorption

Here the photon energy is [Diebold, 2003]:

$E = (h.c)/\lambda$ Where,

E: photon energy, J

h: Planck's constant, 6.626×10^{-34} kgm^2/s

c: speed of light, $3x10^8$ m/s

λ: Wavelength, m

1eV = $1.6x10^{-19}$ J ($Kg.m^2/s^2$)

2.4. Semiconductor Photocatalysis

Semiconductor photocatalysis offers convenient routes to the purification of air and water and the provision of self-maintaining clean surfaces. Semiconductor photocatalysis can be defined as the acceleration of a photoreaction by the presence of a catalyst. The overall process can be summarized as follows:

$$\text{Organic pollutant} + O_2 \xrightarrow[\text{Semiconductor}]{h\nu > Eg} \text{mineralized products}$$

Where E_{bg} is the band gap of the semiconductor, [Mills et al., 2003]. Photocatalytic activity is influenced by the crystal structure of the semiconductor, surface area, size distribution, porosity and surface hydroxyl group density. This will have an influence on the production of electron-hole pairs on the surface adsorption and desorption processes as well as redox process which is related with the photocatalytic process mechanism that will be given later.

The photocatalytic degradation of several liquid and solid organic compounds was studied on TiO_2 thin films on glass under UV illumination [Minabe et al., 2000]. Nearly exact agreement was found between the weight losses of the solid compounds octadecane and stearic acid and weights of CO_2 produced during photocatalytic degradation. Another study was focused on photodegradation of surfactants on the nanosized TiO_2 prepared by hydrolysis of the alkoxide titanium [Zhang et al., 2004].

2.5. Precursors

2.5.1. Alkoxides

Alcohols (R-OH) can be regarded as very weak acids, and the metal salts of alcohols are called alkoxides, $M(OR)_x$, where M is a metal. Due to their polar M-O bond, non-stabilized alkoxides are very sensitive toward hydrolysis, leading to the formation of metal hydroxides (M-OH) with the concurrent release of an alcohol molecule.

If hydrolysis is extensive, precipitation of hydroxide or oxide/hydroxide species may occur. However, the goal in the use of these precursors for film formation is to control the hydrolysis and subsequent condensation reaction [Schwartz et al., 2004].

Transition metal alkoxides are usually highly reactive toward hydrolysis and have to be handled under anhydrous conditions. These alkoxides differ:

- The reactive transition metal alkoxides have to be stabilized in order to avoid uncontrolled precipitation during the deposition process.
- Transition metals often exhibit several stable coordination states, and when coordinately unsaturated, they are able to expand their coordination by different nucleophilic association mechanisms.
- The lower electronegativity of transition metals causes them to be more electrophilic and thus less stable toward hydrolysis, condensation and other nucleophilic reactions [Su et al., 2004].

The effect of precursor on the dispersion and photocatalytic performance of TiO_2 supported on silica has been investigated. The catalysts were prepared by a simple impregnation method with three kinds of titanium complexes of different ligands: (dipyvaroylmetanato) (DPM), acetylacetonato (acac), isopropoxide (O-iPr) [Tanaka et al., 2002].

2.5.2. Mixed Ligand Precursors

Mixed-ligand precursors are also frequently employed in chemical solution deposition (CSD) processing. For example titanium (IV) isopropoxide ($Ti(O^iPr)_4$) and tin tetrachloride pentahydrate ($SnCl_4.5H_2O$), which are very reactive to be directly employed in most CSD routes, may be converted into a more suitable precursor by a reaction with either two equivalents of acetic acid or acetylacetone or just by a hydrolization reaction.

1. Mechanism of the titanium (IV) isopropoxide reactions that takes place during TiO_2 sol-gel processing are as follows [Sonawane et al., 2002]:

$$Ti(OR)_4 + 4\ H_2O \rightarrow Ti(OH)_4 + 4ROH \uparrow$$
$$Ti(OH)_4 \rightarrow TiO_2 + 2H_2O \uparrow$$

2. Mechanism of the tin (IV) chloride pentahydrate reactions that takes place during SnO_2 sol-gel processing are as follows:

$$Sn(OR)_4 + 4H_2O \rightarrow Sn(OH)_4 + 4ROH \uparrow$$
$$Sn(OH)_4 \rightarrow SnO_2 + 2H_2O \uparrow$$

2.6. Solution Processes and Chemical Routes

The coating solution is prepared by mixing, and possibly reacting, the individual precursors or precursor solutions. The chemical interactions that occur between the starting reagents during solution synthesis will depend on the reactivity of the compounds and the solution preparation conditions.

Depending on the procedures utilized during coating solution preparation, the gelation behavior of the deposited film, and the reaction that take place

during thermal annealing, the various chemical routes utilized for oxide film fabrication can be grouped into three principal categories:

- Classical sol-gel processes that use alkoxide solution precursor that undergo primarily hydrolysis and polycondensation;
- Metal organic decomposition (MOD) routes that utilize carboxylate precursors that do not undergo significant condensation reactions during either solution preparation or film deposition;
- Hybrid routes that exhibit condensation reactions at several process stages; frequently, this route is used when multicomponent oxide films are prepared from multiple precursor types [Djaoued et al., 2001].

2.7. Production Techniques for Thin Films

The most common film fabrications are reactive sputtering, chemical vapor deposition (CVD), metal organic vapor deposition (MOCVD) and sol- gel processing (chemical solution deposition). Among the methods of thin film production, reactive sputtering process exhibits very poor step coverage and shadow effects [Sunada et al., 1998].

Various source precursors have been investigated for use in the MOCVD and PECVD (plasma-assisted chemical vapor deposition) processes. These precursors include organic sources such as titanium isopropoxide [$Ti(OC_3H_7)_4$] and titanium ethoxide [$Ti(OC_2H_5)_4$], and inorganic sources such as titanium tetrachloride ($TiCl_4$). However many of the thermal MOCVD approaches required high deposition temperatures, thus limiting their potential applicability in electronic devices and computer chip technology. Alternatively, the realization of low temperature deposition has required the use of plasma process, such as PECVD to provide a portion of the thermal budget required to decompose these source precursors. Unfortunately the application of plasma resulted in the incorporation of carbon as major impurity when organic source precursors of the type [$Ti(OC_3H_7)_4$] were employed. Also chlorine was reported as the primary contaminant in the case of thermal CVD from ($TiCl_4$). Comparison between the

most common processing methods, sol-gel processing due to its many advantages over the other processing methods is the most widely used method [Ting and Chen, 2000].

The chemical solution deposition technique as a highly flexible method for the fabrication of electronic oxide thin films is reviewed. Various chemical aspects of different approaches are discussed, including sol-gel, hybrid, and metallo-organic decomposition routes, which all have been successfully applied for the deposition of this class of materials [Schwartz et al., 2004].

2.7.1. Sol-gel Processes

Sol-gel method is one of the most important techniques for the formation of various functional coatings. This is because of large number of advantages and sol-gel allows synthesis of thin films to have desired properties. Sol-gel technology is a method of fabrication of high quality ceramics and glasses [Kaya, MS Thesis, 2002]. Sol-gel, also known as wet chemical processing, is to form a solution of the elements of the desired compounds in an organic solvent, polymerize the solution to form a gel, and dry and fire the gel to displace organic compounds and form a final inorganic oxide film.

Sol-gel process is quite general and can be applied to a wide range of precursors. This process generally involves the use of inorganic salts or metal alkoxides as precursors. Metal alkoxides are not miscible with water and have to be dissolved in a co-solvent, currently the parent alcohol, prior to hydrolysis [Buscema et al, 2002].

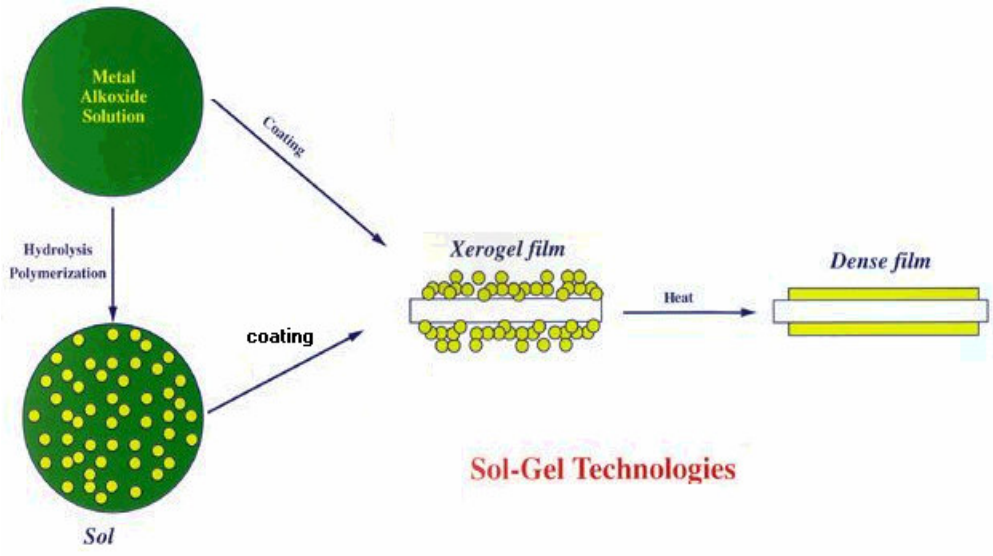

Figure 2.4 Sol-gel Process [URL 2]

In this processing system the key reactions leading to the transformation of the precursor species into an oxide network are hydrolysis and condensation, in which metal-oxygen-metal (M-O-M) bonds are formed which constitutes the backbone of any oxide ceramic structure [Kominami et al., 2001]:

- Hydrolysis

$M(OR)_x + H_2O \rightarrow M(OR)_{x-1}(OH) + ROH$
Where M: Si, Ti, Zr, H, Ta, Nb, and Al
And R: CH_3, C_2H_5, C_3H_7, etc.

- Condensation (alcohol elimination)

$2\ M(OR)_{x-1}(OH) \rightarrow M_2O(OR)_{2x-3}(OH) + ROH$

- Condensation (water elimination)

$2\ M(OR)_{x-1}(OH) \rightarrow M_2O(OR)_{2x-2}(OH) + H_2O$

The sol-gel method of preparing thin films on the substrates has many advantages over other methods such as chemical vapor deposition (CVD), plasma spraying, anodization, and thermal oxidation of the metal as given in Table 2.1. However the method also has some disadvantages as shown in Table 2.2.

Table 2.1 Advantages of the sol-gel method

1. Use of very simple equipment with neither vacuum nor temperature
2. Lower temperature preparation
    - ✓ Save energy
    - ✓ Minimize evaporation losses
    - ✓ No reaction with containers, thus purity
3. New crystalline phase from nanocrystalline solids
4. High homogeneity of the final film
5. Possibility of using great variety of substrates and sizes
6. Controlling the parameters of the process

Table 2.2 Disadvantages of the sol-gel method

1. Large shrinkage during processing
2. Residual hydroxyl
3. Residual carbon
4. Long processing time
5. Health hazardous of organic solutions
6. Continuous hydrolysis and polycondensation reactions; aging period

Thin forbidden zone CdS compounded TiO_2 films were prepared by sol-gel method using spinning technology on the glass surface. Additional TiO_2 layer was coated on the CdS compounded TiO_2 film to inhibit the solubilization of cadmium. Some pore-producing agents, such as trifluoroacetic and polyethylene glycol, had been doped in these additional layers. The degradation efficiency under visible light of compounded films for methyl orange was investigated by atomic absorption spectrophotometer [Chengyu et al., 2003].

Transparent anatase TiO_2 nanometer films were prepared on soda-lime glass and fused quartz via by sol-gel method. The as-prepared TiO_2 films were then treated by dipping them in H_2SO_4 solution. The photocatalytic activity of the samples was evaluated by photocatalytic oxidation of acetone in air [Yu et al., 2002].

TiO_2 sol developed for photocatalytic use, indicating that the excellent photocatalytic activity of original hydrothermal crystallization in organic media-TiO_2 particles was preserved after immobilization on glass substrates by the presented method [Sawunyama et al., 1998].

TiO_2 films on self-assembled monolayers by sol-gel method were deposited on three different kinds of substrates. It was found that octadecyltrichlorosilane self-assembled monolayer induces precipitation of anatase phase at a rather low temperature and accelerates anatase-to-rutile phase transformation [Lin et al., 1998].

2.8. Film Formation

After forming the solution, the next step is the film formation. There are many aspects to the processing of films that are common to all of the deposition techniques. The conditions necessary for the film formation can be outlined as: the solution must wet the substrate, it must remain stable with aging, it should have some tendency toward crystallization into a stable high temperature phase, and for multiple layers the previous layers must be either insoluble or heat treated to make them insoluble before subsequent deposition.

For a solution to wet a substrate the contact angle θ between the surface of a drop of solution and the substrate must be less than 90^{o}. The conditions for this to occur are described by Young's equation [Yusuf et al., 2001]:

$$\gamma_{LV} \times \cos\theta = \gamma_{SV} - \gamma_{SL}$$

Where γ is the surface tension for the liquid-vapor and solid-liquid interfaces, respectively.

For wetting, the easiest variable to control is the surface tension of the solution. In this point of view, alcohol solutions used with metal alkoxides wet best since they have low surface tension.

2.9. Contact Angle

The wetting of a solid with water, where air is the surrounding medium, is dependent on the relation between the interfacial tensions (water/air, water/solid, and solid/air). The ratio between these tensions determines the contact angle θ between a water droplet and the given surface. A contact angle of 0^{o} means complete wetting, and a contact angle of 180^{o} corresponds to complete non-wetting.

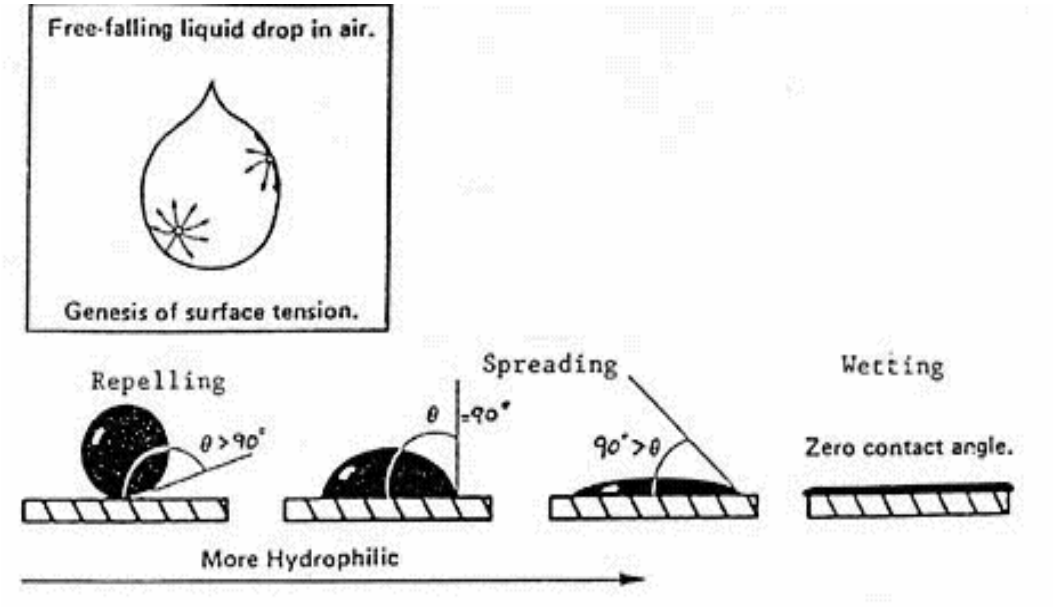

Figure 2.5 Contact angle and hydrophilicity relation [URL 3]

Hydrophilic surfaces with low wettability and contact angles of about 100° are known for a long time. The higher this angle the lower is the value of the adhesion work. Decreasing the contact angle leads to enlarged values of the adhesion work that is hydrophilic surfaces [Kaya, 2003].

Generally detergents reduce the surface tension of water and hence lower the contact angles. Another possibility to cause low contact angles without detergents is the use of active thin films on the material surface. For the preparation of these thin layers mainly photocatalytic active metal oxides or sulfides have been applied. If TiO_2 of the anatase type is exposed to UV light, very low contact angles are obtained (<1°). These materials have the unique property of "attracting" rather than repelling water (super-hydrophilicity). The water lies flat on the surface in sheets instead of forming droplets. If the

illumination is stopped, the super-hydrophilic behavior of TiO_2 surface retained its property for some certain time.

The dependence of critical film thickness, h_{crit}, on the macroscopic contact angle is discussed using measurements of the critical rupture thickness of wetting films on methylated glass surfaces. The rupture thickness increases with increasing contact angles on rather hydrophilic substrates but becomes, however, independent of contact angle on moderately hydrophobic surfaces once contact angle exceeds 45^{o}. Mahnke et al. (1999) suggested that a qualitative estimation of the interaction forces reveal that hydrophobic interaction forces are the primary cause of the film rupture.

2.10. Hydrophilicity

Also termed hydrophilic, is a characteristic of materials exhibiting an affinity for water. Hydrophilic literally means "water-loving" and such materials readily adsorb water. The surface chemistry allows these to be wetted forming a water film or coating on their surface. Hydrophilic materials also possess a high surface tension value and have the ability to form "hydrogen-bonds" with water.

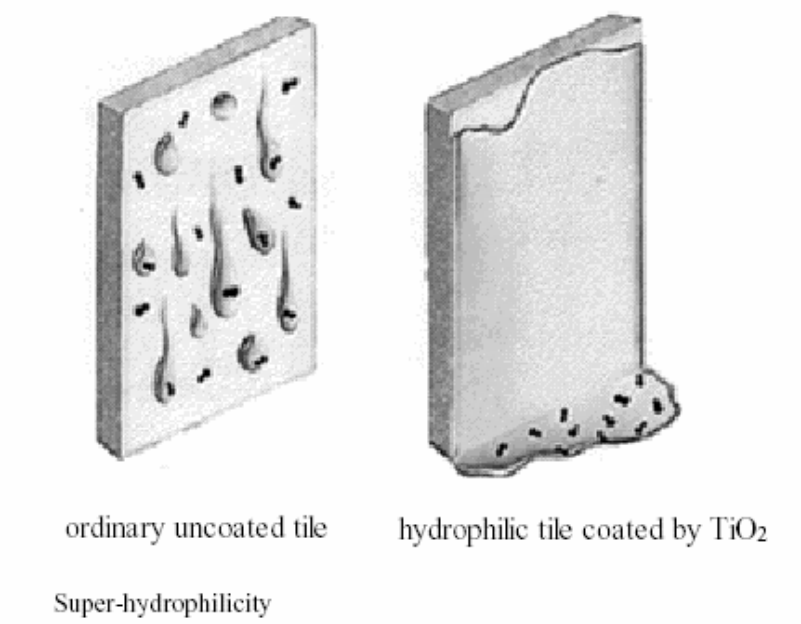

Figure 2.6 Hydrophilic property of coated tile (Benedix et al., 2000)

Photoinduced hydrophilic conversion was evaluated on the different crystal faces of rutile single crystal and also polycrystalline anatase TiO_2 to clarify the dependence of the crystal structure on the photoinduced hydrophilic conversion [Watanabe et al., 1999].

2.11. Hydrophobicity

Also termed hydrophobic, materials possessing this characteristic have the opposite response to water interaction compared to hydrophilic materials. Hydrophobic materials ("water hating") have little or no tendency to adsorb water and water tends to "bead" on their surfaces (i.e., discrete droplets). Hydrophobic materials possess low surface tension values and lack active groups in their surface chemistry for formation of "hydrogen-bonds" with water.

Hydrophobic surfaces with low wettability and contact angles of about 100^{o} are known for a long time. The higher this angle the lower is the value of the adhesion work. Decreasing the contact angle leads to enlarged values of the adhesion work (hydrophilic surfaces). Very interesting possibility to cause low contact angles without detergents is the use of active thin films on the material surfaces [Benedix et al., 2000].

The influence of roughness on the wetting properties of ion-plated poly(tetrafluroethylene) (PTFE) coatings has been investigated using atomic force microscopy. PTFE coatings with different surface roughness have been obtained by applying different substrate bias DC voltages during ion plating. It was found that the majority of surface asperities for rough coatings prepared in this study have dimensions of a few nanometers, 6-13nm. For such coatings, high water contact angles, $150\text{-}160^{o}$, were observed. These measurements provide additional proof on the effect of nanometer-size surface asperities on the wetting characteristics of hydrophobic coatings [Veeramasuneni et al., 1997].

It is stated that by means of an ion assisted deposition method, a TiO_2 photocatalyst was prepared at relatively lower temperature on porous Teflon sheets, are good candidates for the coating materials with super-hydrophobic surfaces. UV light irradiation of TiO_2 photocatalyst led to the photocatalytic degradation of organic pollutants (self-cleaning) that wear off the water-repellent property of the surface [Yamashita et al., 2003].

2.12. Coating Process for Deposition Sol-gel Films

Although there are many factors controlled by the network structure in the solution, the deposition parameters are also important for the final properties of the film.

There are two common techniques for the deposition from solution: dip and spin coating techniques.

2.12.1. Dip Coating

Dip coating is the most common and the easiest way to deposit sol-gel film on a substrate (Figure 2.7). The substrates could be flat panels, cylinders, or in complex geometry. This process may be utilized to coat areas in the order of square meters, and can also operate in either continuous or batch modes. Batch dip coating process is divided into five stages: immersion, start up, deposition, drainage and evaporation. For a coating sol containing volatile solvent, evaporation accompanies the start up, drainage and deposition stages to form a gel film in a relatively short time. The thickness of the film produced with this process is determined by a complex competition between six forces during the film deposition stage: (1) viscous drag upward on the liquid by the moving substrate, (2) force of gravity, (3) resultant force of surface tension in the concavely curved meniscus, (4) inertial force of the boundary liquid layer arriving at the deposition region, (5) surface tension gradient, and (6) the disjoining or conjoining pressure (important for films less than 1 μm thick).

If the substrate speed and liquid viscosities are not high, as is often the case in sol-gel coating process, the thickness may be expressed according to the following relationship [Popielarski, 1998].

$$h = [0{,}94x(\eta x U)^{2/3}]/[\gamma_{LV}^{1/6} \times (\rho g)^{1/2}]$$

Where η, U, ρ, γ_{LV} are sol viscosity, substrate withdrawal speed, density of sol, and liquid-vapor surface tension, respectively. This equation assumes Newtonian fluid behavior and ignores evaporation.

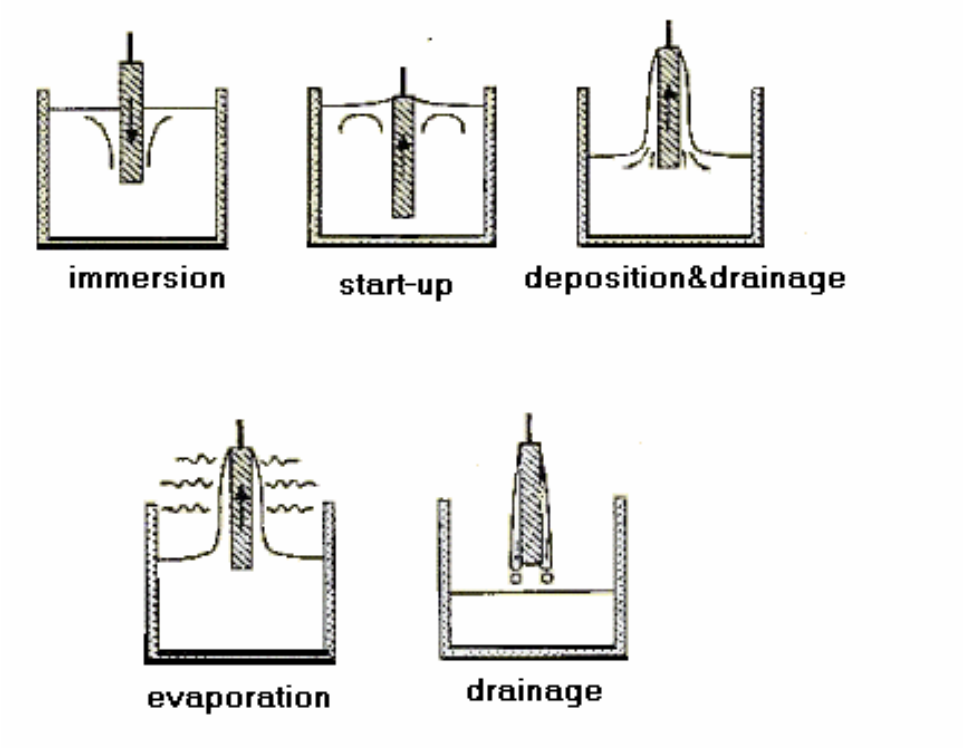

Figure 2.7 The dip-coating technique [URL 4]

2.12.2. Spin Coating

Stage One: The first stage is the deposition of the coating fluid onto the wafer or substrate.

It can be done using a nozzle that pours the coating solution out or it could be sprayed onto the surface, etc. Usually this dispense stage provides a substantial excess of coating solution compared to the amount that will ultimately be required in the final coating thickness. For many solutions it is often beneficial to dispense through a sub micron sized filter to eliminate particles that could lead to flaws. Another potentially important issue is whether the solution wets the

surface completely during this dispensing stage. If not, then incomplete coverage can result.

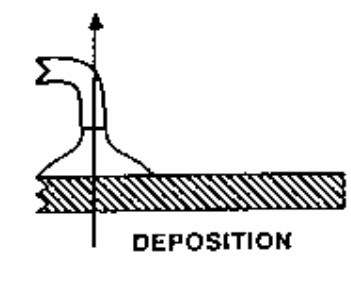

Figure 2.8 Stage one in spin-coating technique, [URL 5]

Stage Two: The second stage is when the substrate is accelerated up to its final, desired, rotation speed.

This stage is usually characterized by aggressive fluid expulsion from the wafer surface by the rotational motion. Because of the initial depth of fluid on the wafer surface, spiral vortices may briefly be present during this stage; these would form as a result of the twisting motion caused by the inertia that the top of the fluid layer exerts while the wafer below rotates faster and faster. Eventually, the fluid is thin enough to be completely co-rotating with the wafer and any evidence of fluid thickness differences is gone. Ultimately, the wafer reaches its desired speed and the fluid is thin enough that the viscous shear drag exactly balances the rotational accelerations.

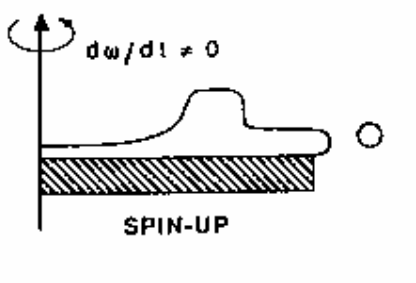

Figure 2.9 Stage two in spin-coating technique, [URL 5]

Stage Three: The third stage is when the substrate is spinning at a constant rate and fluid viscous forces dominate fluid thinning behavior.

This stage is characterized by gradual fluid thinning. Fluid thinning is generally quite uniform, though with solutions containing volatile solvents; it is often possible to see interference colors "spinning off", and doing so progressively more slowly as the coating thickness is reduced. Edge effects are often seen because the fluid flows uniformly outward, but must form droplets at the edge to be flung off. Thus, depending on the surface tension, viscosity, rotation rate, etc., there may be a small bead of coating thickness difference around the rim of the final wafer. Mathematical treatments of the flow behavior show that if the liquid exhibits Newtonian viscosity (i.e. is linear) and if the fluid thickness is initially uniform across the wafer, then the fluid thickness profile at any following time will also be uniform; leading to a uniform final coating (under ideal circumstances).

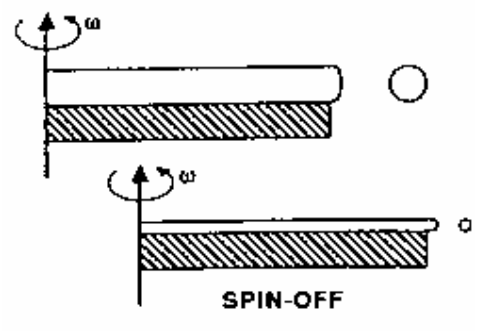

Figure 2.10 Stage three in spin-coating technique, [URL 5]

Stage Four: The fourth stage is when the substrate is spinning at a constant rate and solvent evaporation dominates the coating-thinning behavior.

As the prior stage advances, the fluid thickness reaches a point where the viscosity effects yield only rather minor net fluid flow. At this point, the evaporation of any volatile solvent species will become the dominant process occurring in the coating. In fact, at this point the coating effectively "gels" because as these solvents are removed the viscosity of the remaining solution will likely rise, effectively freezing the coating in place (where he quantified the coating thickness dependence on spin speed and viscosity and its relationship to the evaporation rate) [Meyerhofer, 1978].

After spinning is stopped many applications require that heat treatment or "firing" of the coating be performed (as for "spin-on-glass" or sol-gel coatings). On the other hand, photoresists usually undergo other processes, depending on the desired application/use.

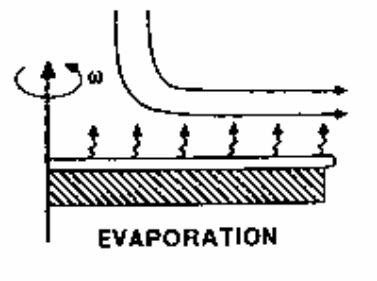

Figure 2.11 Stage four in spin-coating technique, [URL 5]

2.13. Thermal Treatment

The final stages of the processing of a ceramic from the sol-gel solution are drying and heating of deposited material to form the ceramic phase. At that stage transformation reactions and the interaction of amorphous film with the substrate takes place.

2.13.1 Drying

Once the solution applies to the substrate, a sol-gel system is by no means stagnant. The oxide and solvent phases are intimately mixed, and the high solid/liquid surface area drives the network to shrink, a process known as syneresis. Condensation reactions take place, resulting in further shrinkage.

During drying stage, evaporation of alcohol, combustion and carbonization of the organic compounds will take place. After this stage, film is in amorphous stage and crack formation appears at that stage.

Cracks are generally caused by the large internal stresses that are resulting from the thermal mismatch of the substrate and the film. If the thermal expansion coefficients of the film on the substrate are close into each other, then there will be no considerable amount of these stresses. Another factor was the adhesion of the film to the substrate. If the film adheres to the substrate strongly, all of the internal stresses will be relaxed partially during the heat treatment and this will yield a film having minimum amount of cracks [Colgan et al., 2004]

2.13.2 Annealing

Aim of the firing is to convert the dried film to densified ceramic oxide. The heat treatment schedule affects crystal structure, grain size, amount of crystallization, and film cracking. This process includes the removal of residual –OH or –OR groups by polycondensation reactions, pyrolysis of organic compounds or groups left in the film into carbon, oxidation of carbon and gradual densification of the film.

TiO_2 powder was immobilized on solid support substrates using electrophoretic coating and spray coating. Electrochemical anodization of titanium metal was also carried out to give a thin film of TiO_2 on the surface. The coated substrates were annealed in air at elevated temperatures to improve the adhesion of the catalyst to the supporting substrates. The photocatalytic efficiency of the TiO_2 coatings was compared using the degradation of phenol in aqueous solution as a standard test system. In the case of the powder-derived films, the photocatalytic efficiency was found not to be markedly dependent upon either the substrate used or the annealing temperature employed in the coating process [Byrne et al., 1998].

2.14. Photocatalytic Process Mechanism

Photocatalytic process over a semiconductor is initiated by the absorption of a photon. An electron is promoted from valence band to conduction band. When the electron is transferred to the empty conduction band electron/hole pairs are formed:

$TiO_2\text{-}hv \rightarrow TiO_2\,(h^+ + e^-)$

Holes reacted with H_2O molecules or –OH ions to give •OH radicals:

$h^+ + H_2O \rightarrow \bullet OH + H^+$

$h^+ + 2OH \rightarrow \bullet OH + OH^-$

Photogenerated electrons then react with molecular oxygen (O_2) to produce superoxide radical anions ($\bullet O_2$):

$e\text{-} + O_2 \rightarrow \bullet O_2$

These two types of rather reactive radicals then work together to decompose organic compounds:

$TOC + \bullet O_2 + \bullet OH \rightarrow TOC\ (\text{partially oxidized species}) + CO_2 + H_2O$

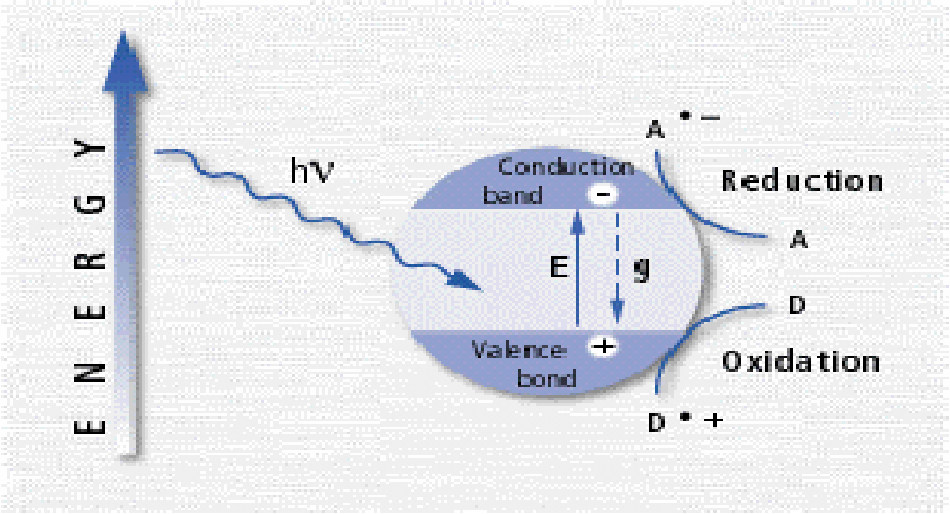

Figure 2.12 Photocatalytic process on the surface of the semiconductor, (Benedix et al., 2000)

For hydrophilicity, electrons and holes are still produced. The electrons tend to reduce Ti (IV) to Ti (III) and the holes oxidize the O^{2-} anions. Holes oxidize the O_2^- anions. In the process O_2 atoms are ejected, creating O_2 vacancies. Water molecules can then occupy these oxygen vacancies. Adsorbed OH^- groups that tend to make the surface hydrophilic are produced.

2.15. Increasing the Photocatalytic Activity

Electrons in the n-type half of the diode are repelled away from the junction by the (-) ions in the p-type region, and holes in the p-type half are repelled by the (+) ions in the n-type region. A space on either side of the junction is left without either kind of current carriers. This is known as the depletion layer, that is, depletion layer is an insulating region within a conductive, doped semiconductor material where the charge carriers have been swept away. Since there are no current carriers in this layer no current can flow. The depletion layer is, in effect, an insulator.

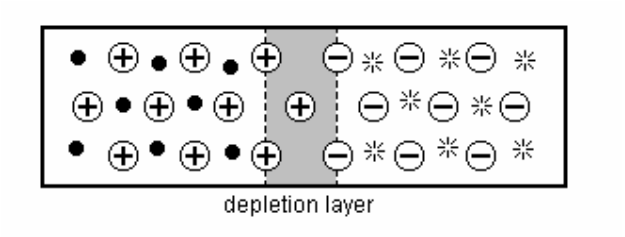

Figure 2.13 Depletion layer of a semiconductor [URL 1]

As mentioned before the photocatalytic activity of semiconductors is due to the production of excited electrons in the conduction band of the semiconductors, along with corresponding (+) holes in the valence band by the absorption of UV illumination. These energetically excited species are mobile and capable of initiating many chemical reactions, usually by the production of radical species at the semiconductor surface. They are unstable, however, and recombination of the photogenerated electrons and holes can occur very quickly, dissipating the input energy as heat. In fact, the photocatalytic efficiency depends on the competition between these two processes, that is, the ratio of the surface charge carrier transfer rate to the electron-hole recombination rate. If recombination occurs to fast, then there is not enough time for any other chemical reactions to occur. In titania, the species are relatively long-lived, allowing the electron or hole to travel to the crystallite surface. To reduce recombination of photogenerated electrons and holes, and to extend its light absorption into the visible region, various transition metal cations have been doped into the semiconductors. Photocatalytic activity is strongly related with the conductivity of the semiconductor surface. The electron mobility on the surface is inhibited by the pores and necks of the crystal structure of the semiconductor surface. By adding dopants, the cavities are filled and the electron mobility increases, hence the conduction on the surface increases, resulting in increase in photocatalytic activity of the semiconductor [Shah et al., 2002].

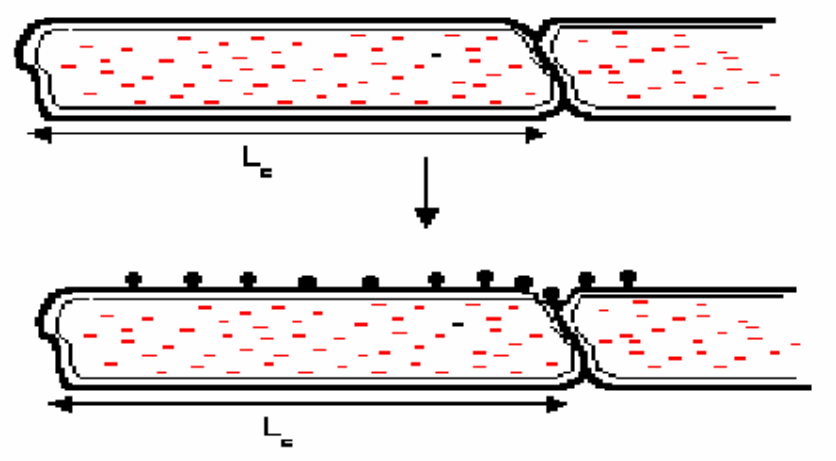

Figure 2.14 Conduction through particles

2.15.1. Microscopic Conduction in Solids

$$\sigma = n_e \cdot e \cdot \mu_e + n_h \cdot e \cdot \mu_h$$

σ: Conductivity $W^{-1}\ m^{-1}$
η: Carrier density (concentration) of electrons (e) and holes (h), (electrons/m^3)
μ: Mobility of electrons (e) and holes (h), (m^2/V-s)
e: electron charge ($1.6x10^{19}$ C)

As a summary, doping increases the mobility of electrons and charge carrier density on the surface resulting in the increase of the conduction of the semiconductor.

2.16. Photocatalytic Effect on Microbial Activity

The reactive oxygen species generated by photocatalytic reactions cause various damages to living organisms. This is not surprising since they consist of abundant organic compounds. For the first time the microbial effect of TiO_2 photocatalytic reactions was reported [Matsunaga et al., 1985]. In this study a

decrease in intracellular coenzyme A (CoA) in the TiO_2 powder-treated cells was detected for various microorganisms. The direct oxidation of CoA that inhibited cell respiration and subsequently caused cell death was proposed as the first killing mode. However, the involvement of cell wall and cytoplasmic membrane in cell death was not taken into account until reported their transmission electron microscopy findings were reported [Saito et al., 1992]. Also it was reported that there was no significant difference between the time required for killing of Gr (+) or Gr (-) bacteria, even though the former has a thicker cell wall [Sjogren and Sierka, 1994]. Different kinds of DNA damages and oxidation of proteins and enzymes were detected [Bornside et al., 1987]. TiO_2 photocatalytic killing studies have revealed that the sensitivity of various biological systems to TiO_2 photocatalysis is likely in the following order: virus > bacterial cells > bacterial spores [Huang et al., 2000]. This suggests that different microorganisms respond differently to TiO_2 photocatalyst due to their structural differences, particularly in the complexity and thickness of the cell envelope. They showed that the cell wall of *Streptococcus sobrinus* was partially broken after cells had undergone TiO_2 photocatalytic treatment for 60 minutes and they recorded cell disruption after 120 minutes [Saito et al., 1992]. They demonstrated that TiO_2 photocatalytic reaction induced the rapid leakage of potassium ions and the 'slow' leakage of RNA and proteins. A second killing mode was therefore proposed. Therefore, the cell envelope may be a significant target for TiO_2 photocatalytic damage in both procaryotic and eucaryotic cells. The intracellular macromolecules, such as nucleic acids, may also be a potential target. Furthermore the TiO_2 photocatalytic inactivation of *E. coli* endotoxin, which is an integral constituent of the outer membrane of Gr (-) bacteria were demonstrated [Trapalis et al., 2003]. This finding suggests that the cell wall damage might take place prior to cytoplasmic membrane damage.

The story of photocatalysis, in particularly TiO_2 photocatalysis, began first as powder TiO_2 in water and air purification applications. Then because of required separation steps and continuous stirring during photocatalytic reactions, film coating of TiO_2 applications were highlighted. Nowadays increasing the photocatalytic activity of semiconductors by doping is being investigated. In the literature in general Pt, Sn, Cu, and Na metals were used as dopants.

The preparation of a colored conductive paint electrode containing In_2O_3, SnO_2, or TiO_2 for the electrochemical inactivation of marine bacteria was performed [Lim et al., 2002]. The results of this study might be effective for preventing bacterial cell accumulation and the formation of biofilms on surfaces immersed in aqueous environments.

It is suggested that using targeted light guidance and a light-guiding sheet (out of a UVA-transmittant, Plexiglas, for example) bacterial inactivation over the entire area is possible. In the presence of water and oxygen, highly reactive OH-radicals are generated by TiO_2 and mild ultraviolet A. The effectiveness of this method was demonstrated using bacteria relevant to hygiene such as *E. coli*, *P. aeruginosa, S. aereus, E. faecium* [Kühn et al., 2003].

The role of active oxygen species in the photocatalytic bactericidal effect was investigated using a thin transparent TiO_2 film. The viable number of *E. coli* significantly decreased on the illuminated TiO_2 film, and the bactericidal effect was observed even when *E. coli* was separated from the TiO_2 surface [Kikuchi et al., 1997]

The photocatalytic inactivation of Gr-(-) *E. coli* and Gr (+) *Lactobacillus helveticus* by both TiO_2 and ZnO with 365nm UV light was studied in a batch reactor. Almost all the initial *E. coli* cell (10^8 CFU/ml) was inactivated in 40 minutes in the presence of 2g/l ZnO [Liu and Yang, 2003].

2.17. Main Cell Types and Their Cell Wall Structures

The complexity and density of the cell walls are different for different types of microbial cells. As given in the previous part, photocatalytic efficiencies are directly related with cell wall structure. The types of microbial cells are given in Figure 2.15 [Shuler and Kargi, 1992].

Observations with the electron microscope have revealed two markedly different kinds of cells, procaryotic and eucaryotic. So far as is known today, all

cells belong to one of these groups. It is clear that in classification, there are differences in the morphology, or the physical form and structure, between these organisms.

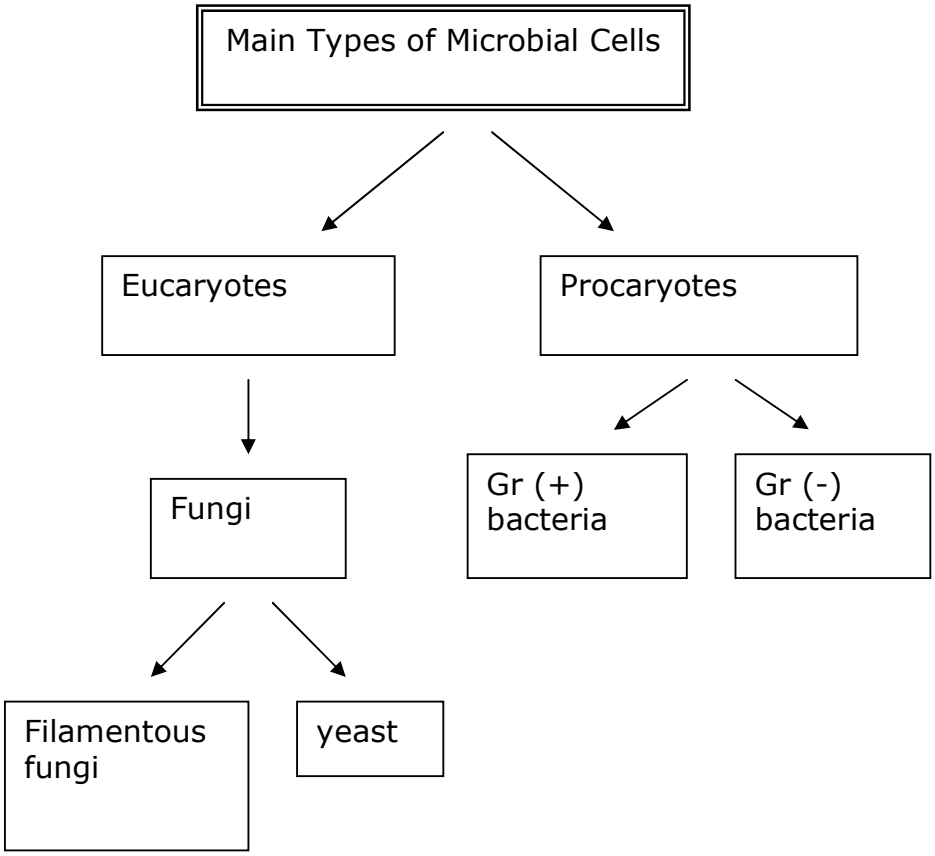

Figure 2.15 Main types of microbial cells

2.17.1. Procaryotic cells

Procaryotic cells, unlike eucaryotic cells, do not contain a membrane-enclosed nucleus and are relatively small and simple cells. Unlike plants and animals, procaryotes are unicellular organisms that do not develop or

differentiate into multicellular forms. Microorganisms of this type grow rapidly and are widespread in the biosphere. Typically, procaryotes are biochemically versatile; i.e., they often can accept a wide variety of nutrients and further are capable of selecting the best nutrient from among several available in their environment. This feature and others to be recounted later make procaryotic cells adaptable to a wide range of environments. Basic features of a procaryotic cell are: the cell is surrounded by a rigid wall. This wall lends structural strength to the cell to preserve its integrity in a wide variety of external surroundings. Immediately inside this wall is *cell membrane*. These membranes play a critical role: they largely determine which chemical species can be transferred between the cell and its environment [Raven and Johnson, 1996].

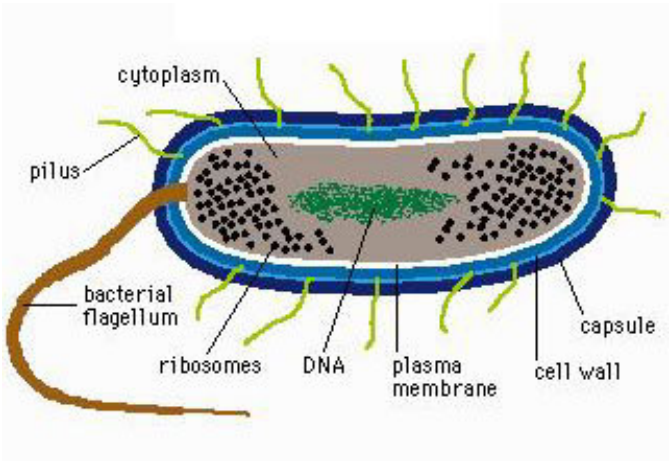

Figure 2.16 Typical procaryotic cell structure [URL 6]

A typical prokaryotic cell structure is given in Figure 2.16. Prokaryotes have a rigid cell wall and this cell wall is an essential structure that protects the cell protoplast from mechanical damage and from osmotic rupture or lysis. Since the membrane is a delicate, plastic structure, it must be restrained by an outside wall made of porous, rigid material that has high tensile strength. Such a material is murein, the abiquitous component of bacterial cell walls.

The cell walls of all bacteria contain a unique type of peptidoglycan called murein. Peptidoglycan is a polymer of disaccharides cross-linked by short chains of aminoacids (peptides), and many types of peptidoglycan exist. All bacterial peptidoglycans contain N-acetylmuramic acid, which is the definitive component of murein [Bailey and Ollis, 1986].

In general, prokaryotes are divided into two main subgroups that are eubacteria and archabacteria as seen in Figure 2.17. Gr (+) and Gr (-) bacteria are subgroups of eubacteria.

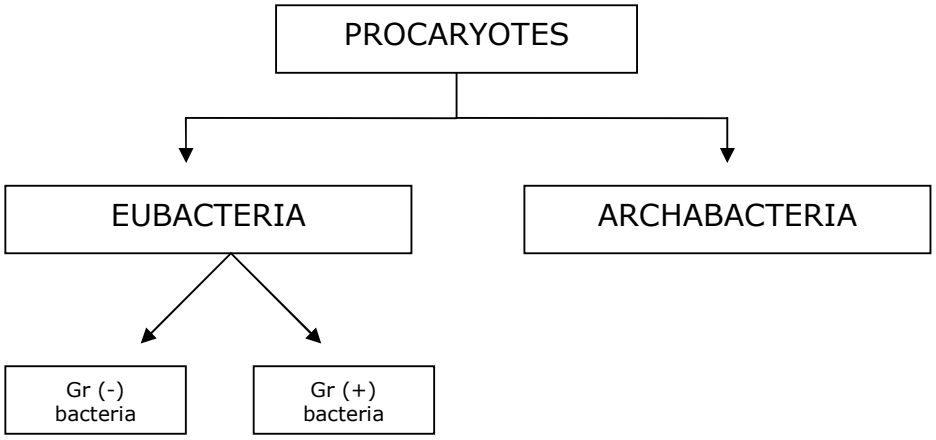

Figure 2.17 Classification of procaryotes

2.17.1.1 Gram-negative Bacteria

It has an outer membrane supported by a thin peptidoglycan layer. Peptidoglycan is a complex polysaccharide with amino acids and forms a structure somewhat analogous to a chain-link fence as mentioned above. A

second membrane (the inner or cytoplasmic membrane) exists and is separated from the outer membrane by the periplasmic space. The cell envelope serves to retain important cellular compounds and to preferentially exclude undesirable compounds in the environment [Laskin and Lechevalier, 1973]. A typical Gr (-) bacterium is *E. coli* and a typical Gr (-) cell wall structure is given in Figure 2.18.

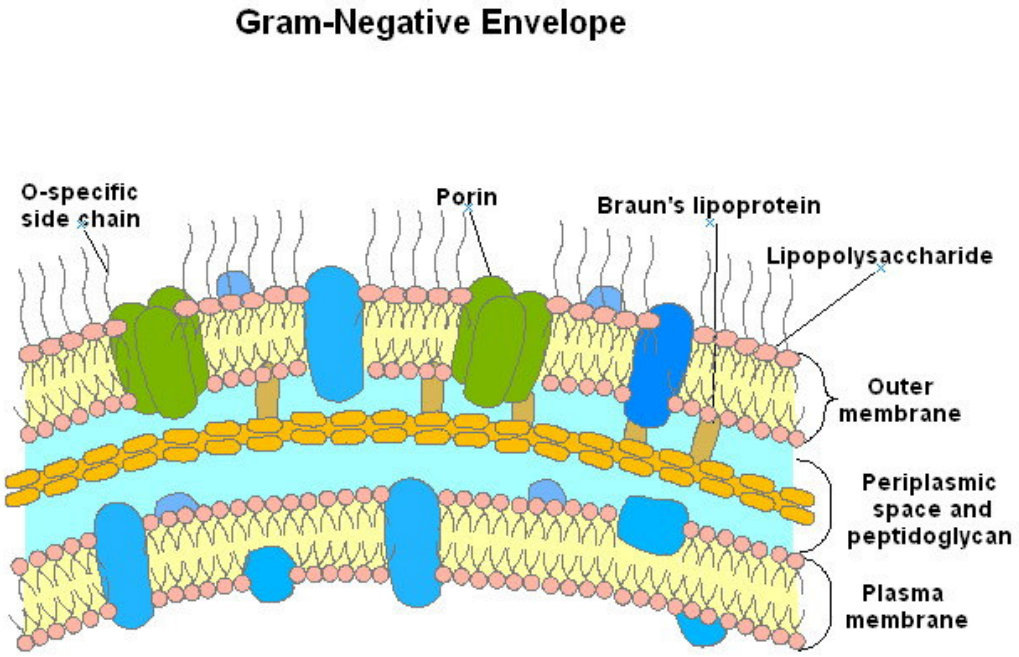

Figure 2.18 Typical gram-negative cell wall structures [URL 7]

2.17.1.2 Gram-positive Bacteria

Typical Gr (+) bacteria are *Bacillus subtilis* and *S. aereus.* Gr (+) bacteria do not have an outer membrane. Rather they have a very thick, rigid cell wall with multiple layers of peptidoglycan. The cell wall structure of a Gr (+) bacterium is shown in Figure 2.19. Because Gr (+) bacteria have only a

cytoplasmic membrane, they are often much better suited to excretion of proteins. In Figure 2.20, the cell wall structures of Gr-(+) and Gr-(-) bacteria were compared [Todar, 2000].

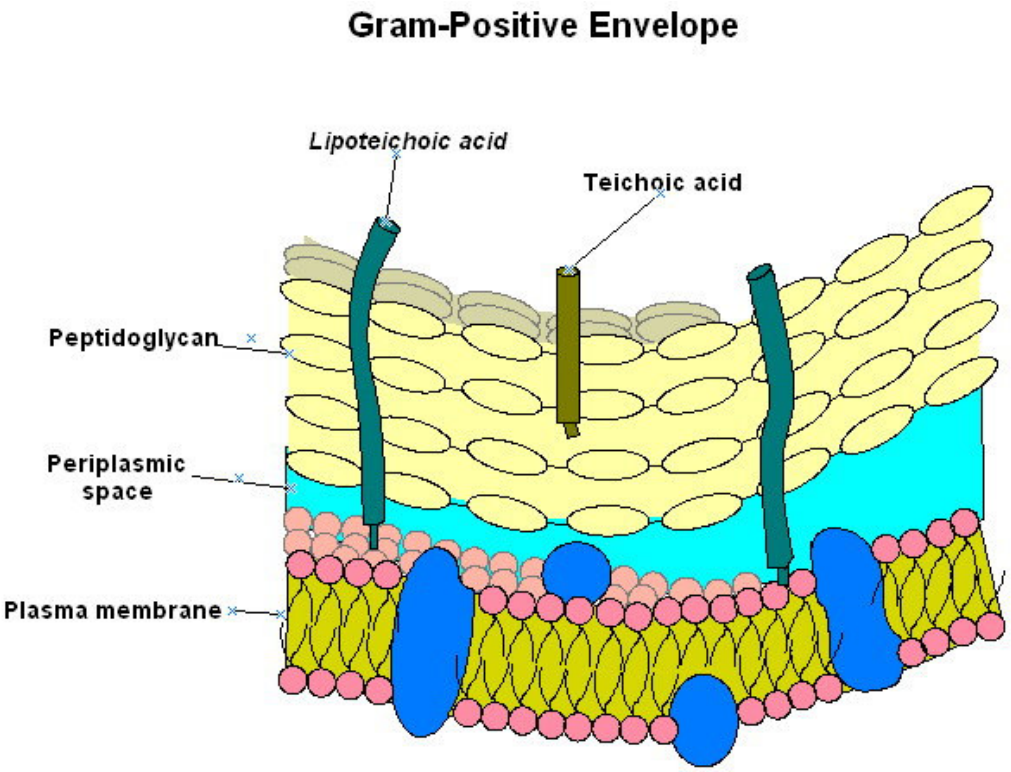

Figure 2.19 Typical gram-positive cell wall structures [URL 7]

As explained above there are simple but important differences between Gr-(+) and Gr-(-) cells. A general comparison of these two cells is given in Figure 2.20.

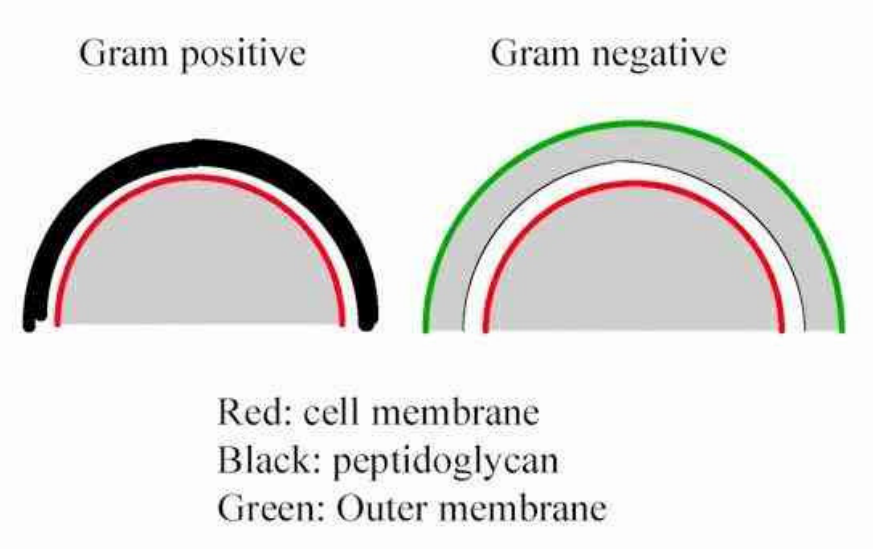

Figure 2.20 Comparison of cell wall complexity of gram-positive and gram-negative bacteria [URL 8]

2.17.2. Eucaryotic cells

Eucaryotic cells, or eucaryotes, make up the other major class of cell types. As a rule these cells are 1000 to 10,000 times larger than procaryotes. All cells of higher organisms belong to this family. The internal structure of eucaryotes is considerably more complex than that of procaryotic cells. The cell is surrounded by a plasma membrane. On the exterior surface of this membrane may be a cell coat or wall. Important to the internal specialization of eucaryotic cells is the presence of unit membranes within the cell. A complex, convoluted membrane system called the *endoplasmic reticulum,* leads from the cell membrane into the cell. The *nucleus* here is surrounded by a porous membrane. *Ribosomes* are embedded in the surface of much of the *endoplasmic reticulum*. Furthermore *mitochondria, chloroplast, golgi complex, lysosomes*, and *vacuoles* are the existing organelles in the cell structure of an eukaryote [Bailey and Ollis, 1986]. Animals, plants and microbial cells are the subgroups of eukaryotes. Yeasts and filamentous fungi are microbial cell group of the eukaryotes.

2.17.2.1. Fungi

Fungi, like bacteria, are widespread in nature although they usually live in the soil and in regions of lower relative humidity than bacteria. They are unable to extract energy from sunlight and usually are free-living.

In Figure 2.21, a typical filamentous fungi cell wall structure is given. The structural building material in many fungi is called chitin. Chitin is a modified form of cellulose in which a nitrogen group has been added to the glucose units. When cross-linked by proteins, it forms a tough, resistant surface material.

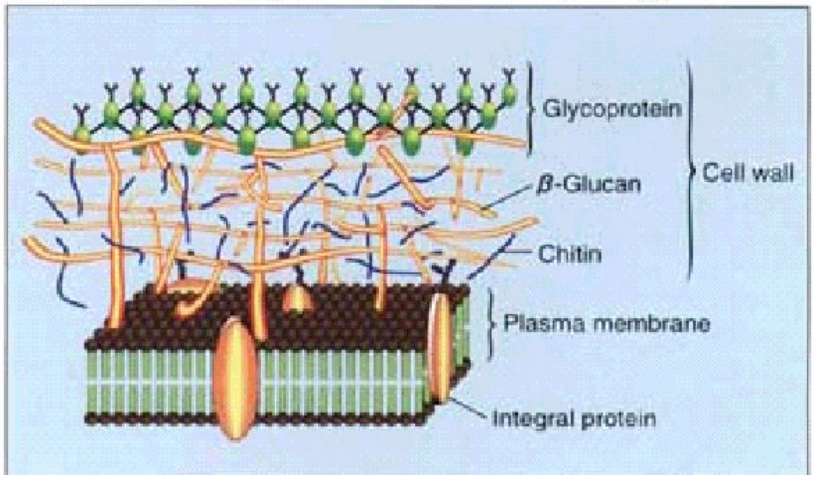

Figure 2.21 Cell Wall structure of a filamentous fungi (mold) cell [URL 9]

As mentioned before most fungi grow as tubular filaments called hyphae. The walls of hyphae are often strengthened with chitin, a polymer of N-acetylglucosamine. The linkage between the sugars is like cellulose and peptidogycan and produces the same sort of structural rigidity.

2.17.2.2. Yeasts and Molds

Yeasts and molds form important subgroups of fungi. Although most fungi have a relatively complex morphology, yeasts are distinguished by their usual existence as single, small cells. The yeast cell envelope is a protecting capsule, consisting of three major constituents (inside out): the plasma membrane, the periplasmic space, and the cell wall. In *S. cerevisiae*, the cell envelope takes 15% of the total cell volume and has a major role in controlling the osmotic and permeability properties of the cell. The plasma membrane is a lipid bilayer with proteins inserted into this layer. The cell wall of yeast is remarkably thick envelope. Major structural constituents of the cell wall are polysaccharides, mainly glucans and mannans, with a minor percentage of chitin. Glucans provide strength to the cell wall. Chitin is a polymer of N-acetylglucosamine representing only 2-4% of the cell wall and mainly located in bud scars [Moses and Cape, 1991]. A typical cell wall structure of yeast, *S. cerevisiae* is given in Figure 2.22.

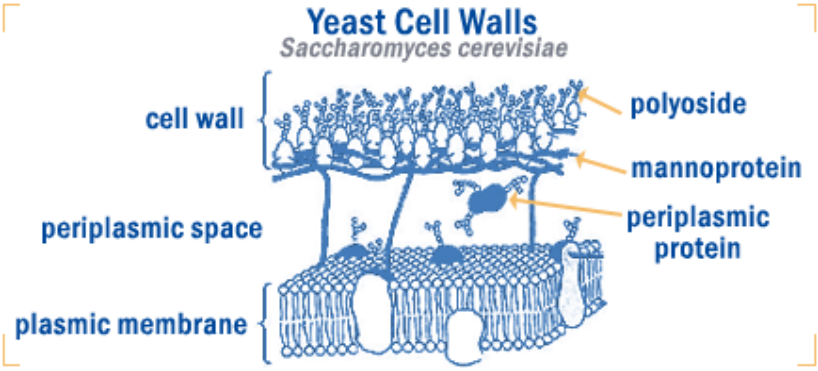

Figure 2.22 Cell Wall structure of a yeast cell [URL 10]

The yeast cell wall is made of 30 - 60 % polysaccharides (beta-glucan and mannan sugar polymers), 15 - 30 % proteins, 5 - 20 % lipids and a small

amount of chitin. Most of the protein is linked to the Mannan-Oligo-Saccharides (MOS) and is referred to as the mannoprotein complex.

Molds are higher fungi with a vegetative structure called a mycelium. Mycelium is a highly branched system of tubes. Dense mycelium structure can cause complexities in their cultivation, since the mycelium can represent a substantial mass-transfer resistance. Industrially the most important classes of molds are Aspergillus and Penicillium.

Molds usually form long, highly branched cells and easily grow on moist, solid nutrient surfaces. Long, thin filaments on the mycelium structure are called hyphae. Certain branches of mycelium may grow in the air, and asexual/sexual spores are formed on these aerial branches. These spores provide resistance against heat, freezing, drying, and some chemical agents.

The onset of asexual reproduction of fungal spores is controlled by many different things. Some are environmental, like nutrient levels, chemical agents, and temperature or pH level. Others can have internal time clocks and sporulate anyway in a preset part of the fungal life cycle. In general, cell walls of spores are generally not fibrillar, but they are multi-layered and often contain melanin and have ornamentations.

CHAPTER 3

EXPERIMENTAL PROCEDURE

3.1. Preparation of Monolayers

3.1.1. Pretreatment of the glasses

The pretreatment step is a critical step for the proper adhesion of the coatings. Quality of the films is directly related with the cleanliness of the substrates. The soda-lime microscope glass plates (75mm x 25mm x 1mm) were cleaned first using surfactants by hand with finger sacks carefully and rinsed with water. Then hydroxylation and etching of the glass plates was performed by treatment with saturated NaOH solution for 5 minutes before use and rinsed with water. As a next step glass plates were ultrasonicated in distilled water for 10 minutes and in a boiling ethanol:chloroform mixture (1:1 by volume) for 10 minutes. Then drying was performed as a final step [Lin et al., 1998].

3.1.2. Preparation of coating solutions

3.1.2.1. Sol-gel Preparation of Titanium dioxide (TiO_2)

Glass samples were fabricated by the sol-gel procedure. Precursor solutions such as alkoxide solutions were used for sol-gel processing (chemical solution deposition) during the synthesis of thin films. There are some requirements that must be satisfied by the precursor solutions:

- high solubility in the selected solvent,
- should decompose without evaporating,
- should be stable for a period of time [Bornside et al., 1987].

In this study chemically extra pure titanium tetraisopropoxide (TTIP, Aldrich), ethanol (C_2H_5OH) and 35% $HCl_{aq.}$ were utilized as starting materials

without further purification. Distilled water was used for hydrolysis. Because of its high solubility, decomposition without evaporating, availability, and stability titanium tetraisopropoxide was used as precursor in this study. Titanium tetraisopropoxide (8.4ml) was dissolved in ethanol (20ml) as the solvent. Then ethanol (130ml), HCl (0.24ml) and distilled water (0.5ml) mixture was prepared separately and added to the above solution by dropwise under continuous stirring at $0^{o}C$ to start hydrolysis. The final solution was kept at the same temperature for 30 min. to finish the hydrolysis, resulting in the TiO_2 sol (Figure 3.1).

Depending on the application, coating solutions need to be stable. It is possible to increase the solution stability by storing in an inert atmosphere, in a dessicator, so that further hydrolysis is minimized.

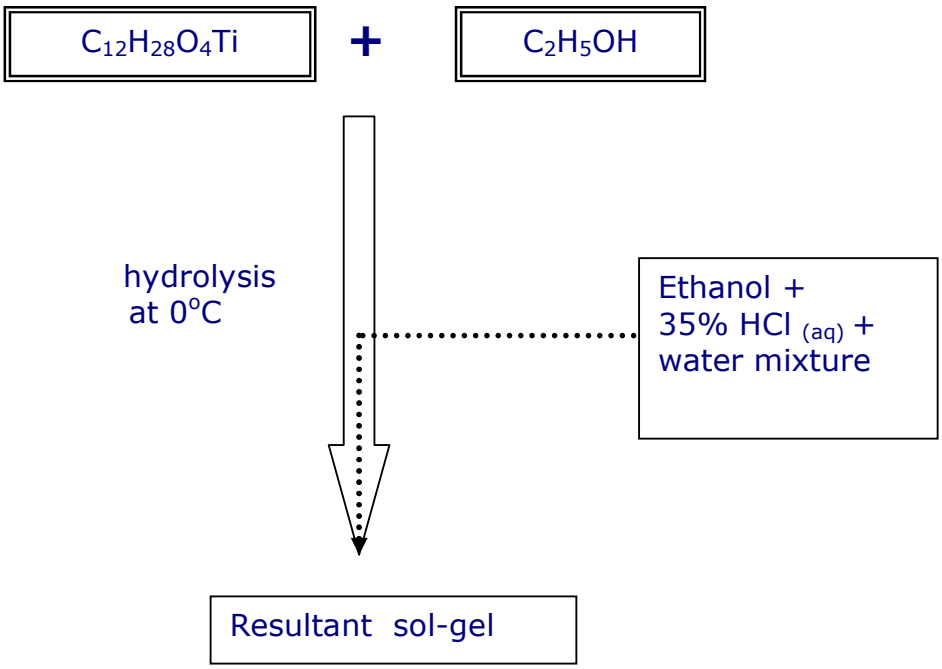

Figure 3.1 Flow diagram for the sol-gel processing of TiO_2 thin films

Color change and the precipitate formation with time are related with the limit of the stability of the coating solution. After some time, due to the continuous hydrolysis reaction solution, viscosity changes together with the change in color [Watanabe et al., 1999].

3.1.2.2. Sol-gel Preparation of Tin dioxide (SnO_2)

For the SnO_2 sol-gel preparation tin tetrachloride pentahydrate (12.37g), obtained from Acros and used as received, as the precursor was dissolved in isopropanol (15g), from Riedel-de Haen, as the solvent. Then water (3.42g) and isopropanol (10g) mixture was prepared separately and added to above solution to start hydrolysis under vigorous stirring. The resultant solution was allowed to stand on magnetic stirrer overnight for aging, resulting in SnO_2 sol (Figure 3.2).

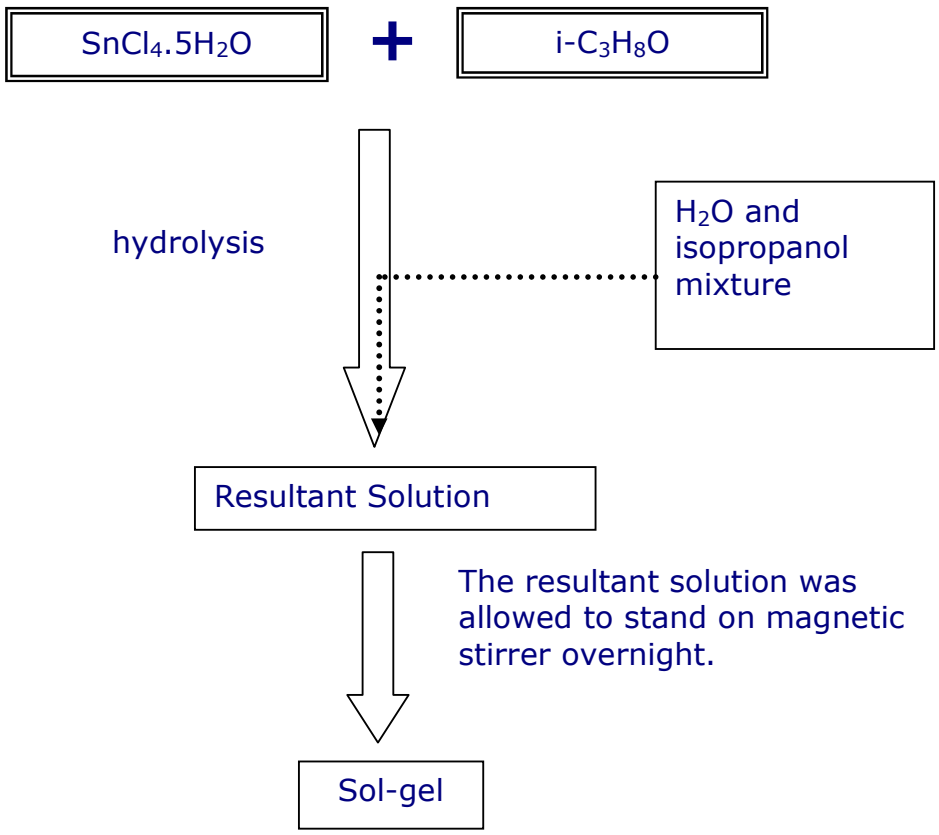

Figure 3.2 Flow diagram for the sol-gel processing of SnO_2 films

3.1.2.3. Palladium doping to the TiO_2 and SnO_2 solutions

1% (wt/wt) Pd promoted TiO_2 and SnO_2 sol-gels were prepared. After TiO_2 and SnO_2 sol-gels were obtained 0.045g and 0.0985g Palladium Acatate (Aldrich) was added respectively before aging.

3.1.3. Coating of the films

Deposition of the films onto the substrates was done by dip coating technique. Dip coating consists of immersion of the substrates into the coating solution. Then withdrawal of the solutions begins, film deposition, solvent evaporation, and contiued drainage takes place as the substrate is completely removed from the liquid bath. As a summary, the substrates were dipped into the coating solution and withdrawn which was repeated 5 times. The gel films thus obtained were dried at 120^{o}C for 20 minutes between following coating steps. Detailed information about the dip-coating was given in chapter 2. Soda-lime glass plates were dipped in titaniumdioxide and palladium doped solution and the steps explained above were performed. For tin dioxide and palladium doped solution coating, soda-lime glass plates, previously coated with silica thin film by directly applying tetraethylorthosilicate (TEOS), then were dipped in tin dioxide and palladium doped solution and were slowly pulled from the solution.

3.1.4. Heat Treatment of the Films

The purpose of the heat treatment step is to change the amorphous structure to crystalline structure. Annealing includes rapid temperature raise by inserting the films into a furnace preheated to the crystallization temperature (stage1) of 650^{o}C then maintaining the constant temperature for a short period of time (stage2), 10 minutes, and then reduction of the temperature to room temperature (stage3). Processing steps were described in details in section 2.13.

(W. C. Heraeus Hanau, KT 500 type) oven was utilized for drying of the as-deposited films and (Heraeus D-6450 Hanau, K 1252 type) oven was utilized in annealing of the amorphous films.

3.2. Analysis of the Films

Analysis of the films was done by using scannig electron microscopy (SEM), by Jeol JSM-6400 SEM. During SEM studies film surfaces were investigated. SEM samples were coated by gold (Au) to prevent discharge using BAL-TEC SCD 050 sputter coater.

Spectroscopic analysis of the films was performed by using a UV-Vis spectrophotometer (Shimadsu, UV-1601) in the wavelength range 290-550 nm.

3.3. Antimicrobial Tests

3.3.1. Microorganisms and growth conditions

E. coli (XL1-blue) was cultured aerobically in Luria-Bertani (LB) broth (Appendix A) at 35^{o}C on a rotary shaker (170rpm) overnight. *E. coli* was maintained on LB agar (Appendix A). The plates were incubated at 35^{o}C overnight and then stored at 4^{o}C until use.

Identification of *S. aereus* was performed on the Baird-Parker agar (Difco) (Appendix A) containing egg yolk-telluride emulsion (EYT enrichment) at 35^{o}C for 24 hours. *S. aereus* cells appeared in black colored colonies with a white shiny hollow around on the Baird-Parker agar after incubation period [Speck, 1989]. From a single colony streak plating was performed and stock cultures were prepared. Then, pure S. *aereus* was cultivated aerobically in LB broth at 35^{o}C on a rotary shaker (170rpm) for 24 h.

The cell concentrations were determined before photocatalytic reactions by viable count procedure on agar plates after serial dilutions of the culture in peptone water (0,1%).

S. cerevisiae was cultured aerobically in YPD broth (Appendıx A) at 35^{o}C on a rotary shaker (170rpm) for 24 hours. *S. cerevisiae* was maintained on YPD agar (Appendix A). The plates were incubated at 35^{o}C for 24 hours and then stored at 4^{o}C until use.

A. niger was maintained on the potato-dextrose agar. The plates were incubated at 35°C for 4 days until complete sporulation occured. Spores were transfered and homogenized by vortex in peptone water and directly used as the spore suspension for the inactivation tests.

3.3.2. Illumination

In the system for photocatalytic process, illumination is performed by a solar light simulator lamp, Ultra-Vitalux light (Osram), to eliminate the outdoor sun light intensity changes.

Solar light simulator should be a good representative of natural sunlight, i.e., the spectral distribution should be comparable.

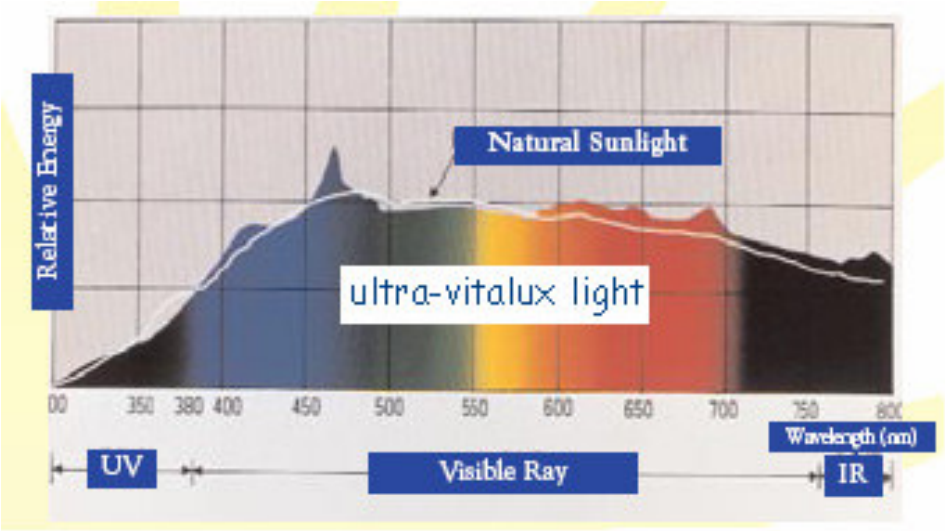

Figure 3.3 Comparison of spectral distribution of solar simulator with the natural light

3.3.3. Irradiation and testing antimicrobial effect

After cell counting, the required bacterial cell count was adjusted by dilution in peptone water. A concentration of about 10^3 cells per ml for *E. Coli*, *S. aereus* and S. *cerevisiea* were prepared by dilution. 200µl of the microbial suspension was pipetted onto the (19 cm^2) coated and uncoated control surfaces and spread out to give a uniform liquid film. Then the samples were illuminated from above with artificial solar light simulator (Osram, ultra-vitalux, 300W). A window glass was placed between the glass samples and lamp as a UVC filter. There was no temperature increase around the samples after 180 minutes irradiation since the lamp was placed three meters above the glass surfaces. During 2-3 h illumination, cell suspensions were removed from the surfaces at various time intervals. Removed suspensions were directly spread onto the LB agar and incubated at 35°C for 16 h to determine the survival of *E. coli and S. aereus* cells; spread onto YPD agar and incubated at 35°C for 24 h to determine the survival of *S. cerevisiae* cells by counting the colony-forming units (CFUs). *A. niger* spores were spread onto Potato-Dextrose agar (Merck) and incubated at 35°C for 29 h to determine the survival of *A. niger* spores by counting the colony-forming units (CFUs). In the case of the slow-growing S. *aereus,* S. *cerevisiae* and A. *niger,* the plates were checked after a further 8 h. Each evaluation was carried out in dublicate.

Controls: The effect of UVA light alone on the microorganisms and *A. niger* spores were determined on uncoated glasses. The stability of the microorganisms and the effect of coating materials alone were measured on coated samples in the dark. In addition, to determine the initial number of microbial cells that applied to surfaces, liquid cell suspension of 200µl was spread onto agar plates and incubated at 35°C. Empty agar plates were also incubated to test the sterilization conditions [Kühn et al., 2003].

CHAPTER 4

RESULTS AND DISCUSSION

4.1. Determination of Optical Absorption Edge Energy of the Films Depending on the Spectra

As mentioned in chapter 2, UV-Vis absorbance and reflectance spectroscopy of semiconductors contain valuable information in the sense of crystallite size, electronic properties of surface, oxidation states of species and metal support interaction. Depending on the crystallite size of the semiconductor material, either band gap or absorption edge energy must be determined to characterize the property. Spectroscopic analysis of the films were performed by using a UV-Vis spectrophotometer (SHIMADZU, UV-1601) in the wavelength range of 290-550nm.

In Figure 4.1, the UV-Vis spectrum of both bare titanium dioxide (TiO_2) and 1% Palladium doped titanium dioxide (1%PdO-TiO_2) deposited glass samples are given. During the analysis, the bare glass slide was used as reference channel of the spectrophotometer in order to cancel absorbance effects rising from substrate. As it is shown in Figure 4.1, wide absorbance bands were obtained from both bare TiO_2 and 1%PdO-TiO_2 samples within the range of 295-370 nm. The intensity of absorbance for 1% Pd-TiO2 is much higher than bare TiO_2 indicating the immense effect metal doping even at 1% loading. The absorption edge energy of the bare TiO_2 was determined as 3.4 eV which is attributed to the O^{-2} – Ti^{+4} [O (2p) – Ti (3d)] transition and this result shows that there is 0.2 eV red shift compared with the literature value (3.2 eV) [Popielarski, 1998]. The 1%PdO doped TiO_2 sample yielded 3.3 eV absorption edge energy which indicates metal oxide addition enhances the conductance of sol gel produced TiO_2 by 0.1 eV blue shift. The wide absorbance band with small intensity on 1%PdO/TiO_2 spectrum between 395-495 nm is assigned as Pd^{2+} d-d transitions or $Pd(O)_n^{2+}$ clusters. The peak widening indicates these clusters are very small

and Pd^{2+} ions might be anchored to the surface oxygen of TiO_2 support. The literature reports the Pd d-d transition occur in two distinct band ranges as A(300 nm) and B (400 nm) [(Tessier et al., 1992) and (Rakai et al., 1992)]. The A(300nm) band which is within the range of optical absorbance of TiO_2 and is not resolved as separate peak in the present case, but increase of absorbance on the 295-370 nm can be attributed as d-d transition peak of Pd^{2+} ions.

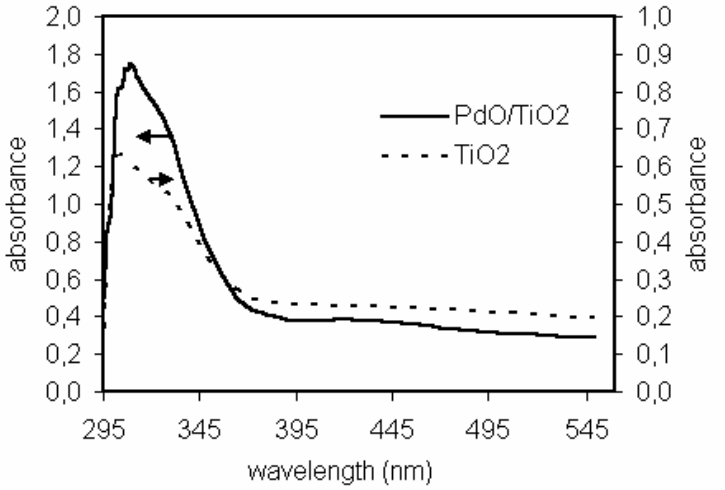

Figure 4.1 UV-Vis spectra of TiO_2 and PdO-TiO_2 deposited glass substrates

Similarly, the optical absorbance of bare tin dioxide (SnO_2) and 1% palladium doped tin dioxide (1%PdO-SnO_2) samples were analyzed. As it is seen from Figure 4.2, the wide absorbance band between 200-360 nm were obtained for bare SnO_2 and 270-360 nm for 1%PdO-SnO_2 samples. Similar to the TiO_2 based samples, 1%PdO doped sample yields much higher absorbance compared to the bare SnO_2 indicating the metal doping dominates the optical absorbance in the UV range. The most important point of this analysis is the wide blue shift of bare SnO_2 absorbance band to the higher energy, while the optical edge around 360 nm was observed for both bare and PdO doped sample. The peak widening which extends asymmetrically to the blue (higher energy) indicates the inherent long range disordered structure and the presence of smaller crystallites with

more fragments and defects and comparatively more amorphous structure exists over the bare surface of SnO_2 than the 1%PdO doped surface. The absorption edge of bare SnO_2 was determined as 3.7 eV and this value represents the less conductivity (+0.2 eV red shift) than the literature value of band gap (Eg SnO_2 = 3.5 eV) [Benedix et al., 2000]. The spectra of 1%PdO-SnO_2 represents completely different structure of PdO exists over the surface compared with the TiO_2 counterpart. The shoulder at 350 nm indicates the presence of dispersed Pd^{2+} ions and the sharp peak around 480 nm can be attributed to the isolated PdO crystallites over the SnO_2 surface with is typical for the PdO bulk phase. Similar results were also reported in literature [(Tessier et al., 1992) and (Rakai et al., 1992)]. This result reveals that the complete PdO dispersion over the SnO_2 surface is not completely achieved and the surface contains both ionic Pd^{2+} species which interacts with the O^{2-} ions of SnO_2 and larger crystallites which comprised of PdO crystals. The adsorption edge energy of 1%PdO-SnO_2 surface is determined as 3.6 eV which indicates higher conductivity than the bare SnO_2 sample.

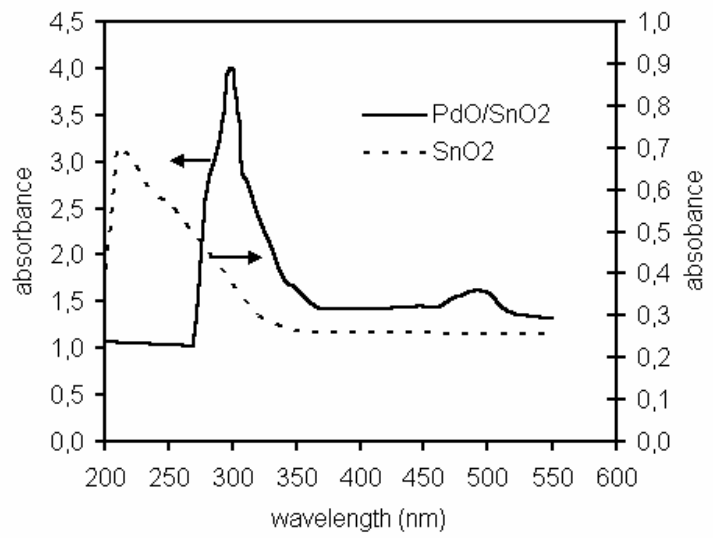

Figure 4.2 UV-Vis spectra of SnO_2 and PdO-SnO_2 deposited glass substrates

The results of absorption edge energy analysis by UV-Vis spectrophotometer indicated that both PdO promoted and bare samples of TiO_2 have superior conductivity over SnO_2 counterparts. The addition of 1% PdO to both TiO_2 and SnO_2 yields higher conductance and promotes the semiconductor properties and alter the optical absorbance character. Both SnO_2 and TiO_2 and their PdO doped counterparts are useful for photo-catalysis because of their validated semiconductor properties and their activity with respect to the UV radiation. The difference in their absorption edge energies requires different wavelength and intensities of UV radiation for photochemical activity. Therefore, depending on the availability of light source, and its spectral distribution (Intensity versus wavelength), activity of these materials can be tuned for specific application.

4.2. Film Morphology

SEM investigation is important stage for the thin film qualification. Film morphology, film thickness and continuity of the final film affect the properties of the film. The aim of this study was to produce homogeneous and thin anatase TiO_2 films as mentioned previously.

4.2.1. SEM analysis for TiO_2 and PdO-TiO_2 deposited glass substrates

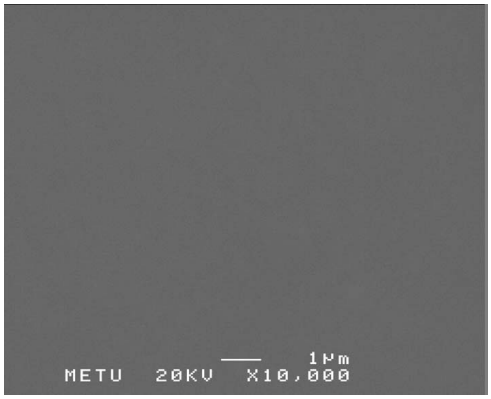

Figure 4.3 SEM micrograph of TiO_2 film surface, x10,000 magnification

The surface and particle morphology of the thin TiO_2 films which were produced by the five successive applications of sol-gel layers of TiO_2 over the glass substrate and the heat treatment at 650^oC for 10 minutes were examined by SEM imaging. The samples were coated with gold in order to achieve sufficient conductivity for analysis. The representative SEM images of TiO_2 films coated on glass substrates are given in Figure 4.3 and Figure 4.4. The formation of continuous TiO_2 was observed over the samples that were examined and the smooth, glassy, defect free structure is the general appearance. At 10,000X magnification, where 0.1μm resolution is achieved, neither particle structure, nor grains were observed over the surface. Some defects were observed due to the drying and calcination steps and the presence of solid impurities within the sol-gel solution may lead to the thermal stresses over the film. However, the periodicity of film defects per unit area is very small. The representative sample image of the surface defects is given in Figure 4.4. The formation of these cracks was also explained by the internal tension during thermal treatment in literature [Kwon et al., 2003].

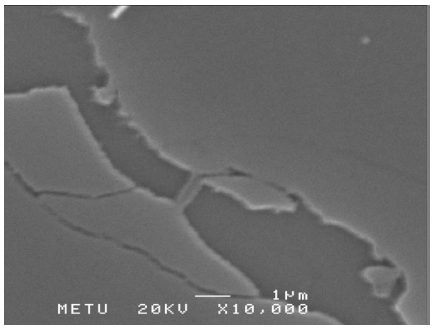

Figure 4.4 SEM micrograph of surface defects over the TiO_2 film surface at x10,000 magnification.

Figure 4.5 and 4.6 present the SEM micrographs of glass surfaces which are coated with PdO doped TiO_2 films which were obtained after five step coating of sol-gel solution and calcinations at 650°C for 10 minutes. The formation of smooth, homogeneous and defect free adhesion of the PdO-TiO_2 film was evidenced in these micrographs. It can be said that the coating solution

completely wetted the surface and well adhered to the glass surfaces and PdO doping has no adverse effect on TiO_2 thin films. Similar to the bare TiO_2 films, the presence of particles and grains were not observed at 10,000 magnifications. Due to the drying and calcination stage that causes thermal stresses created in the film, micro cracks can appear on the coating surface as seen in Figure 4.6.

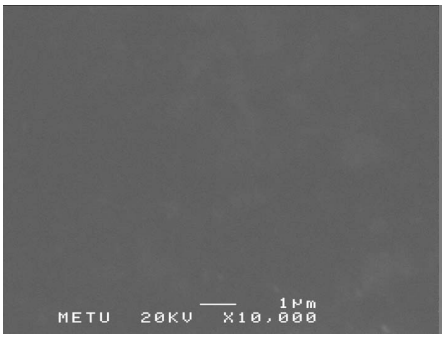

Figure 4.5 SEM micrograph of PdO-TiO_2 film surface, x10,000 magnification

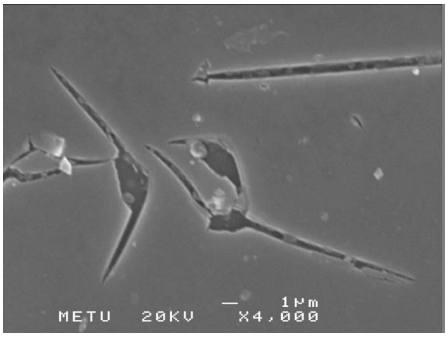

Figure 4.6 SEM micrograph of surface defects over the PdO-TiO_2 film surface, x10,000 magnification

4.2.2. SEM analysis for SnO_2 and PdO-SnO_2 deposited glass substrates

Figure 4.7 shows the surface SEM image of SnO_2 film, coated on the glass substrate which are prepared from the precursor solutions and method which are

described in Experimental part. In overall, the SnO_2 film surface represents the grainy structure even at 1000 magnification. Although shrinkages were observed from the figure, the coated under layer can be seen from the grains over the surface. The overlap of five layers of coatings may barely form a continuous SnO_2 matrix over the surface. This fact may lead to the loss of apparent electrical conductance over the surface (macro-range) as a result of 3-5μm large gaps between the grains, although the UV-Vis analysis indicates the semiconductor structure in micro-range.

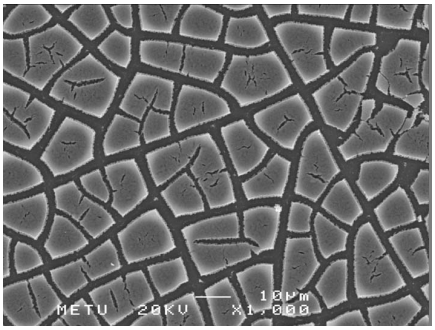

Figure 4.7 SEM micrograph of SnO_2 film surface, x1,000 magnification

It is believed that the shrinkages and cracks were due to the heat treatment step that is due to initiation of internal tension during thermal treatment and large density variation between the sol-gel solution and SnO_2 solid film.

The surface morphology of the PdO doped SnO_2 samples which are prepared by the same method with TiO_2 counterparts was also examined by SEM. In Figure 4.8 the representative image of the PdO-SnO_2 film is presented. The surface structure of PdO doped SnO_2 film surface is similar to the bare SnO_2 which has grainy structure. As observed from the Figure 4.8, smaller (1-3μm) gaps between the grains were observed which cannot be explained by the effect of addition of PdO to the SnO_2 sol.

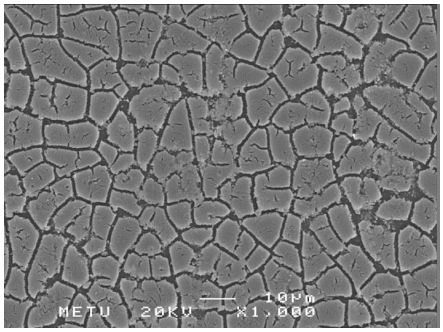

Figure 4.8 SEM micrograph of PdO-SnO_2 film surface, x1,000 magnification

4.3. Reusability of the Films

Each prepared coating on glass surfaces was used for at least 20 times during 1 year period. After each experiment the coated surfaces were washed with ethanol and detergents. The antimicrobial effect of these coatings did not change during this period, showing time, water contact and rubbing do not affect the coating's stability.

4.4. Antimicrobial Properties of the Films

In order to test the antimicrobial properties of the coatings, their effects on several microorganisms having different cell wall structures were tested. Considering the initial destructive effect of photocatalytic activity that takes place on the cell wall [Huang et al., 2000], *E. coli* and *S. aereus* were used as Gr(-) and Gr(+) procaryotic cells, *S. cerevisiae* was used as an eucaryotic cell and *A. niger* spores were used as fungal spores.

For each microorganism, cell suspensions in peptone water were prepared and 200µl of cell suspension was applied on glass surfaces. Before each experiment the number of the cells in the microbial suspension was determined by viable count method. The effect of UVA only was measured by incubating the microbial suspension on uncoated surface and the effect of coating only was

measured by incubating the microbial suspension on the coated surfaces in the dark.

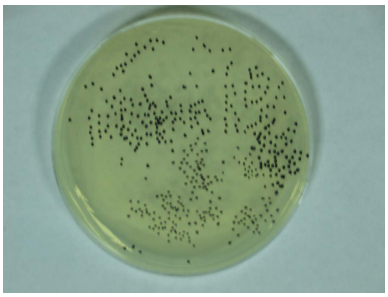

Figure 4.9 Number of *E. coli* cells in the 200μl microbial suspension that applied on the surfaces, [352±5 CFU/200μl were counted]

Figure 4.9 shows the number of *E. coli* cells in the *E. coli* suspension applied on the surfaces that was used in the photocatalytic experiments. In all the experiments, number of cells in the sample applied to the surface was determined almost equal to the number of survived cells illuminated on uncoated glass surfaces (Figure 4.10) and to the number of survived cells on coated samples in the dark (Figure 4.11). Therefore, neither illumination nor coating alone has antimicrobial effect.

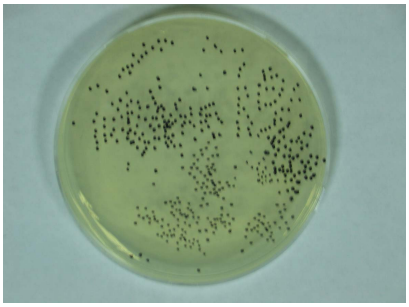

Figure 4.10 Number of *E. coli* cells in the microbial suspension of 200μl applied on the uncoated surface and illuminated i.e., the UVA effect alone [350±7 CFU/200μl were counted].

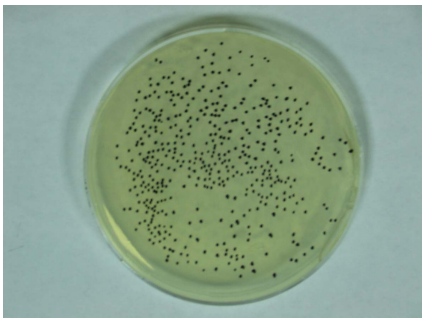

Figure 4.11 Number of *E. coli* cells in the microbial suspension of 200μl applied on the TiO_2 coated surface and kept in the dark [350±5 CFU/200μl were counted].

As observed from Figures 4.9-4.11, numbers of *E. coli* cells in the 200μl microbial suspension, in the suspension applied on the TiO_2 surface after incubation in the dark and in the suspension after incubation on uncoated surface are counted as 352, 350 and 350 CFUs, respectively. These control experiments were also performed for *S. aereus* and *S. cerevisiae*. The results of these experiments for all the microorganisms are given in Table 4.1. Therefore

the coating itself and UVA alone do not have any antimicrobial effect against *E. coli, S. aereus* and *S. cerevisiae*.

Table 4.1 Results of the illumination and coating material control experiments

	Number of Cells/200μl		
	Original microbial suspension applied on the surfaces	On the TiO_2 coatings incubated in the dark	On the illuminated uncoated surfaces
E. coli	352±5 CFUs	350±5 CFUs	350±7 CFUs
S. aereus	330±5 CFUs	325±10 CFUs	337±8 CFUs
S. cerevisiae	434±8 CFUs	430±10 CFUs	432±12 CFUs

Similarly no antimicrobial effect was observed for other coatings, PdO-TiO_2, SnO_2 and PdO-SnO_2 against *E. coli, S. aereus* and *S. cerevisiae* after incubated in the dark.

4.5. Photocatalytic Effect on the Antimicrobial Properties of the Films

4.5.1. Antimicrobial Effect Against of *Escherichia coli*

4.5.1.1. TiO_2 Films

The results of photocatalytic effect, after 2 hours illumination against *E. coli* on the TiO_2 coated and uncoated control glasses were given in Figures 4.12 and 4.13. After 2 hours illumination, the numbers of cells on the coated and uncoated glasses were counted as 350 and 50 CFUs showing 85% decrease in survival ratio of *E. coli* due to the photocatalytic effect.

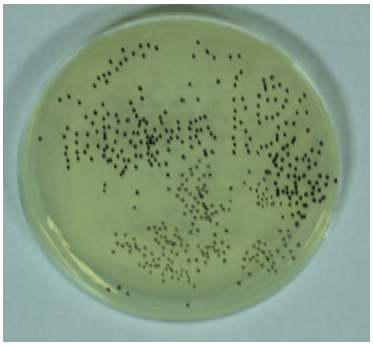

Figure 4.12 Number of *E. coli* cells survived on uncoated (control) glass surface, [350±7 CFUs/200µl were counted]

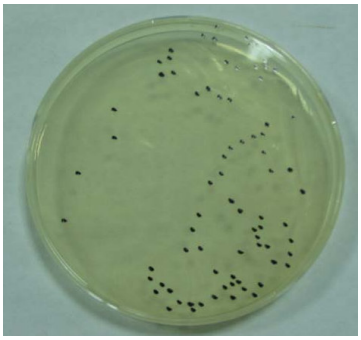

Figure 4.13 Number of *E. coli* cells survived on TiO_2 coated glass surface [50±4 CFUs/200μl were counted]

Huang et al. (2000) reported 99% inactivation of *E. coli* cells after 60 minutes illumination period. However, TiO_2 powder was used in their study. They also observed better activity by increasing TiO_2 surface area and decreasing the particle size, with the help of sonication.

Another study was performed by Kikuchi et al. (1997), in which a complete inactivation of *E. coli* cells on TiO_2 film was observed after 1 hour illumination. However, because of their light source, 20% and 30% of *E. coli* had been inactivated after 1 and 2 hours of illumination. Our light source and UV filter was adjusted to provide no cell inactivation by illumination itself.

4.5.1.2. Palladium doped TiO_2 Films

Metal doping into a semiconductor catalyst increases the conductivity on the surface of the semiconductor as known from literature (Zaharescu et al., 1993; Ranjit and Viswanathan, 1997). The effect of palladium doping (as a metal doping) on the photocatalytic activity of semiconductor coatings has not been investigated before. Since no report is present in the literature, the effect of

palladium doping on photocatalytic activity was studied considering a possible increase in the photocatalytic efficiency, against microorganisms.

As observed from Figures 4.14 and 4.15, photocatalytic efficiency of Pd doped TiO_2 coated glasses is considerably higher than the ones coated with only TiO_2. After 2 hours illumination, 8 and 356 CFUs were counted on Pd doped TiO_2 and uncoated (control) glasses showing 98% decrease in the survival ratio of *E. coli*. So, as expected palladium doping increased the photocatalytic activity possibly by increasing the conductivity on the surface of the PdO-TiO_2 coated glass.

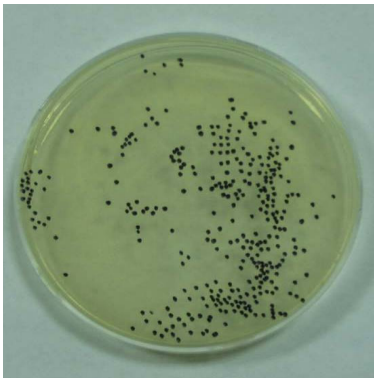

Figure 4.14 Number of *E. coli* cells survived on uncoated (control) glass surface, [356±5 CFUs/200µl were counted]

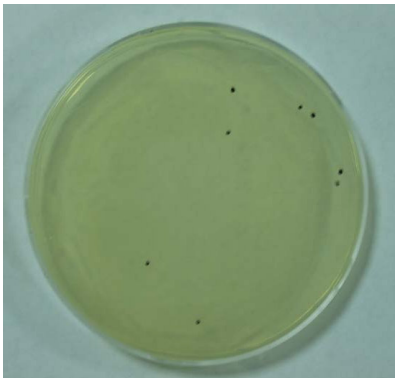

Figure 4.15 Number of *E. coli* cells survived on PdO-TiO_2 coated glass surface [8±1 CFUs/200µl were counted]

In Figure 4.16, time-dependent survival ratios of *E. coli* under illumination on TiO_2 and PdO-TiO_2 coated glasses are given.

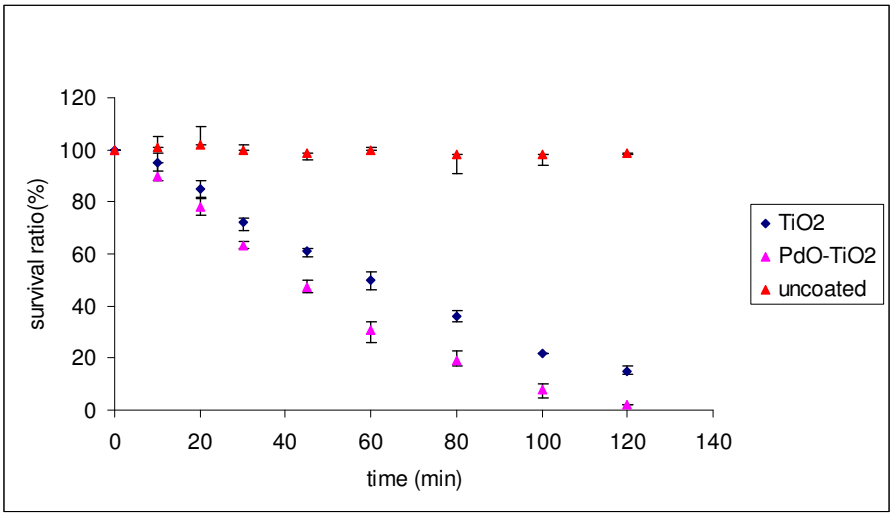

Figure 4.16 Survival ratio of *E. coli* under illumination on TiO_2 and PdO-TiO_2 coated glasses (initial number of *E. coli*: 352±5 CFUs/200µl)

The effect of palladium doping is obviously seen in Figure 4.16. The photocatalytic activity of palladium doped TiO_2 coated glass shows higher efficiencies when compared with only TiO_2 coated glass through 2 hours of illumination. After 40 minutes of illumination, survival ratio of *E. coli* decreases significantly. After 2 hours illumination of *E. coli* on the PdO-TiO_2 coated glass, almost all *E. coli* cells were killed, that is, 98% efficiency was achieved.

4.5.1.3. SnO_2 Films

SnO_2, as a semiconductor photocatalyst, with its reasonable band gap energy, is known as an efficient photocatalyst. SnO_2 is a good alternative to TiO_2 semiconductor photocatalyst since it has a similar photocatalytic process mechanism. As seen from Figures 4.17 and 4.18, the number of *E. coli* cells on uncoated (control) and SnO_2 coated glass surfaces were counted as 352 and 153 CFUs. So, a 56% decrease in survival ratio of *E. coli* was achieved with the photocatalytic effect of SnO_2. The antimicrobial effect of SnO_2 coatings showed lower photocatalytic efficiency with respect to TiO_2 coatings. The band gap energy was higher for SnO_2 and hence the surface conductivity of SnO_2 was lower. Since the conductivity and band gap concepts strongly affect the photocatalytic activity, this lower photocatalytic efficiency was not surprising.

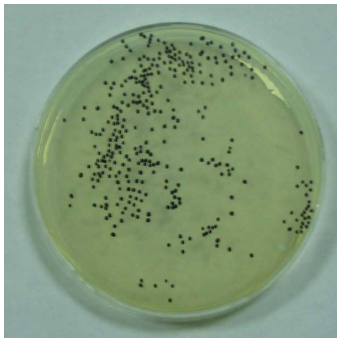

Figure 4.17 Number of *E. coli* cells survived on uncoated (control) glass surface, [352±5 CFUs/200μl were counted]

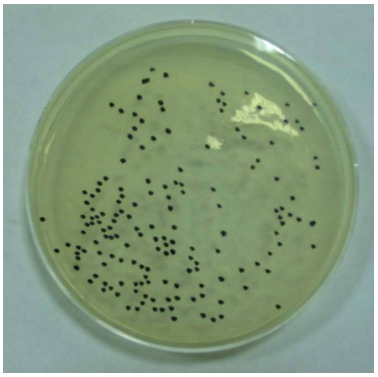

Figure 4.18 Number of *E. coli* cells survived on SnO_2 coated glass surface [153±4 CFUs/200µl were counted]

4.5.1.4. Palladium doped SnO_2 Films

Similarly in TiO_2, palladium doping to the SnO_2 semiconductor catalyst was expected to increase the photocatalytic activity by increasing the conductivity on the surface of the semiconductor.

As observed in Figures 4.19 and 4.20, 351 and 109 CFUs were counted on uncoated (control) glass and PdO-SnO_2 coated glass after 2 hours illumination showing a 68% decrease in survival ratio of *E. coli*.

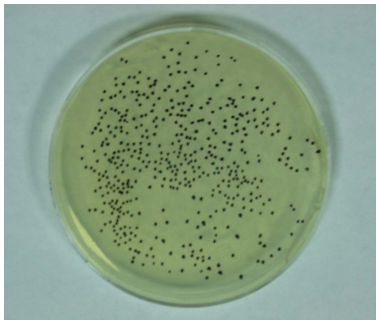

Figure 4.19 Number of *E. coli* cells survived on uncoated (control) glass surface, [351±2 CFUs/200µl were counted]

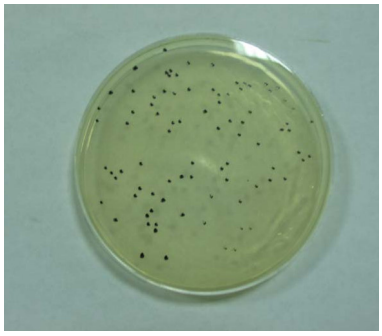

Figure 4.20 Number of *E. coli* cells survived on PdO-SnO_2 coated glass surface [109±1 CFUs/200µl were counted]

As seen from Figure 4.21, palladium doped SnO_2 coated glass shows higher photocatalytic efficiencies on the inactivation of *E. coli* when compared with the SnO_2 coated glass surface. Although, the photocatalytic efficiencies of SnO_2 and PdO-SnO_2 are lower than that of TiO_2 and PdO-TiO_2, respectively, the effect of palladium doping to the photocatalytic activity is obvious by increasing the electron mobility on the semiconductor surface in any case. However the antimicrobial effect of Pd was higher on TiO_2 than SnO_2 coated surfaces.

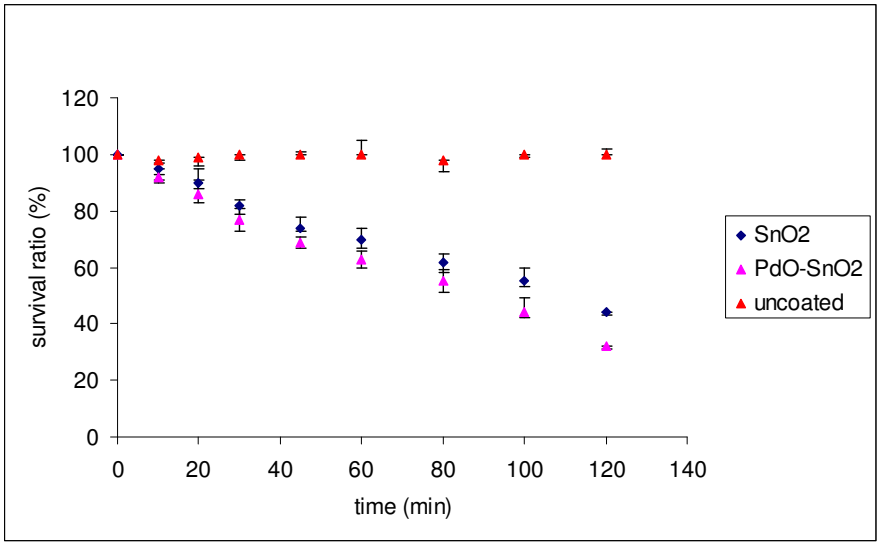

Figure 4.21 Survival ratio of *E. coli* under illumination on SnO_2 and PdO-SnO_2 coated glasses (initial number of *E. coli*: 352±5 CFUs/200μl)

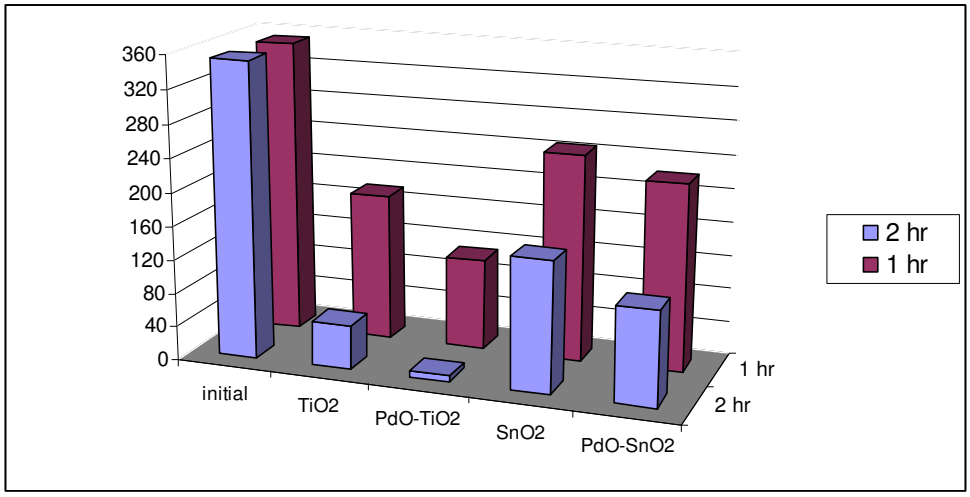

Figure 4.22 Number of residual cells of *E. coli* under illumination on TiO_2, PdO-TiO_2, SnO_2 and PdO-SnO_2 coated glasses (initial number of *E. coli*: 352±5 CFUs/200μl)

4.5.2. Antimicrobial Effect against *Staphylococus aereus*

4.5.2.1. Isolation and Identification of *S. aereus*

Since *S. aereus* cells were obtained in a liquid culture, it was necessary to isolate a single colony and perform its identification. From literature, it is known that *S. aereus* cells were appeared in black colored colonies with a white shiny hollow around when cultivated on Baird-Parker agar containing egg-yolk tellurite emulsion (Speck, 1989). The appearance of the isolated microorganism is given in Figure 4.23 indicating the identity of the microorganism as *S. aereus.*

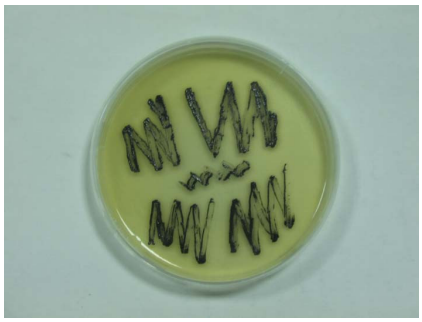

Figure 4.23 Identification of *S. aereus* on Baird-Parker agar

4.5.2.2. TiO_2 Films

Illumination period was increased to 3 hours by considering the thick and strong cell wall structure of *S. aereus*. The results of photocatalytic effect after 3 hours illumination against *S. aereus* on the TiO_2 coated and uncoated control glasses are given in Figures 4.24 and 4.25. The number of cells on the coated and uncoated glasses was counted as 337 and 44 CFUs showing 87% decrease in survival ratio of *S. aereus* due to photocatalytic effect.

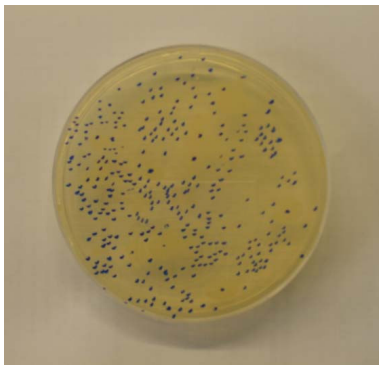

Figure 4.24 Number of *S. aereus* cells survived on uncoated (control) glass surface, [337±5 CFUs/200µl were counted]

Photocatalytic efficiency of TiO_2 coating on the inactivation of *S. aereus* was lower than *E. coli* since comparable results could be obtained after 2 and 3 hours of illumination for *E. coli* and *S. aereus,* respectively.

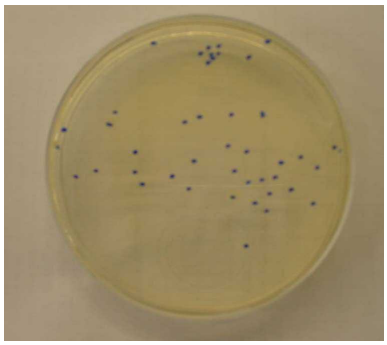

Figure 4.25 Number of *S. aereus* cells survived on TiO_2 coated glass surface [44±6 CFUs/200µl were counted]

The different cell structures, particularly cell wall structures, play an important role. Since *E. coli* is Gr (-) and *S. aereus* is Gr (+) bacteria and as explained in chapter 2, *S. aereus* is expected to be more resistant to photocatalytic oxidation because of its thicker and stronger cell wall. The presence of an outer membrane and a thin cell wall in Gr (-) bacteria, could not protect the bacterium from photocatalytic effect efficiently. Additionally, the proteins present in the periplasmic space, between the cell wall and outer membrane of Gr (-) bacteria, can be easily inactivated by photocatalytic oxidation and this may also be another reason of higher efficiency of photocatalysis on Gr (-) bacteria.

4.5.2.3. Palladium Doped TiO2 Films

Palladium doping into a semiconductor catalyst was expected to increase the conductivity on the surface of the semiconductor and hence to increase the photocatalytic activity of the semiconductor coating.

As observed from Figures 4.26 and 4.27, the effect of palladium doping is clearly seen that palladium doping increases the photocatalytic activity and increases the inactivation of *S. aereus*. After 3 hours illumination, 7 and 335 CFUs were counted on the PdO-TiO_2 coated and uncoated (control) glass surface showing 98% decrease in the survival ratio of *S. aereus*. However the palladium doping effect on *E. coli* was more striking than *S. aereus*.

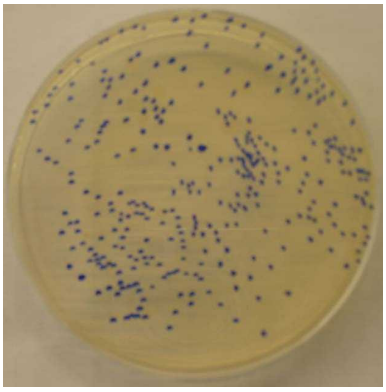

Figure 4.26 Number of *S. aereus* cells survived on uncoated (control) glass surface, [335±7 CFUs/200µl were counted]

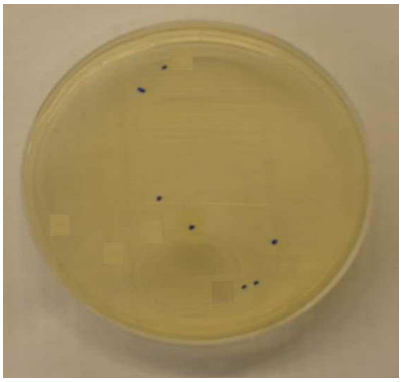

Figure 4.27 Number of *S. aereus* cells survived on PdO-TiO_2 coated glass surface [7±2 CFUs/200µl were counted]

The photocatalytic efficiency of Pd-TiO_2 coated glass surface on the inactivation of *S. aereus* was lower when compared to *E. coli* showing the better protection with the thicker and stronger Gr (+) cell walls than the Gr (-) cell wall. As observed in Figure 4.28, *S. aereus* cells show high resistivity up to 30 minutes of illumination. However, in the case of *E. coli* photocatalysis,

inactivation started immediately (Figure 4.16). The photocatalytic activity of PdO-TiO_2 coating on the inactivation of *E. coli* after 2 hours illumination, 98% decrease, could only be achieved after 3 hours illumination for *S. aereus.*

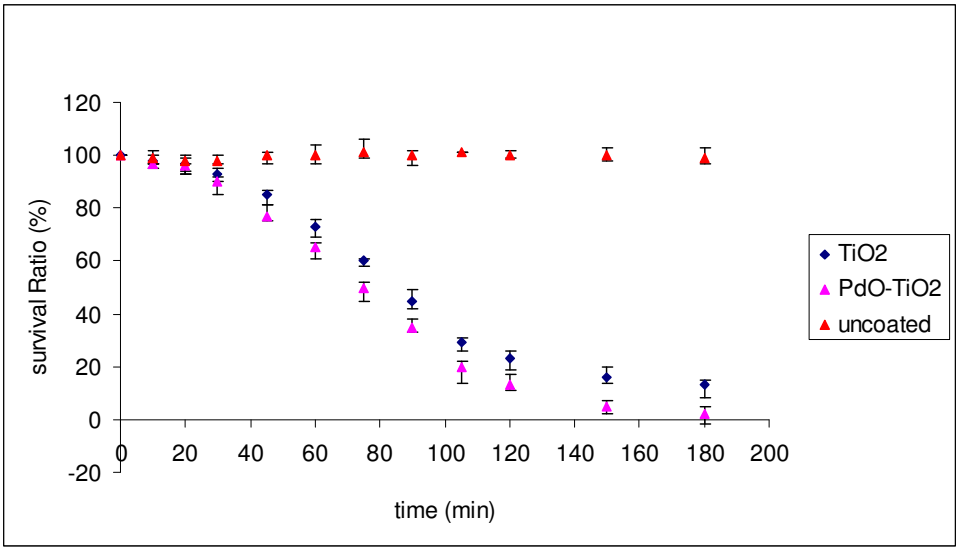

Figure 4.28 Survival ratio of *S. aereus* under illumination on TiO_2 and PdO-TiO_2 coated glasses (initial number of *S. aereus*: 330±5 CFUs/200µl)

4.5.2.4. SnO_2 Films

Antimicrobial effect of SnO_2, as a semiconductor photocatalyst with its reasonable band gap energy, was investigated on the inactivation of *S. aereus*. From Figure 4.29 and 4.30, the number of *S. aereus* cells on uncoated (control) and SnO_2 coated glass surfaces were measured as 327 and 69. So, a 79% decrease in survival ratio of *S. aereus* was achieved with the photocatalytic effect of SnO_2. The photocatalytic efficiency of SnO_2 coating is lower than that of TiO_2 with 87% decrease. The photocatalytic efficiency of SnO_2 coated glass on the inactivation of *S. aereus* and *E. coli* were 56% and 60%, respectively after 2 hours illumination and are comparable with each other.

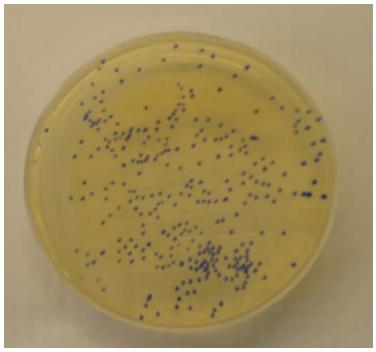

Figure 4.29 Number of *S. aereus* cells survived on uncoated (control) glass surface, [327±7 CFUs/200µl were counted]

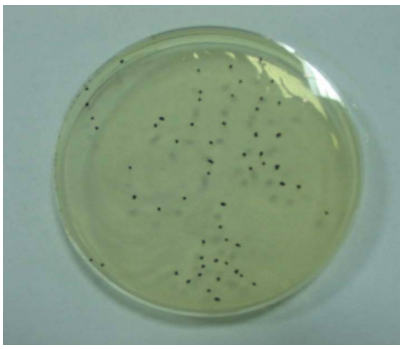

Figure 4.30 Number of *S. aereus* cells survived on SnO_2 coated glass surface [69±3 CFUs/200µl were counted]

4.5.2.5. Palladium doped SnO_2 Films

Palladium doping to the SnO_2 semiconductor catalyst was expected to increase the photocatalytic activity by increasing the conductivity on the surface of the semiconductor. The effect of doping on the photocatalytic activity of SnO_2 films to *S. aereus* was also investigated. After 3 hours illumination, 79%

decrease in survival ratio of *S. aereus* on SnO_2 coated glass surface and 90% decrease in survival ratio of *S. aereus* on PdO-SnO_2 coated glass surface were obtained. From Figures 4.31 and 4.32, the positive effect of palladium doping was clearly observed.

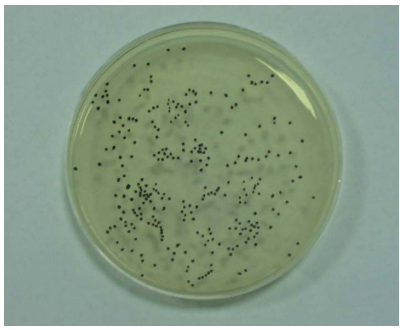

Figure 4.31 Number of *S. aereus* cells survived on uncoated (control) glass surface, [332±7 CFUs/200µl were counted]

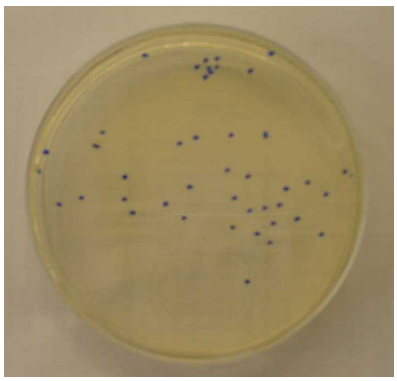

Figure 4.32 Number of *S. aereus* cells survived on PdO-SnO_2 coated glass surface [33±3 CFUs/200µl were counted]

When the photocatalytic efficiency of PdO-SnO_2 coated glass on the inactivation of *E. coli* was compared with *S. aereus* after 2 hours illumination, 71% decrease in *S. aereus* and 68% decrease in *E. coli* on PdO-SnO_2 were obtained. Although, *S. aereus* was expected to be more resistant to the photocatalytic effect than *E. coli*, almost the same efficiency was obtained for these two types of cells on SnO_2 and Pd doped SnO_2 surfaces.

Since S. aereus cells are gram (+) bacteria and have a very thick peptidoglycan layer in their cell wall structure, up to 30 minutes the cells show very high resistivity to photocatalytic effect of SnO_2 and palladium doped SnO_2 coated glasses as seen in Figure 4.33.

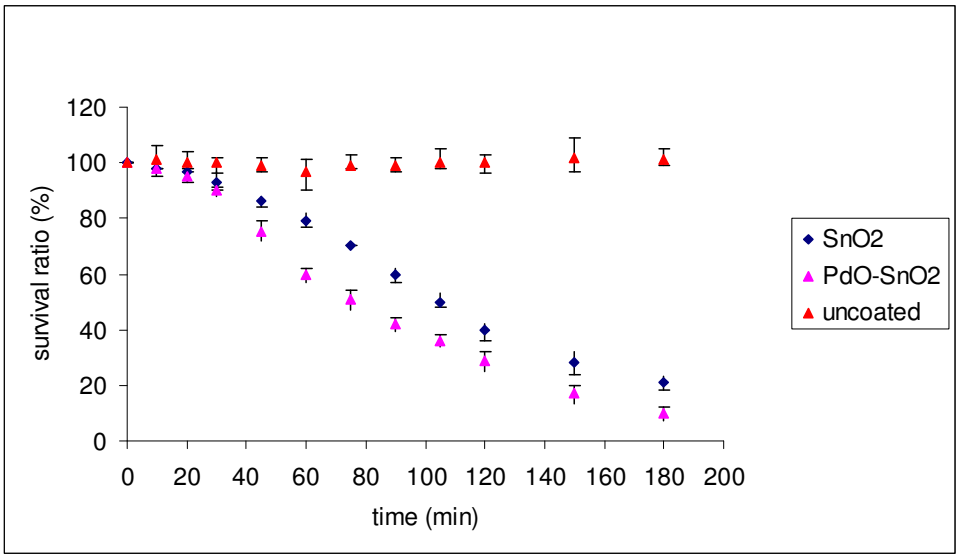

Figure 4.33 The survival ratio of *S. aereus* under illumination on SnO_2 and PdO-SnO_2 coated glasses (initial number of *S. aereus*: 330±5 CFUs/200μl)

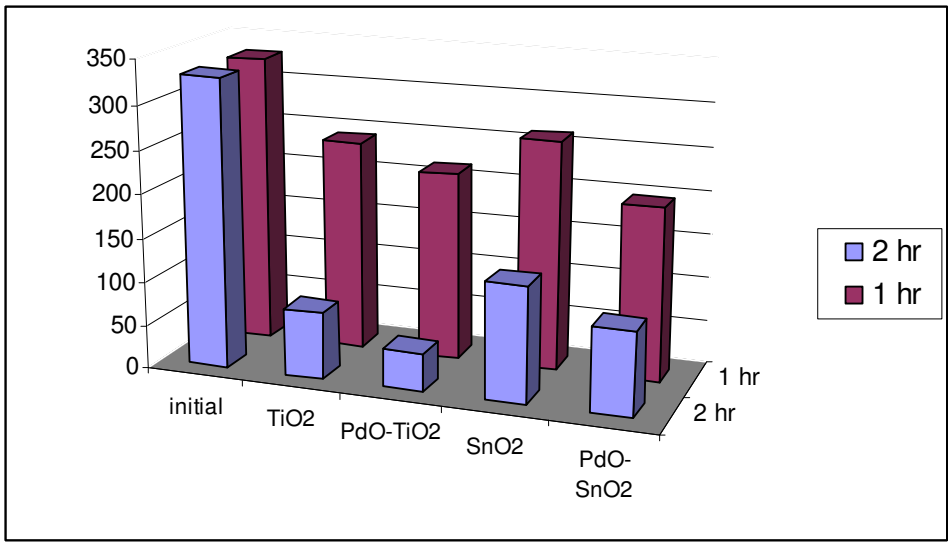

Figure 4.34 Number of residual cells of *S. aereus* under illumination on TiO_2, PdO-TiO_2, SnO_2 and PdO-SnO_2 coated glasses (initial number of *S. aereus*: 352±5 CFUs/200µl)

4.5.3. Antimicrobial Effect against *Saccharomyces cerevisiae*

4.5.3.1. TiO_2 Films

The results of photocatalytic effect after 3 hours illumination against *S. cerevisiae* on the TiO_2 coated and uncoated (control) glasses are given in Figure 4.35 and 4.36. After 3 hours illumination, the number of cells on the coated and uncoated glasses was counted as 432 and 233 CFUs showing 54% decrease in survival ratio of *S. cerevisiae* due to photocatalytic effect.

The number of survived *S. cerevisiae* cells was higher when compared to *E. coli* and *S. aereus* cells after 2 hours illumination. However the size of the colonies was very much smaller than the original colonies probably showing

weak survivors. This result may be due to the higher repair rate of cell wall damage on the agar plates (Davis et al., 1973).

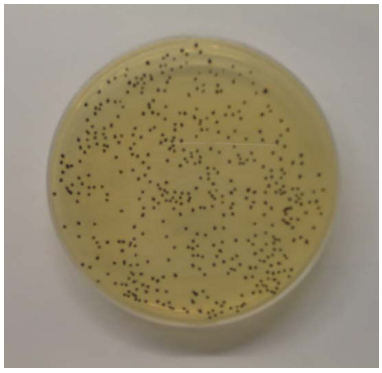

Figure 4.35 Number of *S. cerevisiae* cells survived on uncoated (control) glass surface, [432±12 CFUs/200µl were counted]

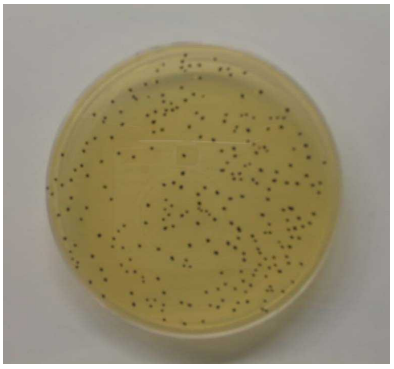

Figure 4.36 Number of *S. cerevisiae* cells survived on TiO_2 coated glass surface [233±8 CFUs/200µl were counted]

After 2 hours illumination, 85% decrease in survival ratio of *E. coli* and 77% decrease in survival ratio of *S. aereus* were achieved on TiO_2 coated glass substrates. For *S. cerevisiae* only 54% decrease in survival ratio was obtained. The cell wall of yeast is remarkably thick and a strong envelope. Probably because of the strong cell wall structure of yeast and better cell repair mechanism, the photocatalytic efficiency of TiO_2 coating against *S. cerevisiae* was the lowest.

4.5.3.2. Palladium doped TiO_2 Films

Palladium doping to the TiO_2 semiconductor catalyst was expected to increase the photocatalytic activity by increasing the conductivity on the surface of the semiconductor. The effect of doping on the photocatalytic activity of TiO_2 films with *S. cerevisiae* was investigated.

As observed from Figures 4.37 and 4.38 that the photocatalytic efficiency of Pd doped TiO_2 coated glass is higher than the ones coated with only TiO_2. After 3 hours illumination 150 and 432 CFUs were counted on Pd doped TiO_2 and uncoated glasses showing 65% decrease in the survival ratio of *S. cerevisiae.* So, as expected, palladium doping increased the photocatalytic activity probably by increasing the conductivity on the surface of the PdO-TiO_2 coated glass. When the photocatalytic effect against *S. cerevisiae* was compared with *E. coli* and *S. aereus*, the inactivation ratio of *S. cerevisiae* was lower. This can be explained by the relatively complex morphology, in particular cell wall structure and may be a better cell wall repair system, of the yeast cells.

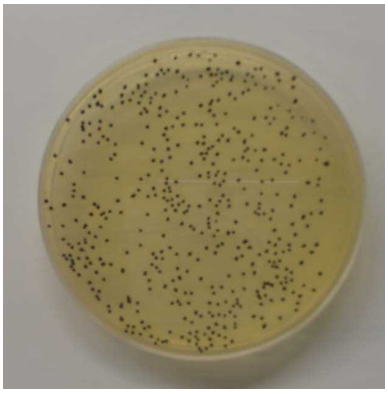

Figure 4.37 Number of *S. cerevisiae* cells survived on uncoated (control) glass surface, [430±8 CFUs/200μl were counted]

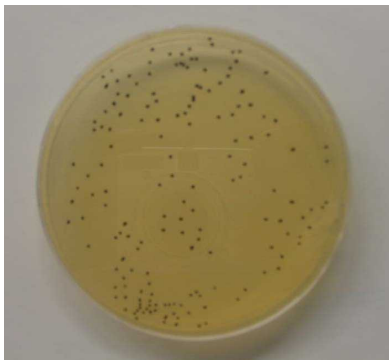

Figure 4.38 Number of *S. cerevisiae* cells survived on PdO-TiO_2 coated glass surface [150±6 CFUs/200μl were counted]

In Figure 4.39, the effect of palladium is obvious on the photocatalytic effect against *S. cerevisiae*. Although only 43% decrease in survival ratio of *S. cerevisiae* was achieved with photocatalytic effect of PdO-TiO_2 coating, the lowest when compared to *E. coli*, 98%, and *S. aereus*, 87%, palladium doping increased the photocatalytic efficiency from 34% to 43%. Since the cell wall of yeast is remarkably thick and glucans and chitin found in the wall structure

strengthen the cell wall of the yeast, the strong cell wall structure of yeast was expected not to be affected much by the photocatalytic effect of the coating as comparable as *E. coli* and *S. aereus*. Additionally, cell wall repair system may be better in *S. cerevisiae.*

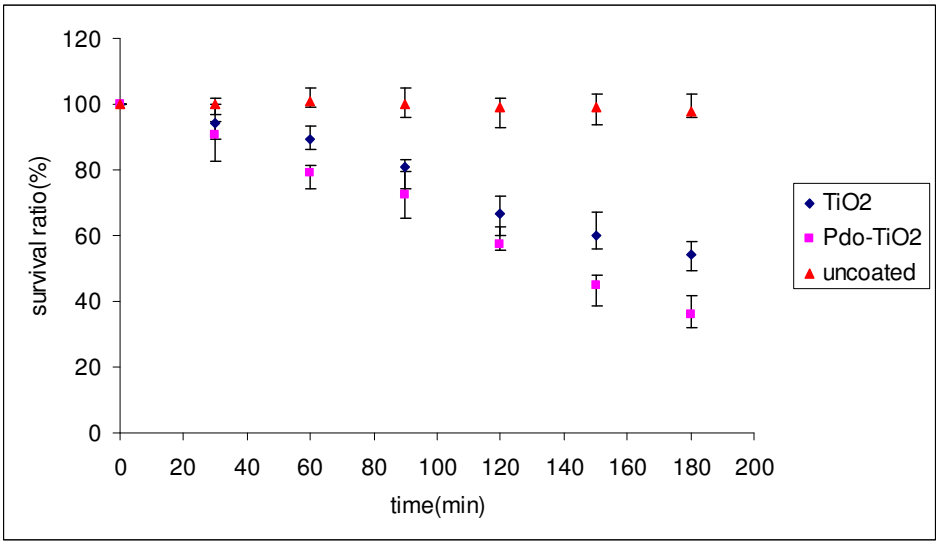

Figure 4.39 Survival ratio of *S. cerevisiae* under illumination on TiO_2 and PdO-TiO_2 coated glass substrates (initial number of *S. cerevisiae*: 434±8 CFUs/200µl)

4.5.3.3. SnO_2 Films

From Figure 4.40 and 4.41, number of *S. cerevisiae* cells on uncoated (control) and SnO_2 coated glass surfaces were counted as 436 and 300 CFUs. So, 31% decrease in survival ratio of *S. cerevisiae* was achieved with the photocatalytic effect of SnO_2. Since the cell wall of *S. cerevisiae* is remarkably thick and strong, the photocatalytic efficiency against *S. cerevisiae* was very low when compared to *E. coli* and *S. aereus*.

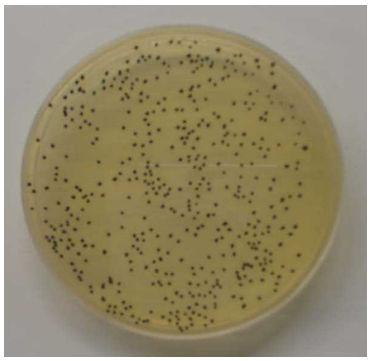

Figure 4.40 Number of *S. cerevisiae* cells survived on uncoated (control) glass surface, [436±8 CFUs/200μl were counted]

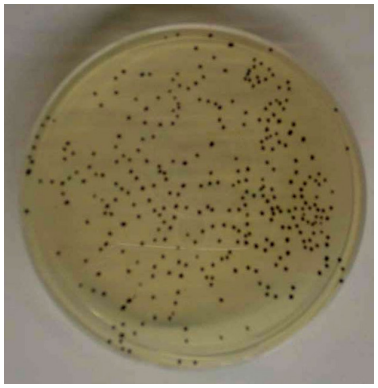

Figure 4.41 Number of *S. cerevisiae* cells survived on SnO_2 coated glass surface [300±9 CFUs/200μl were counted]

4.5.3.4. Palladium doped SnO_2 Films

The effect of Pd dopant on the photocatalytic efficiency was investigated by performing the inactivation of *S. cerevisiae* cells. As discussed before,

palladium doping was expected to increase the photocatalytic efficiency against *S. cerevisiae.*

In the Figures 4.42 and 4.43, 430 and 253 CFUs were counted on the uncoated (control) and PdO-SnO_2 coated glasses, respectively showing 41% decrease in the survival ratio of *S. cerevisiae* due to photocatalytic efficiency of PdO-SnO_2 after 3 hours illumination. Again, very small sized colonies were observed.

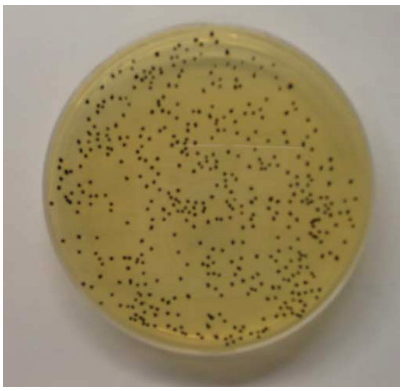

Figure 4.42 Number of *S. cerevisiae* cells survived on uncoated (control) glass surface, [430±8 CFUs/200μl were counted]

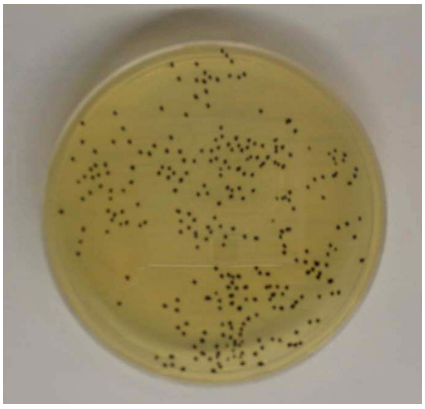

Figure 4.43 Number of *S. cerevisiae* cells survived on PdO-SnO_2 coated glass surface [253±7 CFUs/200μl were counted]

As seen from the figure 4.44, the photocatalytic efficiency was very low when compared to the photocatalytic activity of TiO_2 and PdO-TiO_2 coated glass surfaces. When the microbial cells of *E. coli*, *S. aereus* and *S. cerevisiae* were compared, the photocatalytic efficiency for the inactivation of *S. cerevisiae* was the lowest.

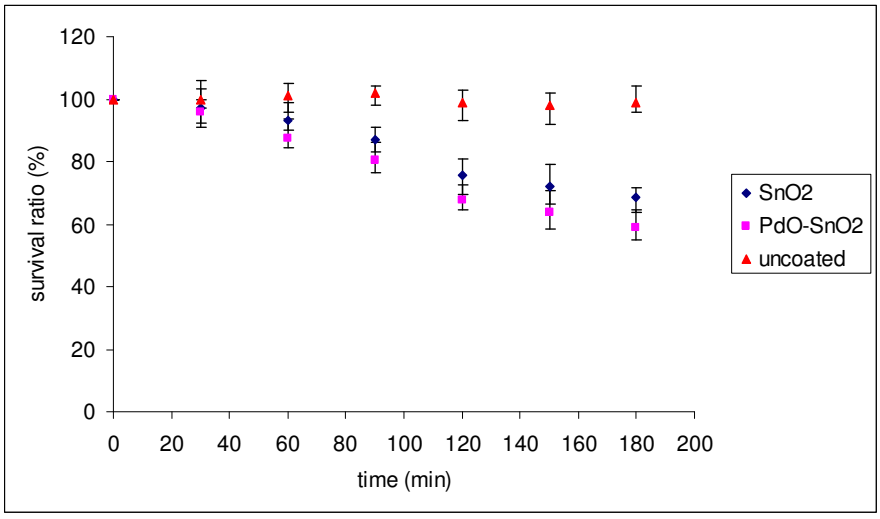

Figure 4.44 Survival ratio of *S. cerevisiae* under illumination on SnO_2 and PdO-SnO_2 coated glass substrates (initial number of *S. cerevisiae*: 434±8 CFUs/200μl)

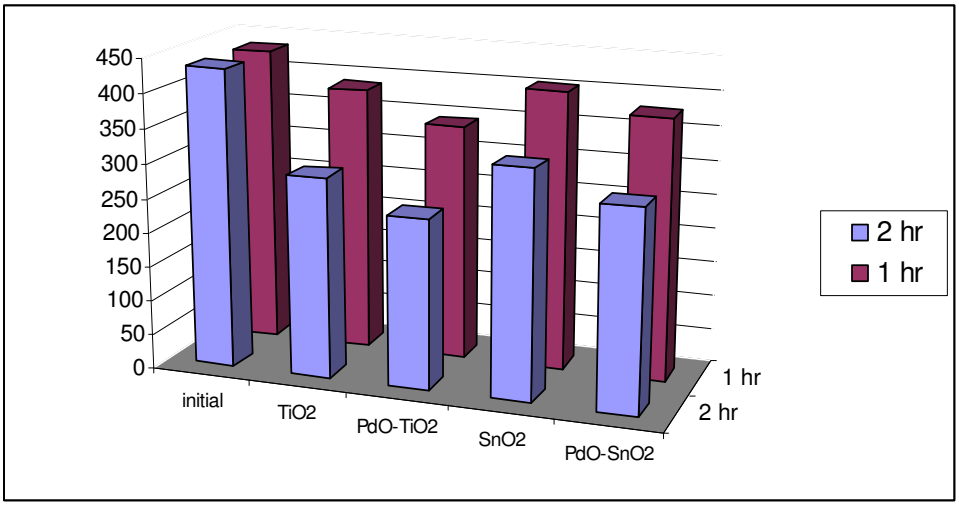

Figure 4.45 Number of residual cells of *S. cerevisiae* under illumination on TiO_2, PdO-TiO_2, SnO_2 and PdO-SnO_2 coated glasses (initial number of *E. coli*: 434±8 CFUs/200μl)

4.5.4. Antimicrobial Test Results of *Aspergilus niger* spores

Most fungi have relatively complex morphology; they have mycelium structure that is a highly branched system of tubes. Dense mycelium structure can cause complexities in their cultivation. Fungi form spores under adverse environmental conditions and for reproduction purposes. In general, cell walls of spores are generally not fibrillar, but they are multi-layered and often contain melanin. The cell wall of a spore is very strong, stronger than any of the microorganism and hence the spores were investigated if they were affected by the photocatalytic property of the coatings. The illumination period on spores increased up to 8 hours to see inactivation of spores by observing no growth or possible differences in the development of mycelia and spore formation. The illumination period could not be increased further because of drying problem of the spore suspension. Unfortunately as observed in Figures 4.46-4.50, significant differences could not be observed. Therefore, no significant deactivation was observed by using neither of coatings up to 8 hours of illumination on *A. niger* spores. To increase the illumination period, to prevent drying, an air-tight container might be used and the glasses can be placed in this box. Pham et al. (1995) has reported that intermittent illumination reduced the viable *Bacillus pumilus* spores more effectively than continuous exposure to UV. Therefore, intermittent and stronger illumination together with extended time periods can be tried.

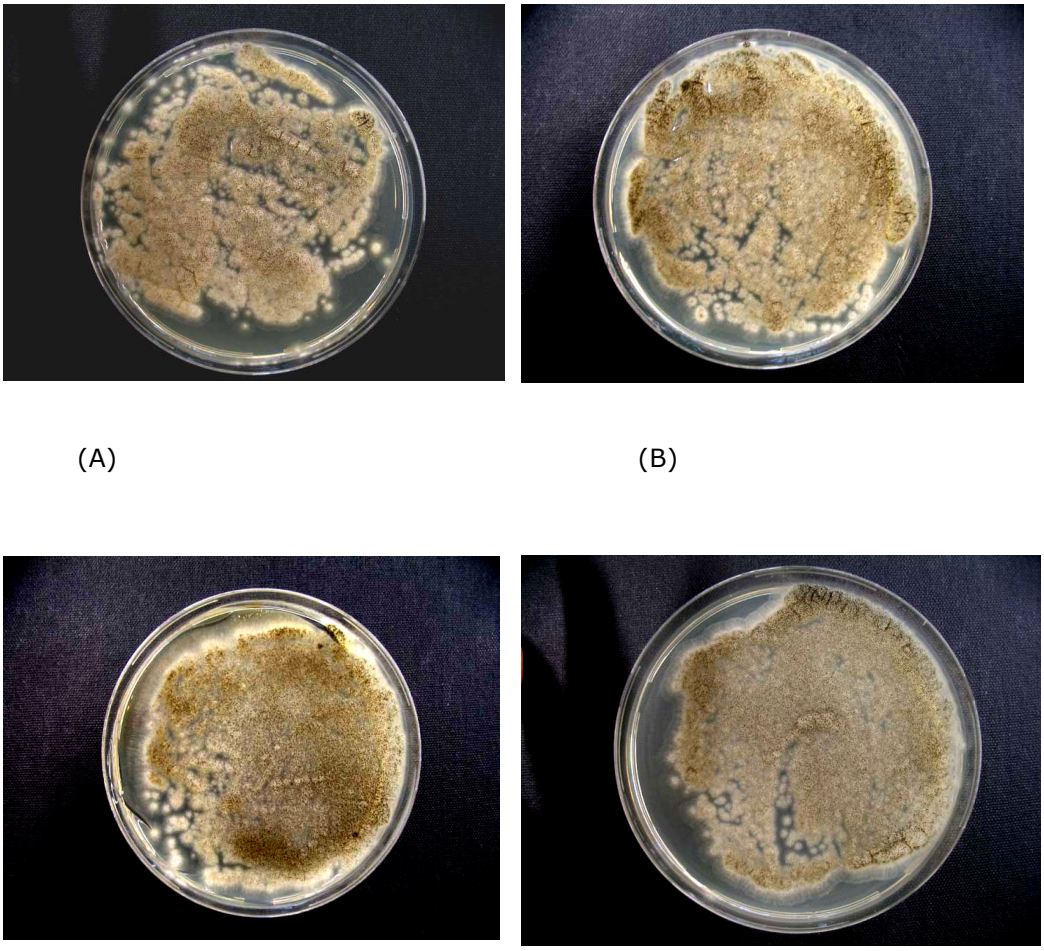

(A) (B)

(C) (D)

Figure 4.46 Growth of *A. niger* spores on the uncoated (control) glass after (A) 2h illumination; (B) 4h illumination (C) 6h illumination (D) 8h illumination. Plates were incubated at 35^{o}C for 29 hours.

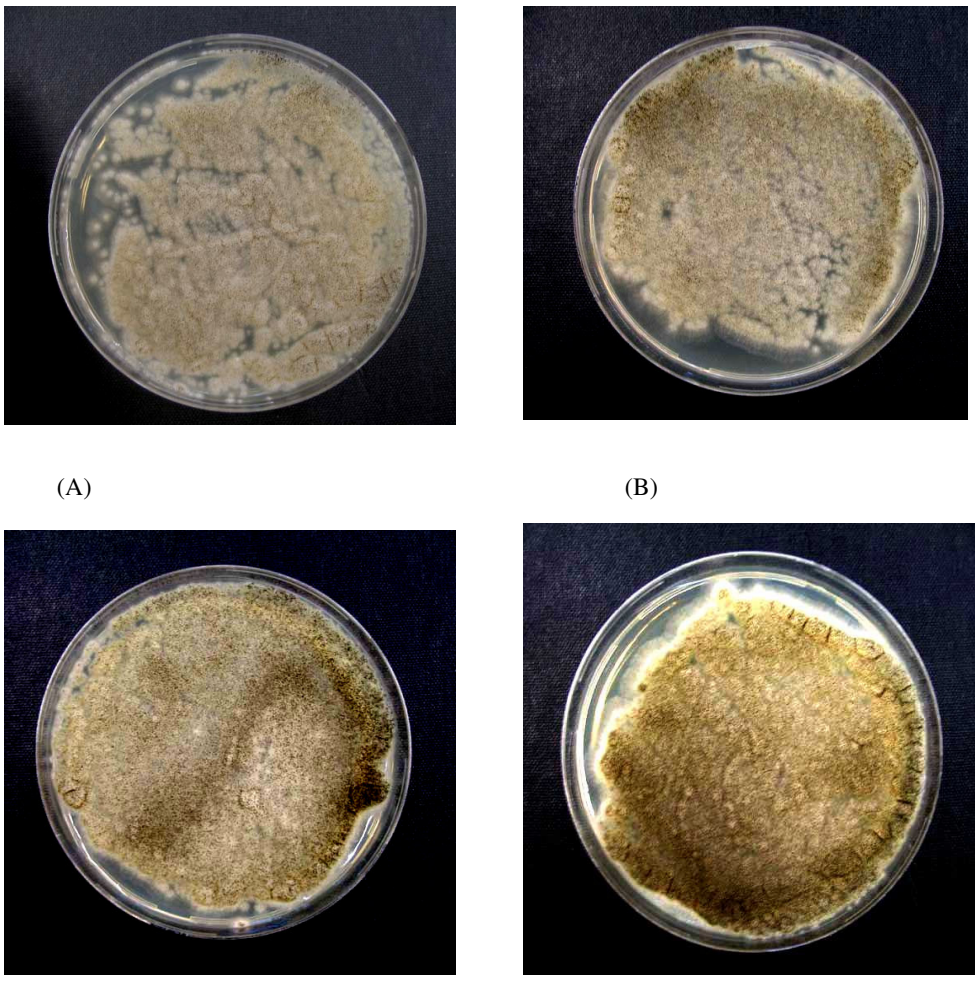

(A) (B)

(C) (D)

Figure 4.47 Growth of *A. niger* spores on TiO_2 coated glass after (A) 2h illumination; (B) 4h illumination (C) 6h illumination (D) 8h illumination. Plates were incubated at 35°C for 29 hours.

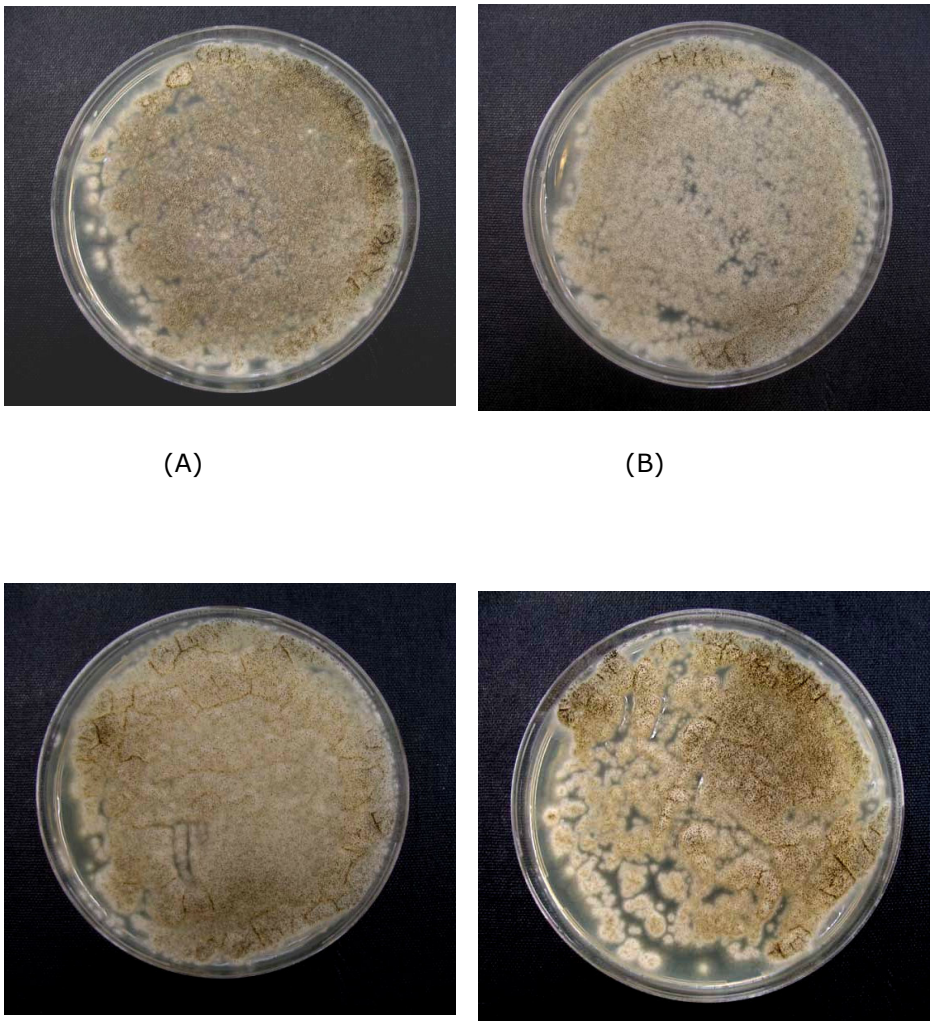

(A) (B)

(C) (D)

Figure 4.48 Growth of *A. niger* spores on PdO-TiO_2 coated glass after (A) 2h illumination; (B) 4h illumination (C) 6h illumination (D) 8h illumination. Plates were incubated at 35^{o}C for 29 hours.

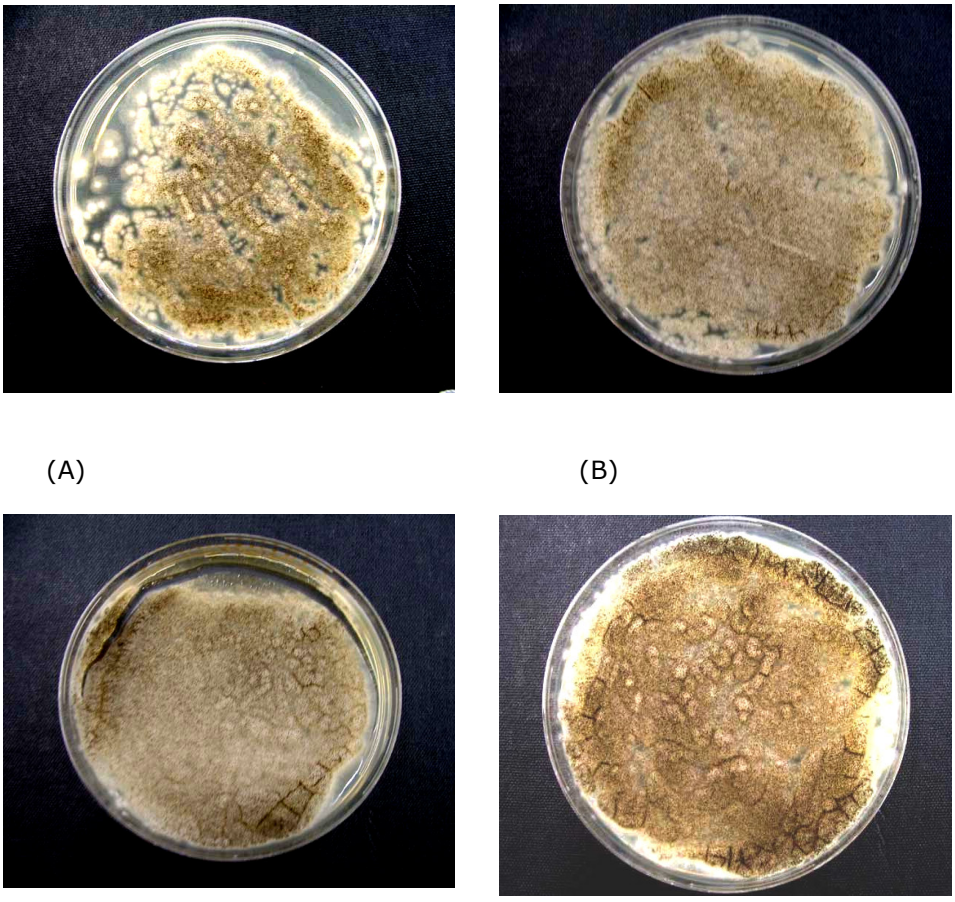

Figure 4.49 Growth of *A. niger* spores on SnO_2 coated glass after (A) 2h illumination; (B) 4h illumination (C) 6h illumination (D) 8h illumination. Plates were incubated at 35^{o}C for 29 hours.

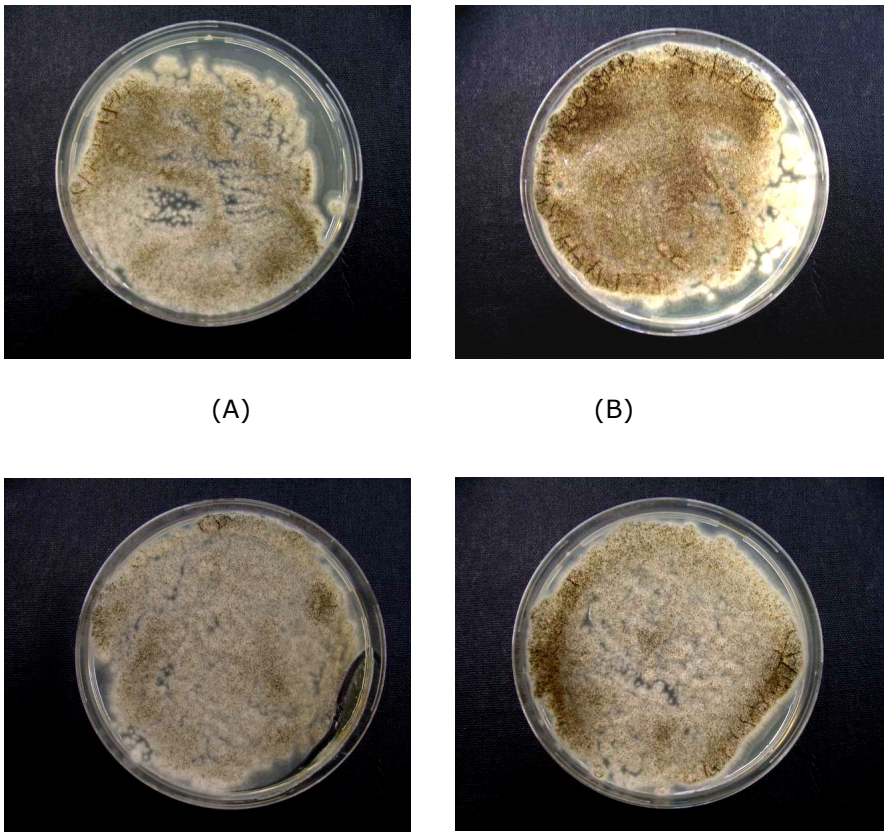

Figure 4.50 Growth of *A. niger* spores on PdO-SnO_2 coated glass after (A) 2h illumination; (B) 4h illumination (C) 6h illumination (D) 8h illumination. Plates were incubated at 35^{o}C for 29 hours.

As a final summary, the microbial cells *E. coli, S. aereus, S. cerevisiae* and *A. niger* spores were illuminated on different coated surfaces up to 8 hours.

The antimicrobial efficiencies against different microorganisms were found to decrease in the following order: *E. coli* > *S. aereus* > *S. cerevisiae* > *A. niger* spores. The complexity and strength of the cell walls increased in the same order of precedence: *E. coli* have thin, slack cell walls [Gr (-) bacteria] and has a periplasmic space having proteins, *S. aereus* have thicker and denser cell walls

[Gr(-) bacteria], the cell wall of *S. cerevisiae* is remarkably thicker and stronger and *A. niger* spores have very thick and strong walls to protect the genetic material from various adverse conditions. This order of precedence appears reasonable if it is assumed that the primary step in photocatalytic decomposition consists of an attack to the cell wall, leading to punctures (Kühn et al., 2003). This is supported by our finding that it was not possible to reduce easily the spores of *A. niger* by photocatalytic treatment even after 8 hours.

In any case, the effect of palladium doping was clearly observed from the results except the case of *A. niger* spores. A final comparison of microorganisms and coatings after 1 and 2 hours of illumination is given in Figure 4.51.

As observed from Figure 4.51, in general the best photocatalytic efficiency against all of the microorganisms, was achieved with Palladium doped TiO_2 coating. The highest antimicrobial efficiency was against *E. coli* because of the simple cell wall structure. The antimicrobial properties of SnO_2 and PdO-SnO_2 coatings, in general, were less effective than TiO_2 and PdO-TiO_2 coatings. However, in the case of SnO_2 and PdO-SnO_2 coatings against *E. coli* and *S. aereus* after 2 hours of illumination were almost equal to each other. After extended period of time, the effect of bacterial cell wall structure on SnO_2 based coatings became unimportant. Up to 1 hr illumination, the effect of Pd doping on TiO_2 against especially *E. coli* but also *S. cerevisiae* was 5% more striking. However, the effect of Pd doping on SnO_2 was higher against *S. aereus*. Therefore, decrease of the gaps between grains of the SnO_2 coatings and formation of isolated palladium crystallites over the SnO_2 surface might make the coating more effective against cell wall disruption of thick Gr (+) cell wall of *S. aereus*. However, in *E. coli* case, formation of uniformly distributed palladium ions and consequently having superior conductivities increased the coating's antimicrobial activity much more than in the case of *S. aereus*. This might be because of switch from cell wall disruption to cell wall component inactivation. The effect of Pd doping on TiO_2 and SnO_2 coatings in (%) increase in reduction efficiencies against different microorganisms were given in Table 4.2.

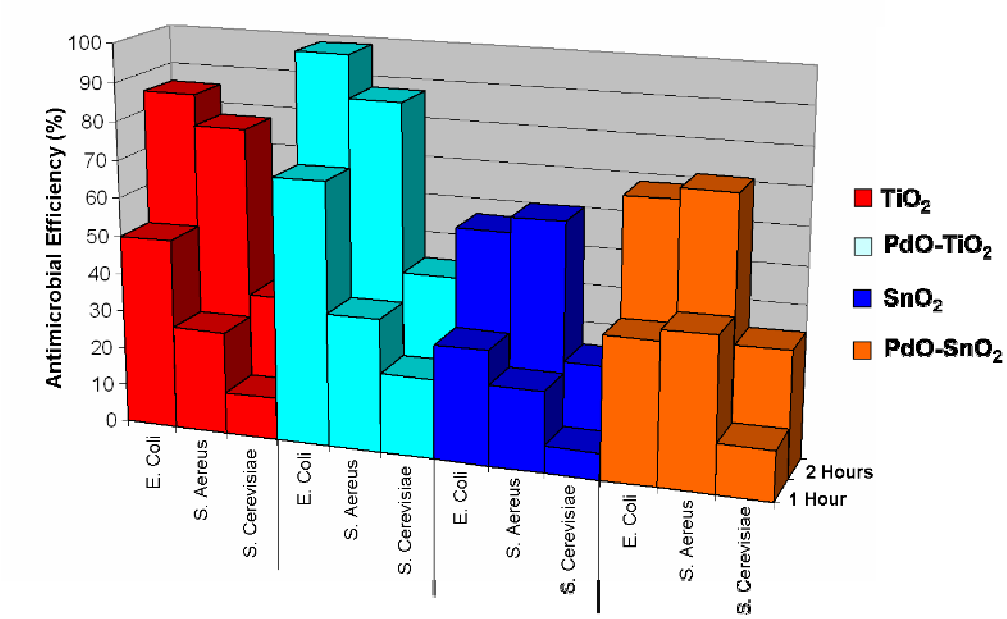

Figure 4.51 Comparison of antimicrobial efficiencies of different coatings against different microorganisms after 1 and 2 hours of illumination

Table 4.2 The increasing effect of Pd doping on TiO_2 and SnO_2 coatings

		Effect of Pd doping on TiO_2 coating (%)	Effect of Pd doping on SnO_2 coating (%)
1 hr illumination	*E. coli*	19	7
	S. aereus	8	19
	S. cerevisiae	10	6
2 hr illumination	*E. coli*	13	12
	S. aereus	10	11
	S. cerevisiae	10	9

CHAPTER 5

CONCLUSIONS

This study focused on the preparation of TiO_2, SnO_2 and palladium doped TiO_2, SnO_2 coatings on glass surfaces and their antimicrobial properties, that is, photocatalytic effect of the coating materials and how palladium doping to these coating materials effect the photocatalytic efficiency. The following conclusions were drawn with the results obtained:

- For both TiO_2 and SnO_2 coatings palladium doping decreased the optical absorption edge energy.

- Photocatalytic antimicrobial efficiency of TiO_2 coating was better than SnO_2 coating.

- Pd doping increased the cell inactivation process for both of the coatings, TiO_2 and SnO_2.

- The assumption of an initial attack on the microbial cells by OH radicals from outside was highly supported since the photocatalytic activity decreases as the cell wall structure complexity increases. The reduction efficiencies were found to decrease in the following order of *E. coli* [Gr(-)] > *S. aereus* [Gr (+)] > *S.cerevisiae* (yeast) > *A. niger* spores. Hence the photocatalytic efficiency against *E. coli* was the highest.

- With the coating that shows the best photocatalytic activity, PdO-TiO_2, 98% of *Escherichia coli*, 87% of *Staphylococcus aereus*, 43% *Saccharomyces cerevisiae* were killed after 2 hours illumination.

- No significant inactivation was observed by using all types of coatings up to 8 hours of illumination on *A. niger* spores.

CHAPTER 6

RECOMMENDATIONS

In this contribution it was shown that it is possible to disinfect surfaces consisting of a light-guiding material coated with a specific semiconductor (TiO_2, SnO_2) and stimulated by direct UVA.

- As for the future effort for developing complete understanding of the photocatalyst behavior, other high organized cells should be investigated such as filamentous fungi and algae.

- Once the mechanisms lying beneath the promoting effect of palladium clarified thoroughly, the synergistic effects of other metal dopants in such system should be investigated.

- Surfaces other than glasses such as ceramic surfaces can be coated and the antimicrobial property can be gained to these ceramic surfaces.

- The effect of initial cell concentration on surfaces can be investigated to determine whether cell protection at high cell concentrations is possible.

- The effect of uniform distribution of Pd ions vs formation of isolated PdO crystallites on antimicrobial effect can be investigated in detail by formation of PdO crystallites on TiO_2 and uniform Pd ion distribution on SnO_2 coatings.

REFERENCES

Bailey J. E. and Ollis D. F., 1986, Biochemical Engineering Fundamentals, 2nd ed., McGraw-Hill Inc., NY.

Benedix R., Dehn F., Quaas J. and Orgass M., 2000, Application of Titanium Dioxide Photocatalysis to Create Self-Cleaning Building Materials, LACER, 5, pp. 157-167.

Bornside D. E., Macosko C. W. and Scriven L. E., 1987, On the modeling of spin coating, Journal of Imaginang Technology 13, pp. 122-130.

Buscema C. L., Malibert C. and Bach S., 2002, Elaboration and Characterization of Thin Films of TiO2, Prepared by Sol–gel Process, Thin Solid Films, 418, 2, pp. 79-84.

Byrne J. A., Eggins B. R., Brown N. M. D., McKinney B. and Rouse M., 1998, Immobilisation of TiO_2 Powder for the Treatment of Polluted Water, Applied Catalysis B: Environmental, 17, pp. 25-36.

Chang H. T., Wu N. M. and Zhu F., 2000, A Kinetic Model for Photocatalytic Degradation of Organic Contaminants in a Thin-Film TiO_2 Catalyst, Water Environment Research, 34(2), pp. 407-416.

Chengyu W., Huamei S., Ying T., Tongsuo Y. and Guowu Z., 2003, Properties and Morphology of CdS Compounded TiO_2 Visible-light Photocatalytic Nanofilms Coated on Glass Surface, Separation and Purification Technology, Journal of Photochemistry and Photobiology A: Chemistry, 32, pp. 357-362.

Colgan M. J., Djurfors G., Ivey D. G. and Brett M. J., 2004, Effects of Annealing on Titanium Dioxide Structured Films, Thin Solid Films, 466(1-2), pp. 92-96.

Davis B. D., Dulbecco R., Eisen H. N., Gingsberg H. S., Wood W. B. and McCarty M., 1973, Microbiology, 2nd Ed., Harper and Row, pp. 128-134.

Diebold U., 2003, The surface science of titanium dioxide, Surface Science Reports, 48(5-8), pp. 53-229.

Djaoued Y., Badilescu S., Ashrit P.V. and Robichaud J., 2001, Vibrational Properties of the Sol-gel Prepared Nanocrystalline TiO_2 Thin Films, Journal Of Vibrational Spectroscopy, 5(6) pp. 4-11.

Fujishima A., Rao T. N. and Tryk D. N., 2000, Titanium Dioxide Photocatalysis, Journal of Photochemistry and Photobiology C: Photochemistry Reviews, 1, pp. 1-21.

Fukayama S., Kawamura K., Saito T., Iyoda T., Hashimoto K. and Fujishima A., 1995, Proceedings of the Extended Abstracts of the 18th Meeting of the electrochemical Society, The Electrochemical Society, Pennington, NJ, USA.

Hoffmann M. R., Martin S. T., Choi W. and Bahnemann D. W., 1995, Environmental Applications of Semiconductor Photocatalysis, Chemical Review, pp. 69-96.

Huang Z., Maness P. C., Blake D: M:, Wolfrum E. J. Smolinski S. L. and Jacoby W. A., 2000, Bactericidal Mode of Titanium Dioxide Photocatalysis, Journal of Photochemistry and Photobiology A: Chemistry, 130, pp. 163-170.

Izgi E., 1998, Characterization of Superconducting Bi-Sr-Ca-Cu-O System Prepared by Sol-Gel Processing, M. S. Thesis, Middle East Technical University.

Kato K., Tsuzuki A., Torii Y., Taoda H. and Butsugan Y., 1995, Crystal structures of TiO_2 thin coatings prepared from the alkoxide solution via the dip coating technique affecting the photocatalytic decomposition of aqueous acetic acid, Journal of Materials Science, 30, pp. 837-841.

Kaya Ö., 2002, Characterization of Titanium Dioxide Thin Films Prepared by Sol-gel Processing, MS Thesis, Ankara.

Kikuchi Y., Sunada K., Iyoda T., Hashimoto K. and Fujishima A., 1997, Photocatalytic Bactericidal Effect of TiO_2 Thin Films: Dynamic View of the Active Oxygen Species Responsible for the Effect, Journal of Photochemistry and Photobiology A: Chemistry, 106, pp. 51-56.

Kominami H., Kumamoto H., Kera Y. and Ohtani B., 2001, Immobilization of Highly Active Titanium(IV) Oxide Particles A Novel Strategy of Preparation of Transparent Photocatalytic Coatings, Applied Catalysis B: Environmental, 30, pp. 329-335.

Kühn K. P., Chaberny I. F., Massholder K., Stickler M., Benz V. W., Sonntag H. G. and Erdinger L., 2003, Disinfection of Surfaces by Photocatalytic Oxidation with Titanium Dioxide and UVA Light, Chemosphere, 53, pp. 71-77.

Kwon C. H., Kim J. H., Jung I. S., Shin H. and Yoon K. H., 2003, Preparation and Characterization of TiO_2-SiO_2 nano-composite Thin Films, Ceramics International, 29, pp. 851-856.

Laskin A. I. and Lechevalier, H. A., 1973, Handbook of Microbiology, volume 1, CRC Press, USA.

Lim T.K., Murakami T., Tsuboi M., Yamashita K. and Matsunaga T., 2002, Preparation of a Colored Conductive Paint Electrode for Electrochemical Inactivation of Bacteria, Biotechnology and Bioengineering, 81(3), pp. 299-304.

Lin H., Kozuka H. and Yoko T., 1998, Preparation of TiO_2 Films on Self-Assembled Monolayers by Sol-Gel Method, Thin Solid Films, 315, pp. 111-117.

Liu H. and Yang T. C. K., 2003, Photocatalytic Inactivation of *Escherichia coli* and *Lactobacillus helveticus* by ZnO and TiO_2 Activated with Ultraviolet Light, Process Biochemistry, 39, pp. 475-481.

Mahnke J., Schulze H. J., Stöckelhuber K. W. and Radoev B., 1999, Rupture of Thin Wetting Films on Hydrophobic Surfaces Part I: Methylated Glass Surfaces, A: Physicochemical and Engineering Aspects, 157, 1-9.

Marzan L. and Luis M., 2003, Nanoscale materials, Kluwer Academic Publishers.

Matsunaga T., Tomoda R., Nakajima T. and Wake H., 1985, Photoelectrochemical Sterilization of Microbial Cells by Semiconductor Powders, FEMS Microbiology Letters, 29(1-2), pp. 211-214.

Meyerhofer, 1978, Characteristics of Resist Films Produced by Spinning, Journal of Applied Physics, 49, pp. 3993

Mills A., Hill G., Bhopal S., Parkin I. P. and O'Neil S. A., 2003, Thick Titanium Dioxide Films for Semiconductor Photocatalysis, Journal of Photochemistry and Photobiology A: Chemistry, 160, 3, pp. 185-194.

Minabe T., Tryk D. A., Sawunyama P., Kikuchi Y., Hashimoto K. and Fujishima A., 2000, TiO_2-Mediated Photodegradation of Liquid and Solid Organic Compounds, Journal of Photochemistry and Photobiology A: Chemistry, 137, pp. 53-62.

Moses, V. and Cape, R. E., 1991, Biotechnology: The Science and The Business, Harwood Academic Publishers, Switzerland.

Okudera H. and Yokogawa Y., 2001, Formation of TiO_2 Thin Films by Hydrolysis of Ti-tetraethoxide in Ethanol: Kinetics, Surface Morphology, Constituent Phases and Their Formation Mechanism, Thin Solid Films, 401, pp. 124-130.

Pham N. H., Mcdowell T. and Witkins E., 1995, Journal of Environmental Science Health A, 30, pp. 627.

Popielarski S., 1998, Photocatalysis on Nano-Sized Semiconductors, Chemical Reviews, 95, pp. 735.

Rakai A., Tessier D. and Verduraz B. F., 1992, Palladium-alumina catalysts: a diffuse reflectance study, New Journal of Chemistry, 16, pp. 869-875.

Ranjit K. T. and Viswanathan B., 1997, Photocatalytic Reduction of Nitrite and Nitrate Ions Over Doped TiO_2 Catalysts, Journal of Photochemistry and Photobiology A: Cemistry, 107(1-3), pp. 215-220.

Raven P. H. and Johnson G. B., 1996, Biology, McGram-Hill Inc., NY.

Reddya K. M., Manorama S. V. and Reddy A. R., 2002, Bandgap Studies on Anatase Titanium Dioxide Nanoparticles, Materials Chemistry and Physics, 78(1), pp. 239-245.

Saito T., Iwase T., Horis J. and Morioka T., 1992, Mode of photocatalytic bactericidal action of powered semiconductor TiO_2 on mutans streptococci, Journal of Photochemistry and Photobiology B: Biology, 14, pp. 369.

Sawunyama P., Yasumori A. and Okada K., 1998, The Nature of Multilayered TiO2-Based Photocatalytic Films Prepared By a Sol-Gel Process, Materials Research Bulletin, 33(5), pp. 795-801.

Schwartz R. W., Schneller T. and Waser R., 2004, Chemical Solution Deposition of Electronic Oxide Films, C.R. Chimie, 7, pp. 433-461.

Schwitzgebel J., Ekerdt J. G., Gerischer H. and Heller A., 1995, Role of oxygen molecule and the photogenerated electron in TiO_2-photocatalysed air oxidation reactions, Journal of Physics and Chemistry, 99 pp. 5633-5638.

Serpone N. and Pelizetti E., 1988, Photocatalysis: Fundamentals and Applications, Wiley, New York.

Shah S. I., Li W., Huang C. P. and Ni C., 2002, Study of Nd^{3+}, Pd^{2+}, and Fe^{3+} dopant effect on photoreactivity of TiO2 nanoparticles, Journal of Photochemistry and Photobiology A: Chemistry, 99(2), pp. 6482-6486.

Shuler M. L. and Kargi K., 1992, Bioprocess Engineering Basic Concepts, Prentice Hall, Englewood Cliffs, NJ, USA

Sjogren J. C. and Sierka S. A., 1994, Inactivation of phage MS2 by iron-aided titanium dioxide photocatalysis, Applications of Environmental Microbiology, 60, pp. 344.

Sonawane R. S., Hegde S. G. and Dongare M. K., 2002, Preparation of Titanium(IV) Oxide Thin Film Photocatalyst by Sol-Gel Dip Coating, Materials Chemistry and Physics, 77, pp. 744-750.

Speck M. L., 1989, Compendium of Methods for the Microbiological Examination of foods, by APHA Intersociety, Agency Committee.

Su C., Hong B. Y. and Tseng C. M., 2004, Sol-gel Preparation and Photocatalysis of Titanium Dioxide, Catalysis Today, 96(3), pp. 119-126.

Sunada K., Kikuchi Y., Hashimoto K. and Fujishima A., 1998, Environmental Science Technology, 32, pp. 726.

Tanaka T., Teramura K., Yamamoto T., Takenaka S., Yoshida S. and Funabiki T., 2002, TiO_2/SiO_2 Photocatalysts at Low Levels of Loading: Preparation, Structure and Photocatalysis, Journal of Photochemistry and Photobiology A: Chemistry, 148, pp. 277-281.

Tang H., Berger H., Schmid P. E. and Levy F., 1995, Urbach Tail of Anatase TiO_2, Solid State Comminications, Physical Reviews, 87, pp. 847-850.

Tessier D., Rakai A. and Verduraz B. F., 1992, Spectroscopy Study of The interaction of Carbon monoxide with cationic and metallic palladium-alumina catalysts, Journal of Chemistry Society of Faraday Transformations, 88, 741-749.

Tiller J., Lee S. B., Lewis K. and Klibanov A. M., 2002, Polymer Surfaces Derivatized with Poly(Vinyl-N-Hexylpyridinium) Kill Airbone and Waterborne Bacteria, Biotechnology and Bioengineering, 79(4), pp. 465-471.

Tiller J., Liao C. J., Lewis K. and Klibanov A. M., 2001, Designing Surfaces that Kill Bacteria on Contact, PNAS, 98(11), pp. 5981-5985.

Ting C. C. and Chen S. Y., 2000, Influence of ligand groups in Ti precursors on phase transformation and microstructural evolution of TiO_2 thin films prepared by the wet chemical process, Journal of Material Research, 16, pp. 1712-1719

Todar, K., 2000, Nutrition and Growth of Bacteria, University of Wisconins-Madison.

Trapalis C. C., Keivanidis P., Kordas G., Zaharescu M., Crisan M., Szatvanyi A. and Gartner M., 2003, $TiO_2(Fe^{3+})$ Nanostructured Thin Films with Antibacterial Properties, Thin Solid Films, 433(1-2), pp. 186-190.

Veeramasuneni S., Drelich J., Miller J. D. and Yamauchi G., 1997, Hydrophobicity of Ion-Plated PTFE Coatings, Progress in Organic Coatings, 31, pp. 265-270.

Walters A. B., Na B. K., Liu C. C. and Vannice M. A., 2000, Distinguishing Surface and Bulk Electron Charge Carriers for ZnO Powders, Journal of Molecular Catalysis A: Chemical, 162, pp. 287-295.

Watanabe T., Nakajima A., Wang R., Minabe M., Koizumi S., Fujishima A. and Hashimoto A., 1999, Photocatalytic Activity and Photoinduced Hydrophilicty of Titanium Dioxide Coated Glass, Thin Solid Films, 351, pp. 260-263.

Yamashita H., Nakao H., Takeuchi M., Nakatani Y. and Anpo M., 2003, Coating of TiO_2 photocatalysts on Super-Hydrophobic Porous Teflon Mambrane by an Ion Assisted Deposition Method and Their Self-Cleaning Performance, Nuclear Instruments and Methods in Physics Research B, 206, pp. 898-901.

Yu J. C., Jiaguo Yu and Zhao J., 2002, Enhanced Photocatalytic Activity of Mesoporous and Ordinary TiO_2 Thin Films by Sulfuric Acid Treatment. Applied Catalysis B: Environmental, 36, pp. 31-43.

Yusuf M. M., Imai I. and Hirashima H., 2001, Preparation of mesoporous TiO_2 thin films by surfactant templating, Journal of Non-Crystalline Solids, 285, pp. 90-95.

Zaharescu M., Pirlog C., Crisan M., Gartner M. and Vasilescu A., 1993, TiO_2-based vitreous coatings obtained by sol-gel method, Journal of Non-Crystalline Solids, 160, pp. 162-166.

Zhang R., Gao L. and Zhang O., 2004, Photodegradation of surfactants on the nanosized TiO_2 prepared by hydrolysis of the alkoxide titanium, Chemosphere, 54(3), pp. 405-411.

WEB REFERENCES

URL 1 EISF, Last updated January 2005, Lesson 4 – Semiconductors, http://www.madlab.org/electrnx/lesson4.html, Last visited July 19, 2005.

URL 2 Chemat Technology, Last updated 1998, Sol-gel Technology, http://www.chemat.com/html/solgel.html, Last visited July 19, 2005.

URL 3 Water & Process Technology, Last updated 2005, Hydrophilicity and Hydrophobicity, http://www.gewater.com/library/tp/772_Hydrophilicity_and.jsp, Last visited July 19, 2005.

URL 4 CSMFO, Last updated July 8 2005, The dip-coating technique, http://www.science.unitn.it/~gcsmfo/index_.html, Last visited July 19, 2005.

URL 5 Dunbar P. B., Last updated December 1999, Coating quality and Spin coating, http://www.mse.arizona.edu/faculty/birnie/Coatings/index.htm, Last visited July 19, 2005.

URL 6 Kenneth Todar University of Wisconsin-Madison, Last updated 2001, Biological identity of Procaryotes, http://www.bact.wisc.edu/Bact303/TheProcaryotes, Last visited July 19, 2005.

URL 7 ConceptDraw, Last updated 2005, Ejemplos de conceptdraw medical, http://www.conceptdraw.com/sp/sampletour/medical/, Last visited July 19, 2005.

URL 8 Washington State University, Last updated December 16 1999, Microbiology 101/102 internet text, http://www.slic2.wsu.edu:82/hurlbert/micro101/pages/chap3.html, Last visited July 19, 2005.

URL 9 Washington State University, Last updated 2005, Introduction to kingdom fungi, http://classes.plantpath.wsu.edu/plp321/Powerpoint%20Lecture%20Presentations/1, Last visited July 19, 2005.

URL 10 EURAASYP, Last updated 2005, Definition of yeast cell wall, http://www.eurasyp.org/public.levure.ecorce.screen, Last visited July 19, 2005.

APPENDIX A

MEDIUM AND AGAR BASES

1. **Luria-Bertani (LB) Broth:**

Basis: 1L (in distilled water)

- Bacto-tryptone (Sigma), 10g
- Bacto-yeast extract (Merck), 5g
- NaCl, 10g

pH: 7.0

2. **Luria-Bertani (LB) Agar:**

Basis: 1L (in distilled water)

- Bacto-tryptone (Sigma), 10g
- Bacto-yeast extract (Merck), 5g
- NaCl, 10g
- Agar (Merck), 15g

pH: 7.0

3. **Baird-Parker Agar:**

Basis: 1L (in distilled water)

- Baird-Parker Agar complex (Difco), 63g

Containing:

- ✓ Bacto-tryptone, 10g
- ✓ Bacto-beef extract, 5g
- ✓ Bacto-yeast extract, 1g
- ✓ Glycine, 12g
- ✓ Na-pyruvate, 10g
- ✓ Lithium Chloride, 5g
- ✓ Bacto-agar, 20g

50 ml Egg-yolk tellurite (EYT enrichment) (Merck) emulsion was added to Baird-Parker agar complex for the identification of *S. aereus*.

4. **YPD Broth:**

Basis: 1L (in distilled water)

- Glucose (Sigma), 20g
- Peptone (Sigma), 10g
- Bacto-yeast extract, 10g

pH: 7.0

5. **YPD Agar:**

Basis: 1L (in distilled water)

- Glucose (Sigma), 20g
- Peptone (Sigma), 10g
- Bacto-yeast extract, 10g
- Agar (Merck), 20g

6. **Medium for *Aspergilus niger:***

Basis: 1L (in distilled water)

- Glucose (Sigma), 10g
- Ammonium Hydrogen Phosphate, $[(NH_4)_2HPO_4]$ (Merck), 5g
- Potassium Phosphate, $[K_2HPO_4]$ (Merck), 1g
- Magnesium Sulphate, $[MgSO_4.7H_2O]$ (Merck), 1g
- Zinc Sulphate, $[ZnSO_4.7H_2O]$ (Merck), 0,1g
- NaCl, 0,0025g

PH: 5.5

7. **Potato-Dextrose Agar:**

Basis: 1L (in distilled water)

- Potato-dextrose agar complex (Merck), 39g

pH: 5.5

APPENDIX B

SAMPLE CALCULATIONS

A.1 Calculations For SnO_2 Preparation

The molecular weights of species necessary for the calculations are presented in Table A1.

Table A.1 Molecular Weights of Reactants And Products

Specie	Molecular Weight(gr/mol)
Tin Tetrachloride Pentahydrate [$SnCl_4.5H_2O$]	350.58
Palladium Acetate [$Pd(CH_3CO_2)_2$]	224.45
Isopropyl Alcohol [C_3H_7OH]	60,06
Water [H_2O]	18.02
Palladium Oxide [PdO]	122.41
Tin Oxide [SnO_2]	150.69

Basis: 1 g of SnO_2 product

$n_{SnO2} = m_{SnO2} / (M_{wt})_{SnO2} = 1g / 150.69g/mol = 6.636*10^{-3}\ mol$

$n_{SnO2} = n_{Sn} = n_{SnCl4.5H2O} = = 6.636*10^{-3}\ mol$

$m_{SnCl4.5H2O} = n_{SnCl4.5H2O} \times (M_{wt})_{SnCl4.5H2O} = 6.636*10^{-3}\ mol x 350.58g/mol$

$= 2.326g$

Isopropyl alcohol is added to $SnCl_4.5H_2O$ in 7:1 molar ratio.

$n_{C3H7OH} = 7 \times n_{SnCl4.5H2O} = 7 \times 6.636*10^{-3}\ mol = 0.0464mol$

$m_{C3H7OH} = n_{C3H7OH} \times (M_{wt})_{C3H7OH} = 0.0464mol x 60.06g/mol$

$= 2.790g$

The molar ratio of $SnCl_4.5H_2O$ to water is 1:5.38, for the course of hydrolysis reaction

$n_{H2O} = 5.38 \times n_{SnCl4.5H2O} = 5.38 \times 6.636*10^{-3}\ mol = 0.0357mol$

$m_{H2O} = n_{H2O} \times (M_{wt})_{H2O} = 0.0357mol \times 18.02g/mol = 0.643g$

The molar ratio of isopropyl alcohol to water for the course of the hydrolysis reaction is 1:1.14

$n_{C3H7OH} = n_{H2O} / 1.14 = 0.0357mol / 1.14 = 0.0313mol$

$m_{C3H7OH} = n_{C3H7OH} \times (M_{wt})_{C3H7OH} = 0.0313mol \times 60.06g/mol = 1.88g$

B.2 Calculations for 1 wt. %Pd/SnO_2 Preparation

1 g SnO_2 constitutes 99% of the resultant powder

0.01 g PdO constitutes 1% of the resultant powder

$n_{PdO} = m_{PdO} / (M_{wt})_{PdO} = 0.01g/122.41g/mol = 8.170*10^{-5}mol$

$n_{PdO} = n_{Pd(CH3CO2)2} = 8.170*10^{-5}$

$m_{Pd(CH3CO2)2} = n_{Pd(CH3CO2)2} \ x \ (M_{wt})_{Pd(CH3CO2)2} =$

$$8.170*10^{-5}mol* \ 224.45g/mol = 0.0183g$$

For the synthesis of 1 wt.% PdO/SnO_2 0.0183g $Pd(CH_3CO_2)_2$ should be added to the sol described in section A.1.

B.3 Calculations for 1 wt. %Pd/TiO_2 Preparation

The molecular weights of species necessary for the calculations are presented in Table B1.

Table B.1 Molecular Weights of Reactants And Products

Specie	Molecular Weight(gr/mol)
Titanium Tetra Isopropoxide $[C_{12}H_{28}O_4Ti]$	283,879
Palladium Acetate $[Pd(CH_3CO_2)_2]$	224.45
Water $[H_2O]$	18.02
Palladium Oxide [PdO]	122.41

$C_{12}H_{28}O_4Ti + 4\ H_2O \longrightarrow TiO_2$

(Titanium tetra isopropoxide)

$m_{C12H28O4Ti}\ (g)/V_{C12H28O4Ti}\ (ml) = \rho_{C12H28O4Ti}\ (g/ml)$ $x(g)/8.4ml = 0.995g/ml$

$x = 8.4ml*0.995g/ml$ $x_{C12H28O4Ti} = 8.36g$

$n_{C12H28O4Ti}\ (mol) = m_{C12H28O4Ti}\ (g)/MW_{C12H28O4Ti}\ (g/gmol)$

$n = 8.36g/283.87g/gmol$

$n = 0.03mol$

$n_{C12H28O4Ti} = n_{TiO2} = 0.03mol$

$n(mol) = m(g)/MW(g/gmol)$ $0.03mol = m(g)/79.879g/gmol$

$m_{C12H28O4Ti}\ (g) = 2.4g$

$x(g) \longrightarrow 100\%$

$2.4g \longrightarrow 99\%$

$x = 2.4242g$

$m_{PdO} = 2.4242g - 2.4g$ $m_{PdO} = 0.02424g$

$n_{PdO} = 0.02424g/122.41(g/gmol) = 1.980*10^{-4}mol$

$n_{PdO} = n_{Pd(CH3CO2)2} = 1.980*10^{-4}mol$

$m_{Pd(CH3CO2)2} = n_{Pd(CH3CO2)2}\ x\ (M_{wt})_{Pd(CH3CO2)2}$

$m_{Pd(CH3CO2)2} = 1.980*10^{-4}mol\ x\ 224.49\ g$

$m_{Pd(CH3CO2)2} = 0.045g$

For the synthesis of 1 wt.% PdO/TiO_2 0.045g $Pd(CH_3CO_2)_2$ should be added to the sol described in chapter 3.

APPENDIX C

DATA OF GRAPHICS

Table 9.1 Data of Figure 4.1, UV-Vis spectra of TiO_2 and PdO-TiO_2 deposited glass substrates

TiO_2		**PdO-TiO_2**	
nm	abs	Nm	abs
295	0,115	296	0,501
296	0,204	297	0,79
297	0,356	298	0,873
298	0,456	299	0,983
299	0,555	300	1,173
300	0,613	301	1,354
301	0,604	302	1,519
302	0,621	303	1,613
303	0,629	304	1,613
304	0,632	305	1,635
305	0,63	306	1,713
306	0,622	307	1,715
307	0,624	308	1,71
308	0,62	309	1,736
309	0,612	310	1,748
310	0,605	311	1,727
320	0,558	312	1,682
330	0,52	313	1,673
340	0,444	314	1,657
350	0,352	315	1,636
360	0,291	320	1,56
370	0,254	330	1,371
380	0,241	340	1,05
390	0,236	350	0,765

Table 9.1 Data of Figure 4.1, UV-Vis spectra of TiO_2 and PdO-TiO_2 deposited glass substrates (cont'd)

TiO_2		**PdO-TiO2**	
nm	abs	nm	abs
400	0,233	360	0,573
410	0,231	370	0,454
420	0,229	380	0,408
430	0,227	390	0,385
440	0,226	400	0,379
450	0,224	410	0,38
460	0,222	420	0,382
470	0,22	430	0,381
480	0,218	440	0,377
490	0,215	450	0,368
500	0,212	460	0,357
510	0,209	470	0,346
520	0,205	480	0,335
530	0,202	490	0,325
540	0,198	500	0,317
550	0,196	510	0,309
		520	0,303
		530	0,299
		540	0,293
		550	0,29

Table 9.2 Data of Figure 4.2, UV-Vis spectra of SnO_2 and PdO-SnO_2 deposited glass substrates

SnO_2		**PdO-SnO_2**	
nm	abs	nm	abs
200	0,365	200	1,079
210	0,702	210	1,066
220	0,679	220	1,055

Table 9.2 Data of Figure 4.2, UV-Vis spectra of SnO_2 and PdO-SnO_2 deposited glass substrates (cont'd)

SnO_2		**PdO-SnO_2**	
nm	abs	nm	abs
230	0,622	230	1,046
240	0,589	240	1,04
250	0,572	250	1,039
260	0,536	260	1,043
270	0,489	270	1,048
280	0,456	280	2,642
290	0,412	290	3,245
300	0,375	295	3,812
310	0,336	296	3,887
320	0,302	297	3,965
330	0,287	298	3,997
340	0,274	299	4
350	0,263	300	3,998
360	0,262	301	3,926
370	0,261	302	3,874
380	0,261	303	3,736
390	0,259	304	3,652
400	0,26	305	3,482
410	0,261	306	3,279
420	0,26	307	3,125
430	0,259	308	2,965
440	0,26	309	2,846
450	0,26	310	2,834
460	0,259	320	2,438
470	0,258	330	2,121
480	0,257	340	1,765
490	0,256	350	1,634
500	0,256	360	1,513
510	0,257	370	1,427
520	0,257	380	1,426

Table 9.2 Data of Figure 4.2, UV-Vis spectra of SnO_2 and PdO-SnO_2 deposited glass substrates (cont'd)

SnO_2		**PdO-SnO_2**	
nm	abs	nm	abs
530	0,256	390	1,425
540	0,255	400	1,424
550	0,256	410	1,423
		PdO-SnO_2	
		nm	abs
		420	1,424
		430	1,435
		440	1,441
		450	1,449
		460	1,443
		470	1,515
		480	1,572
		490	1,624
		500	1,612
		510	1,46
		520	1,365
		530	1,348
		540	1,332
		550	1,316

Table 9.3 Data of Figure 4.16, Survival ratio of *E. coli* under illumination on TiO_2 and PdO-TiO_2 coated glass substrates

	TiO_2	**PdO-TiO_2**
time(min)	%survival	%survival
0	100	100
10	95	90
20	85	78
30	72	63
45	61	47

Table 9.3 Data of Figure 4.16, Survival ratio of *E. coli* under illumination on TiO_2 and PdO-TiO_2 coated glass substrates (cont'd)

60	50	31
80	36	19
100	22	8
120	15	2

Table 9.4 Data of Figure 4.21, Survival ratio of *E. coli* under illumination on SnO_2 and PdO-SnO_2 coated glass substrates

	SnO_2	**PdO-SnO_2**
time(min)	%survival	%survival
0	100	100
10	95	92
20	90	86
30	82	77
45	74	69
60	70	63
80	62	55
100	55	44
120	44	32

Table 9.5 Data of Figure 4.27, Survival ratio of *S. aereus* under illumination on TiO_2 and PdO-TiO_2 coated glass substrates

	TiO_2	**PdO-TiO_2**
time	%survival	%survival
0	100	100
10	98	98
20	97	95
30	93	90

Table 9.5 Data of Figure 4.27, Survival ratio of *S. aereus* under illumination on TiO_2 and PdO-TiO_2 coated glass substrates (cont'd)

45	86	75
60	79	60
75	70	51
90	60	42
105	50	36
120	40	29
150	28	17
180	21	10

Table 9.6 Data of Figure 4.30, Survival ratio of *S. aereus* under illumination on SnO_2 and PdO-SnO_2 coated glass substrates

	SnO_2	**PdO-SnO_2**
time	%survival	%survival
0	100	100
10	98	97
20	97	96
30	93	90
45	85	77
60	73	65
75	60	50
90	45	35
105	29	20
120	23	13
150	16	5
180	13	2

Table 9.7 Data of Figure 4.37, Survival ratio of *S. cerevisiae* under illumination on TiO_2 and PdO-TiO_2 coated glass substrates

	TiO_2	**PdO-TiO_2**
time (min)	%survival	%survival
0	100	100
30	94	91
60	89	79
90	81	73
120	67	58
150	60	45
180	54	36